The changing influence of permafrost on peatlands hydrology

by

Élise Devoie

A thesis
presented to the University of Waterloo
in fulfillment of the
thesis requirement for the degree of
Doctor of Philosophy
in
Civil Engineering

Waterloo, Ontario, Canada, 2020

Examining Committee Membership

The following served on the Examining Committee for this thesis. The decision of the Examining Committee is by majority vote.

External Examiner:	Andrew Ireson Professor, School for Environment and Sustainability, University of Saskatchewan
Supervisor(s):	James R. Craig Professor, Dept. of Civil & Environmental Engineering, University of Waterloo William L. Quinton Professor, Dept. of Geography, Wilfrid Laurier University
Internal-External Member:	Jonathan S. Price Professor, Dept. of Geography & Environmental Management, University of Waterloo
Alternate:	Behrad Gharedaghloo Adjunct Assistant Professor, Dept. of Geography & Environmental Manage University of Waterloo
Internal Member:	Nandita Basu Professor, Dept. of Civil & Environmental Engineering, University of Waterloo
Internal Member:	Neil R. Thomson Professor, Dept. of Civil & Environmental Engineering, University of Waterloo

Author's Declaration

This thesis consists of material all of which I authored or co-authored: see Statement of Contributions included in the thesis. This is a true copy of the thesis, including any required final revisions, as accepted by my examiners.

I understand that my thesis may be made electronically available to the public.

Statement of Contributions

Élise Devoie was the sole author for Chapters 1, 2, 3, 6 and 8 which were written under the supervision of Dr. James R. Craig and Dr. William L. Quinton. Chapter 6 is written with the intent for publication, but no contributions have been made by other authors yet.

This thesis consists in part of three manuscripts written for publication. Exceptions to sole authorship of material are as follows:

Research presented in Chapter 4:

Élise Devoie developed the model in MATLAB, and collected and aggregated field data from the Scotty Creek Research Station to be used as initial and boundary conditions in the model simulations. She also prepared the manuscript. Dr. Craig provided key insights during model development, benchmarking, and the development of test scenarios. His attention to detail and experience solving PDEs where invaluable in his evaluation of the mathematical formulations and editing the manuscript. Drs. Quinton and Connon provided insight into processes in the field, assisted in design and implementation of field studies and guidance through reviewing the manuscript.

Devoie, É. G., Craig, J. R., Connon, R. F., and Quinton, W. L. (2019). Taliks : A tipping point in discontinuous permafrost degradation in peatlands. *Water Resources Research*. DOI: https://doi.org/10.1029/2018WR024488

Research presented in Chapter 5:

Élise Devoie compares the current Darcy-flux approach to computing subsurface flow in the system to data collected using these instruments. She prepared the field methodology, and performed the data analysis. She also prepared the manuscript. Dr. Craig provided key insights during manuscript preparation. Drs. Quinton and Connon assisted in implementation of field studies and provided feedback on the manuscript.

Devoie, É. G., Craig, J. R., Connon, R. F., and Quinton, W. L. (2020). Passive flux meters as a measure of water movement in low-gradient, variably-saturated cold regions landscapes. *Hydrological Processes* DOI: https://doi.org/10.1002/hyp.13900

Research presented in Chapter 6:

Élise Devoie developed the governing equations and implemented the model in MATLAB. She also prepared the manuscript. Dr. Craig initially suggested the idea, and played a key role in model development and validation as well as manuscript revision.

Devoie, É. G., and Craig, J. R. (2020). A semi-analytical interface model of soil freeze/thaw and permafrost evolution *Water Resources Research* DOI: https://doi.org/10.1029/2020WR027638

Abstract

Hydrology and hydrological modelling in the far north is understudied, and many gaps exist in the current understanding and representation of northern thermal and hydrological systems. A combination of fieldwork and modelling was used to gain a better understanding of landscape evolution and thaw processes in the peatland-dominated discontinuous permafrost region of the Northwest Territories. Data collected at the Scotty Creek Research Station and modelling tools are developed and used to identify and quantify controls on isolated and connected talik formation in discontinuous permafrost peatland systems which include soil moisture, snow cover, surface temperature and subsurface lateral flow. The formation of a talik was shown to be a tipping point in permafrost degradation after which several positive feedback cycles led to more rapid permafrost loss.

Given the widespread prevalence of taliks in this discontinuous permafrost peatlands environment, seasonal pressure and temperature gradients were analyzed in different talik configurations to determine the impacts of taliks on the landscape. It was found that the formation of taliks led to a balance between increased hydrologic storage due to isolated talik prevalence, and increased discharge from the basin due to connected talik features allowing previously inaccessible runoff features to be connected to the drainage network. Thermodynamically speaking, the interplay between subsurface temperature, thaw rates, subsidence, snow accumulation, canopy coverage and soil moisture were discussed supporting the idea that talik formation is a positive feedback for permafrost loss. It is also noted that the loss of permafrost causes subsidence and geophysical destabilization leading to ecosystem change and a change in greenhouse gas emission regimes.

Existing models representing permafrost and other cold-regions processes are either computationally expensive physically-based models, or empirically based. This limits their predictive ability at the watershed scale or larger. Large-scale predictions of the impacts of changing climate and subsequent permafrost thaw are needed to improve our understanding of long-term evolution of semi-discontinuous permafrost landscapes. To extend predictions to this scale, a novel physically-based interface model of active layer and permafrost evolution is developed and validated against both field data and a benchmarked continuum numerical model. This simplified model is designed to be incorporated into a semi-distributed hydrological model that will be used to predict hydrologic impacts of changes in permafrost dynamics at the basin scale. This model was used to inform the current understanding of permafrost thaw mechanisms in this environment.

In order to quantify the rate of permafrost loss, different parts of the landscape are classified based on the mechanisms for permafrost thaw including conduction and advection

in both the vertical and lateral directions. These results help to explain the observed heterogeneity in thaw rates in the landscape. It was found that conduction is responsible for much of the thaw in the vertical direction, while advective processes do play a role in flow-through talik features. Lateral thaw is occurring more rapidly than vertical thaw, due both to conduction and advective heat transfer. Finally, thaw from below is documented both due to geothermal heat flux, and observed deep thermistor temperature profiles. The combined fieldwork and modelling efforts provide a better understanding of the rapidly changing discontinuous permafrost environment, help to predict hydrologic and landscape changes in Canada's north, and create tools which are transferable to other cold-regions environments.

Acknowledgements

Firstly my supervisors who shone a light into the darkness:

Dr. James Craig

Dr. Bill Quinton

Those whose ideas, efforts, curiosity, grammar, trust, guidance and experience made this work possible:

Caren Ackley, Dr. Erfan Amiri, Dr. Nandita Basu, Dr. Michael Braverman, Kevin Brink, Genevieve Brown, Dr. Ryan Connon, Dirk Friesen, Gabriel Hould Gosselin, Sarah Grass, Simon Lin, Dr. Juliane Mai, Dr. Jonathan Price, Mark Ranjram, Leland Scantlebury, Lindsay Stone.

The Tired Doctoral Women:

Melissa Prickaerts & Emma Reesor

The Keepers of Sanity and Good Food:

Christine Maiolo, Danny Aguizi, Ekin Eray.

The Givers of Good Advice:

Robert Gooding-Townsend; Dr. Nicole Hayes; Hannah Ince; Dr. Eric Kennedy; Dr. Kevin Purbhoo.

The Most Loving and Least Likely Cheerleaders:

Lucie Lavoie & Dr. Ken Deacon

Dedication

This thesis is unwisely dedicated to Fred and George, the brothers who got me through the thick and the thin of it, with loads of fur to spare. And to my vacuum cleaner, which often solved the most hairy of problems.

Table of Contents

List of Figures

List of Tables

She is called Mother Earth because from Her come all living things. Water is Her life blood.

– Benton-Banai, E. The Mishomis Book: The Voice of the Ojibway (Indian County Communications, Hayward WI, 1998).

Chapter 1

Introduction

Discontinuous permafrost occurs in a large part of Northern Canada including most of the Northwest Territories, and refers to a landscape which is partially underlain by ground which is frozen for two or more consecutive years (Natural Resources Canada, 1995). Anthropogenic climate change is affecting northern regions with warming at twice the global average rate, resulting in rapid permafrost thaw. The Intergovernmental Panel on Climate Change (IPCC) has projected the widespread disappearance of near-surface permafrost underlying about 25% (by area) of the northern hemisphere by 2100 (Pörtner *et al.*, 2019; Zhang *et al.*, 2008b). The impacts of thaw are expected to be significant, from increased carbon emissions and forest fire frequency to altered hydrologic regimes and ecosystem dynamics including serious impacts on infrastructure due to thaw-induced subsidence (Schaefer *et al.*, 2009; Chen *et al.*, 2012). More than half of global discontinuous permafrost is found in peatlands, where surface soil porosity is upwards of 80% (Tarnocai, 2009). This permafrost is ecosystem-protected, meaning that organic soils insulate remnants of permafrost (Bonnaventure & Lamoureux, 2013). These landscapes generally exhibit little large-scale topographic variation, so thaw processes and the subsequent subsidence strongly impact both surface and subsurface flow paths in the region, increasing the overall hydrologic connectivity and consequently basin discharge (Connon *et al.*, 2015). Permafrost thaw has the potential to impact other components of the water balance as well (Connon *et al.*, 2015; Walvoord & Kurylyk, 2016).

Peatlands overlaying permafrost represent a significant global carbon store, containing 30% of the world's soil carbon on only 3% of the land surface (Kimmel & Mander, 2010). Carbon sequestration in peatlands has therefore been identified as an important control on global climate (Kimmel & Mander, 2010). However, peatlands are fragile ecosystems whose function depends on climate (Rydin & Jeglum, 2013; Price, 1991). It is therefore

important to consider not only the impact of peatlands on the climate, but also the impact of climate on peatlands, especially in discontinuous permafrost regions where climate is changing and impacting local ecology (McBean, 2007). Current literature focuses on the short-term predictions or observed impacts of thaw and climate change without trying to describe the future state of the system. For example Tarnocai (2009) predicts that 87% of perennially frozen and 44% of unfrozen Canadian peatlands will be severely affected by climate change, but does not explain the future state or rate of change of these hydrologic and ecological systems, which will be determined in large part by the changes in hydrology and the water and energy balance.

A small number of field research campaigns have investigated discontinuous permafrost responses to changing climate, and those that do point to a lack of understanding of thaw processes and the interactions between system elements, especially in peatlands (Hayashi, 2013). Current model predictions of future ecosystem states are contradictory; for example, Swindles *et al.* (2015); Chasmer *et al.* (2011) predict an arctic fen as the final successional stage of thawing permafrost peatlands, while Woo (2012); Wright *et al.* (2008) predict that thaw will cause increased evaporation and drying of wetland features. This indicates inadequate and sometimes conflicted understanding of the process of permafrost degradation, and a need for field research to document thaw mechanisms, drivers and processes. Improved conceptual models developed from this additional data need to be tested within a modelling framework to predict long-term change, which can inform future mitigation or adaptation efforts.

This thesis will examine the role of taliks in the evolution of permafrost basins. In the discontinuous permafrost region, taliks (perennially thawed ground in permafrost regions) are well-documented under water bodies such as lakes, fens and streams (Rowland *et al.*, 2011; Yoshikawa & Hinzman, 2003; Connon *et al.*, 2015; Woo, 2012). In contrast, the occurrence of isolated taliks, or taliks sandwiched between the active layer (the region of soil that freezes and thaws annually) and permafrost table is largely undocumented in the literature, though they are likely widespread (Connon *et al.*, 2018). Investigation of talik formation and evolution may lead to a better understanding of wetland evolution in the region. Understanding this process may enhance the numerical descriptions of thaw, resulting in increased confidence in the modelled future system states.

The quantification and understanding of thaw processes at the local and mesoscale is an important step in being able to predict landscape evolution and future system states in the discontinuous permafrost region. While thaw development through talik formation is poorly understood, the numerical representation of thaw is also lacking. Current freeze-thaw models fall into two fairly distinct categories. Firstly, there are continuum physical models which are based on the governing equations of freeze-thaw (Goodrich, 1978). These

models solve coupled differential equations governing heat and moisture transfer numerically, and are computationally demanding, for example McKenzie *et al.* (2007); Frampton *et al.* (2013); Daanen *et al.* (2008); Karra *et al.* (2014); McGuire *et al.* (2016) and others. The second category is empirically based models, which are much less computationally demanding. These models are based on measurements and observed trends in behaviour (Cherkauer & Lettenmaier, 1999). The empirical relationships used in these models are generally not physically-based, and assume temporal stationarity and spatial transferability, such as those presented by Hinzman *et al.* (1998); Krogh *et al.* (2017); Semenova *et al.* (2013); Woo *et al.* (2004) and others. This limits their applicability under changing climate, landscape evolution, and in ungauged basins.

The scale of current freeze-thaw models is also disparate. Physical models act at a local scale, predicting future states of hillslope systems (on the order of metres to tens of metres, e.g., Cherkauer & Lettenmaier (1999); Frampton *et al.* (2011)). Empirical models tend to represent much larger systems, with significantly less detail, and do not capture landscape heterogeneity e.g. Slater *et al.* (1998); Nicolsky *et al.* (2007). Neither type of model scales with landscape size, especially in the discontinuous permafrost region where diverse land-cover regions coexist. A computationally efficient model which can appropriately treat physical processes at a coarser scale is needed in this region to more accurately predict thaw impacts on the landscape, infrastructure, water resources, and the environment.

1.1 Thesis Objectives

The goal of this thesis is to improve our ability to quantify, explain, simulate and predict hydrologic changes due to permafrost thaw in the peatland-dominated discontinuous permafrost region of the Northwest Territories (NWT). Two key questions drive this research.

First, how do small, confined taliks (unfrozen areas sandwiched between the active layer and permafrost table) form and evolve? What is their role in the degradation of permafrost and changing shape of peatlands? The formation of taliks will be studied in the field through the measurement of frost table evolution in conjunction with soil moisture, ground cover and radiation in regions affected and unaffected by advection-driven thaw. This will be combined with modelling work to test hypotheses developed in the field, and to provide a tool to predict future permafrost states and their hydrological impact.

Second, can we fill the existing gap in modelling work that calls for a numerically efficient and physically-based numerical model of freeze-thaw? This model should take our current and new-found process understanding to construct a predictive tool for subsurface

thermal conditions in permafrost environments. This unique model should be applicable to general cold regions hydrological and geophysical models, not only to this investigation.

The specific thesis objectives are to:

1. Identify and quantify controls on local talik formation in the Taiga Plains discontinuous permafrost zone using a mixed field and modelling approach. [Chapters 4,7]
2. Determine and compare the hydrologic function of taliks adjacent to bogs and fens by analyzing seasonal pressure and temperature gradients to understand the evolution and thaw mechanisms in the discontinuous permafrost peatland system. [Chapters 5, 7]
3. Develop, validate and test a physically-based interface model of active layer evolution. Validation will be performed against both field data and a benchmarked numerical model. [Chapter 6]
4. Distinguish thaw mechanisms in the discontinuous permafrost peatlands environment and use a combination of modelling and data collected in the field to determine which processes lead to the spatially variable thaw observed at the Scotty Creek Research Station (SCRS). [Chapter 7]

The following chapters initially review the literature related to the hydrology of discontinuous permafrost peatlands, and hydrological modelling of cold regions. This background material is followed by the methods and results for each research objective, and finally a conclusion and summary of contributions to the field of permafrost hydrology. The contents of chapters 4, 5, and 7 are tied to 3 published manuscripts, as described at the start of these chapters.

Chapter 2

Literature Review

For both the modelling and fieldwork objectives, an understanding of peatlands, permafrost and the cold-regions peatland hydrological system is needed. Because the discontinuous peatland permafrost system is currently changing so rapidly, the field observations collected in this study will likely report thawing trends as opposed to an equilibrium system state. Background information on permafrost peatlands systems is reported here in a manner that highlights these changes, and considers potential trends in behaviour due to thaw processes.

First, peatlands and their interaction with different permafrost regimes are discussed in the context of a changing climate. Then the water balance of a cold-region peatland is presented, with a focus on the role degrading permafrost plays in the system. Once a thorough background of the permafrost-peatlands system is presented, work on modelling similar systems is reviewed, and gaps in process understanding and model representation are highlighted.

2.1 Peatlands

Peatlands are characterized by incomplete cycling of matter, resulting in a net positive carbon balance. They are generally poorly drained areas suitable for wetland vegetation capable of surviving the anaerobic environments favourable to peat formation. A landscape may be classified as a peatland once the peat accumulation exceeds 40 cm according to Canada Soil Survey Committee (1978). Peatlands through which water flows continuously are referred to as fens, whereas bogs are ombrotrophic meaning that they rely on the

atmosphere for nutrients and water. Non-vascular sphagnum moss is one of the few species that can survive the nutrient-poor conditions in a bog, and excludes other plant competitors by acidifying the water through ion exchange (Clymo, 2012; Smith, 1985).

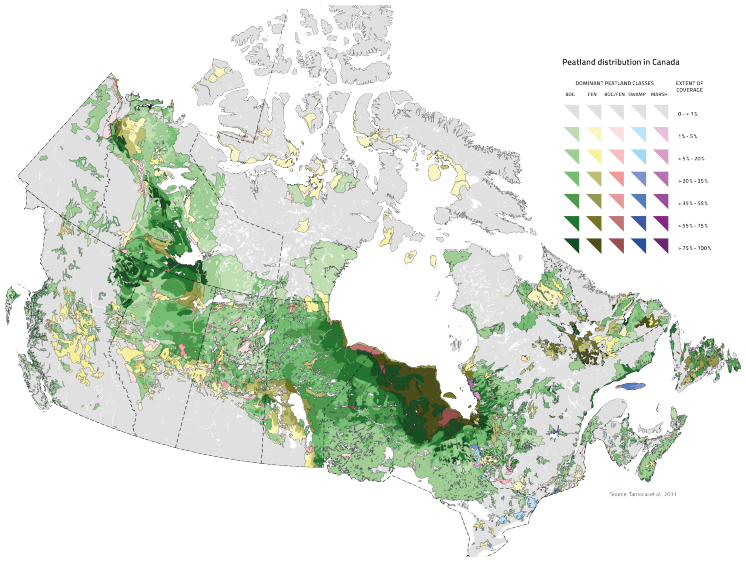

Figure 2.1: Extent of Canadian peatlands. From Tarnocai *et al.* (2011).

Many factors govern the development of peatlands, but a water table near the ground surface leading to waterlogged and anoxic conditions as well as nutrient-poor conditions due to isolation from the regional water table are clear drivers of peat accumulation. These conditions are driven by both the climate, which determines the water and energy balance and hence the water table position, and the geology of the region (Gillespie *et al.*, 2014). Peatlands develop in topographically flat areas with some form of hydraulically confining layer at depth preventing water drainage (Gillespie *et al.*, 2014). Topographic and climatic conditions lead to the geographic distribution of peatlands (figure 2.1), in which peatlands are preferentially found in northern regions in which the precipitation exceeds evapotranspiration and where permafrost acts as the hydraulic confining layer. Peatlands can also be found in silt and clay deposits with low hydraulic conductivity (Woo, 2012). Arctic and sub-arctic peatlands are consistently found in conjunction with permafrost because they co-evolved (Warner, 2016). The permafrost in northern Canada is in large part a remnant from the Little Ice Age, in which the climate was favourable not only for the formation of permafrost, but also for the deposition of peat (Smith, 2011). As peat deposits accumulated, permafrost thickened in these regions, reducing the hydraulic

conductivity and the drainage of the peatlands, thus allowing for the accumulation of additional peat (Warner, 2016). This positive feedback cycle continued while the climate was favourable to the formation of permafrost. Today 37% of Canadian peatlands remain underlain by permafrost (Tarnocai, 2009).

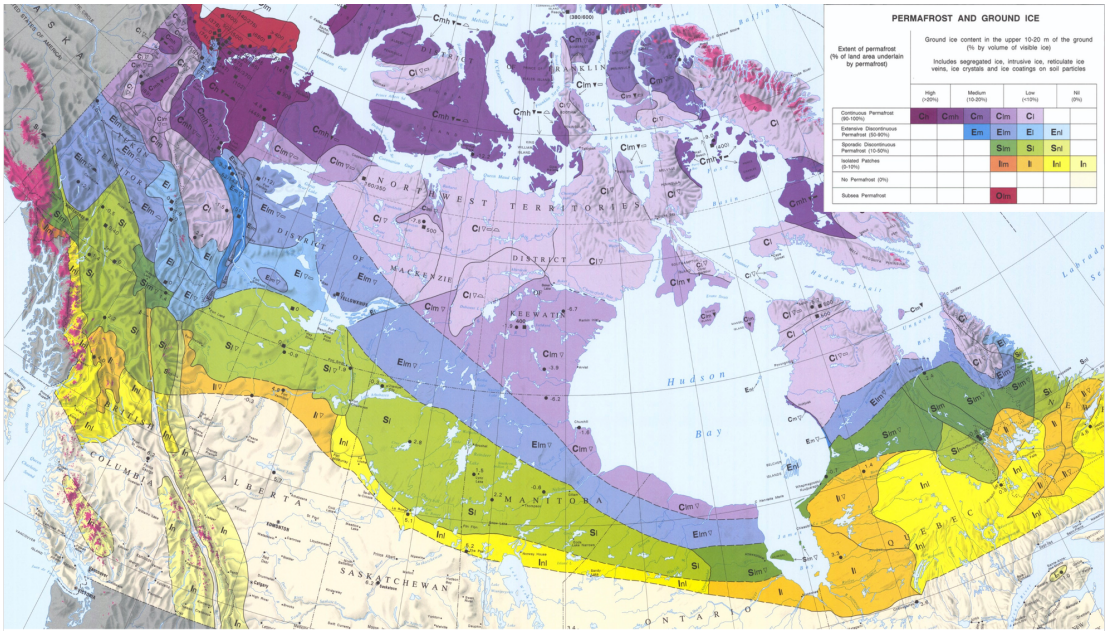

Figure 2.2: Extent of Canadian permafrost. From Natural Resources Canada (1995). Note that continuous permafrost is indicated in purple, while discontinuous to sporadic permafrost is indicated in blue to yellow.

2.2 Permafrost in Peatlands

The permafrost distribution in Canada aligns well with the northern extent of peatlands in topographically flat areas (figure 2.2). Permafrost in peatlands tends to have high ice content because the water table is near the ground surface, and peat has a porosity of 0.7 to 0.9 which is significantly greater than most soils (Boelter, 1966). The hydraulic conductivity, thermal conductivity and heat capacity of peat are highly dependent on the water and ice content of the soil because of the large pore volume of peat soils.

When peat is dry or frozen, a large volume fraction of the soil is occupied by air or ice, respectively. In these cases, few pores are hydraulically connected, and the cross-sectional

area accommodating flow is reduced, resulting in low hydraulic conductivity. Hydraulic conductivity increases rapidly with soil liquid water content as more pore spaces become connected and contribute to flow (Gharedaghloo *et al.*, 2020; Kurylyk & Watanabe, 2013; Côté & Konrad, 2005). Though recent publications indicate that freezing and drying have the same effect on hydraulic conductivity (e.g. Gharedaghloo *et al.* (2020), many studies suggest freezing generally results in lower hydraulic conductivities than drying (for the same medium and moisture content) because changes in pressure result in moisture migration to the freezing front, and greater local impedance to flow (Kurylyk & Watanabe, 2013). This impedance due to the presence of ice can be represented in several ways, but in this work it is taken from Côté & Konrad (2005):

$$K_f = K_u \cdot 10^{-10\theta_i} \tag{2.1}$$

where θ_i is the volumetric ice fraction of the pore water, K_f is the hydraulic conductivity of the frozen (or partially frozen) soil, and K_u is the hydraulic conductivity of the unsaturated soil. Moisture migration is governed by the unsaturated Richards' equation (presented in section 2.6.2), modified by the pressure gradients induced by the presence of freezing soils, which can be obtained from the Clausius-Clapeyron equation. The term accounting for cryosuction was derived using an approach outlined in Edlefsen *et al.* (1943), in which it is assumed that the liquid and solid phases of water must be in equilibrium while they coexist at the same temperature. This leads to a computation considering the change in free energy, f of each phase which is dependent on the pressure ψ and temperature, T (in degrees Kelvin):

$$df_l = \left(\frac{\partial f_l}{\partial \psi}\right)_T \partial\psi + \left(\frac{\partial f_l}{\partial T}\right)_\psi \partial T$$
$$df_i = \left(\frac{\partial f_i}{\partial \psi}\right)_T \partial\psi + \left(\frac{\partial f_i}{\partial T}\right)_\psi \partial T$$

into which is substituted the definition of specific volume v (or $1/\rho$ and entropy s: $\left(\frac{\partial f}{\partial \psi}\right)_T = v$ and $\left(\frac{\partial f}{\partial T}\right)_\psi = -s$, substituting this into the above relation, along with the definition of entropy generation for heat transfer, $\Delta s = \Delta h/T$:

$$\frac{\partial \psi}{\partial T} = \frac{s_i - s_l}{v_i - v_l} = \frac{L\Delta\rho}{T} \tag{2.2}$$

where ρ_l and ρ_i [kg/m^3] are the densities of water and ice, respectively, P_{lf} and P_i [J/m^3] are the soil pressure in the freezing and frozen phase, H_f [J/kg] is the latent heat of fusion, and T is the temperature [°C] (Kurylyk & Watanabe, 2013). It is unclear how this relationship changes when the assumption that phase change happens at a sharp boundary is lifted, and a slushy region is allowed to exist (Amiri *et al.*, 2018). Rather, the relationship is implicitly handled in the soil freezing curve often used to represent the ice content - temperature relationships in soils.

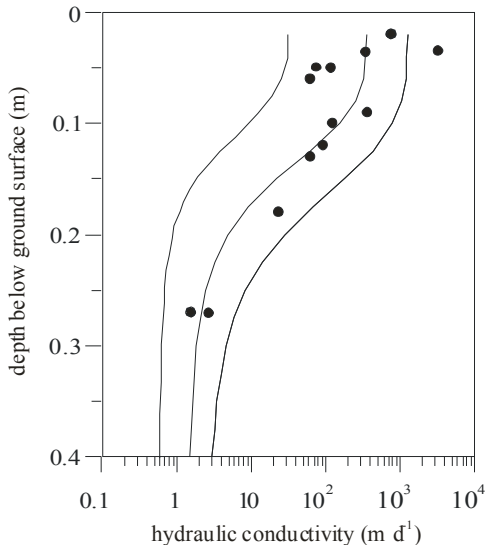

Figure 2.3: Hydraulic conductivity of peat with depth. Points represent field data collected in the southern Northwest Territories, and lines indicate the best-fit profile and upper and lower bounds. From Quinton *et al.* (2008).

The hydraulic conductivity is dependent not only on the cross-sectional area available for flow, but also the pore structure of peat. Near-surface peat tends to be more fibric and have more connected pores than more decomposed peat at depth, leading to increased saturated hydraulic conductivity near the surface (figure 2.3) (Boelter, 1966; Quinton *et al.*, 2008). All other things being equal, the thermal conductivity of peat is less dependent on the pore structure than the hydraulic conductivity. The thermal conductivity is dependent on the air, water and ice content of the pore matrix because the thermal conductivities of air (0.02 W/mK), water (0.58 W/mK) and ice (2.18 W/mK) differ significantly. This difference in thermal conductivities makes peat ideal for permafrost development, because the high hydraulic conductivity and low water retention surface layer drains and dries quickly, allowing it to act as an insulator (Shur & Jorgenson, 2007). Dry peat has very low thermal conductivity, effectively insulating the underlying soil from warm atmospheric temperatures, slowing the seasonal thaw of ground ice. The thermal properties of peat play an important role in determining the state of the permafrost in northern peatlands.

Peatland permafrost regimes can be separated into three classes based on their dependence on climate, ecosystem, and substrate. The first is climate-driven, ecosystem modified (continuous) permafrost, found in the far north (Shur & Jorgenson, 2007). In this regime,

the mean annual temperature is less than -2°C, and the active layer, or uppermost soil layer that freezes and thaws annually, is determined by the maximum thaw depth because all of the soil that thaws will refreeze overwinter.

The second permafrost regime, found further south, is ecosystem-driven (predominantly continuous) permafrost. This is permafrost that exists in regions where the mean annual temperature is near zero, but because of the enhanced ground heat loss during the winter and the relatively small summer heat gain, the peatland system is conducive to the formation and preservation of new permafrost (Shur & Jorgenson, 2007; Jorgenson *et al.*, 2010). Taliks are often found in these regions, in areas that are insufficiently protected by peat accumulation, or in depressions that remain wet through the summer (figure 2.4). Ecosystem-driven permafrost is somewhat susceptible to disturbance, which can impact the energy balance, such as forest fires, peat harvesting, or deforestation. Peatland systems may recover from disturbances if they regain tree-cover, accumulate peat, and the mean annual temperature remains near zero.

The last, and least stable, permafrost regime in northern peatlands is ecosystem-protected (discontinuous) permafrost. The mean annual temperature in these regions is generally well above zero (roughly +2°C), and the areas are unfavourable to the formation of new permafrost (Shur & Jorgenson, 2007; Bonnaventure & Lamoureux, 2013; Quinton *et al.*, 2018). Permafrost in this regime is a remnant from colder climate periods, and would thaw if it were not protected (insulated) by peat deposits. Regions underlain by permafrost are often topographically elevated above the prevalent permafrost-free areas which have subsided as ground ice thawed (Connon *et al.*, 2018). This regime is very sensitive to change, and when exposed to forest fire, deforestation or other disturbance, the permafrost thaws readily (Baltzer *et al.*, 2014). There is no driving mechanism to re-establish the permafrost because it is in disequilibrium with the climate, and permafrost in this regime is changing fastest.

2.3 Arctic Climate Change

Global temperature increases are amplified in the arctic, pushing more and more permafrost regions into disequilibrium with climate (McBean, 2007). Not only is permafrost jeopardized by increases in temperature, but the projected changes in precipitation are also detrimental to permafrost. Cold regions are often referred to as arctic deserts due to their aridity (Woo, 2012). However, it is projected that precipitation in cold regions will increase in the next decades, especially in the winter season (McBean, 2007). This is the worst-case scenario for permafrost, because increases in winter precipitation will result in

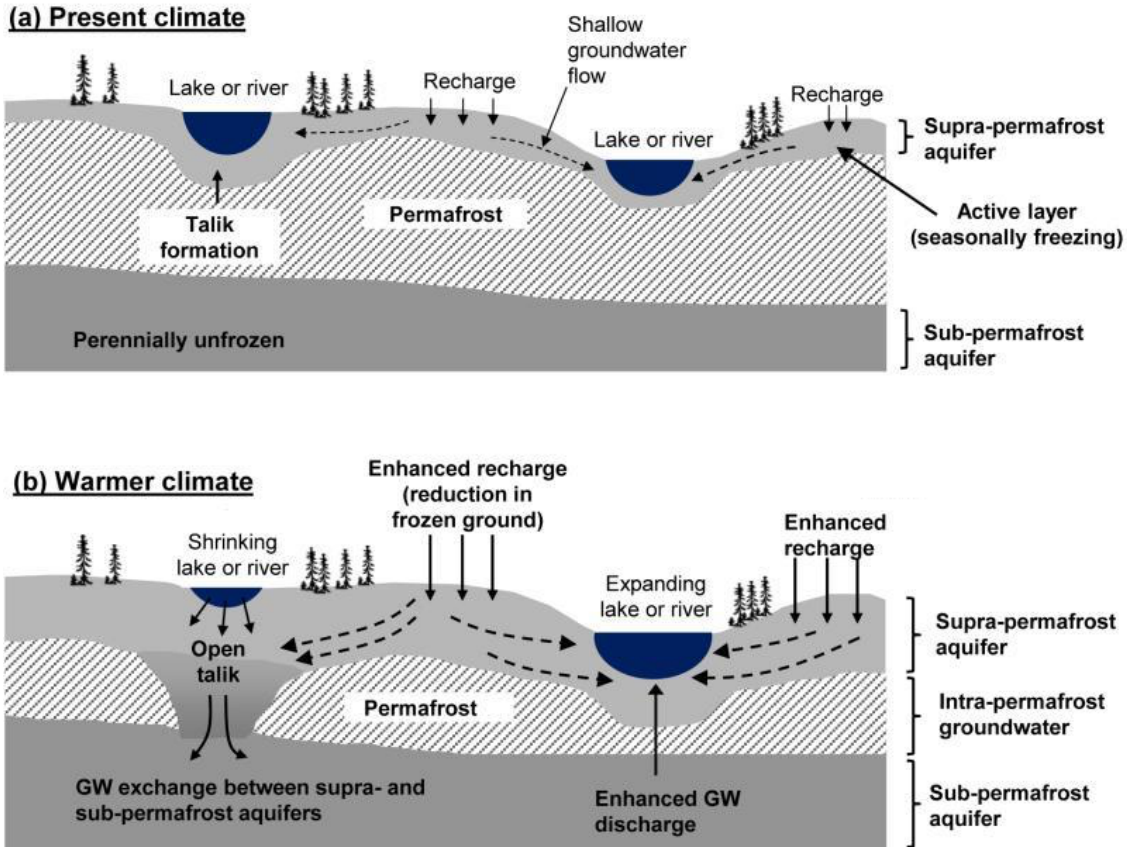

Figure 2.4: Anticipated changes to permafrost regimes under climate warming. Key features of the permafrost landscape are also shown, such as open and confined (in formation) taliks. From Walvoord & Kurylyk (2016).

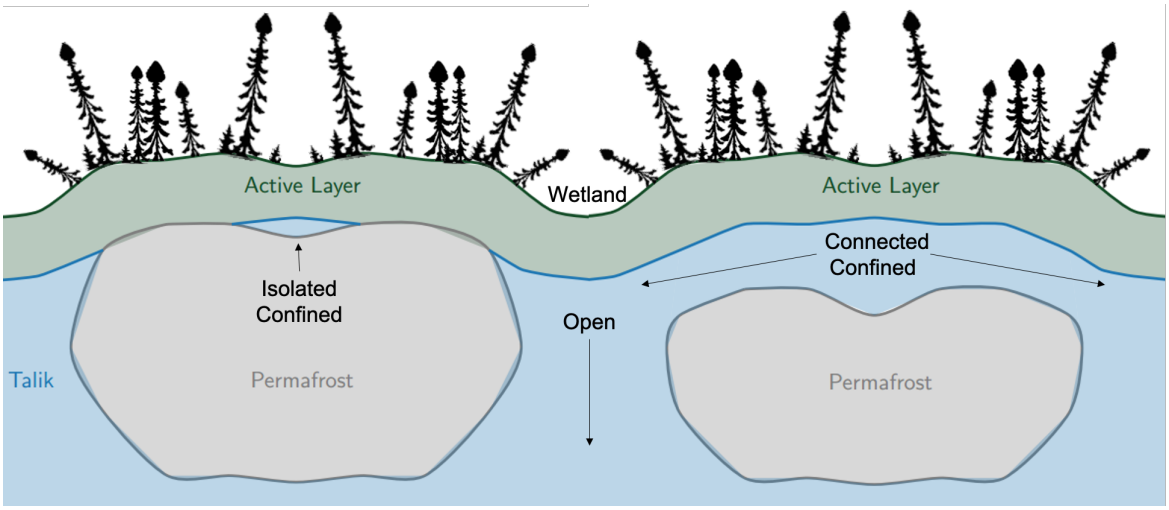

Figure 2.5: Soil profile showing different taliks found in discontinuous permafrost environment.

thicker snow cover earlier in the season (McBean, 2007). Snow, just like dry peat, is an excellent insulator and prevents the soils from losing energy to the cold atmosphere. Under these conditions, the active layer is less likely to refreeze completely, consequently forming a confined talik sandwiched between the active layer and the permafrost table, which can be seen in figure 2.5. Increased summer precipitation will lead to increased soil moisture resulting in higher thermal conductivity, and deepening taliks. As seen in figure 2.5, the deepening of taliks may form a connected confined taliks which allows flow between wetlands over the top of the permafrost table. Once this type of talik is developed, permafrost loss accelerates due to the energy carried with the water flowing through the soil column (see Chapter 7). Taliks isolate the permafrost from the atmosphere during the winter, but reconnect it during the summer, meaning that when a talik exists, the permafrost can only gain energy. The formation of a talik is a tipping point after which the permafrost in an area will degrade and eventually disappear (Connon *et al.*, 2018; Devoie *et al.*, 2019).

Ground thaw in permafrost regions has been found to increase the rate of decomposition in peatlands, releasing increased amounts of methane and carbon dioxide to the atmosphere (Kimmel & Mander, 2010). This process creates a positive feedback loop between thaw and climate warming, compounding the rate and effects of global warming on cold regions.

2.4 Water Balance

Permafrost thaw not only impacts the climate, but also has more immediate and observable effects on the hydrology of peatlands, which can be best observed through the terms of the regional water balance. At any given time, most of the liquid water in the peatlands system can be found in liquid water storage, S [mm], because peat is highly porous and accumulates preferentially in regions where the water table is near the ground surface. The typical water balance in subarctic and arctic peatlands is given by:

$$\frac{dS}{dt} = P - ET - Q - R + SM + IM \tag{2.3}$$

The low relief of peatland landscapes favours stagnation and ponded water, meaning that runoff from rain, R [mm/d], and discharge, Q [mm/d], are a smaller fraction of the water balance than precipitation inputs, P [mm/d], and losses to evapotranspiration, ET [mm/d] (Price & Maloney, 1994; Whitfield *et al.*, 2009). The snowmelt term, SM [mm/d], describes water input from the spring freshet. The freshet can account for more than 70% of the annual water inputs in the arctic and subarctic (Wright *et al.*, 2008). The contribution from ground thaw, IM [mm/d], accounts for water that was held in the soil pores as ice, but melts and becomes available to the system. It is positive if thaw occurs, but negative when ground ice forms.

2.4.1 Storage

In peatlands, the annual change in water storage in the system is generally a small fraction of the total water stored, which has a long residence time in the system (Morris & Waddington, 2011). This storage is transient, such as water accumulation in the annual snowpack, or as soil moisture in the near-surface active layer affected by precipitation and evapotranspiration. However in arctic and sub-arctic systems the bulk of water storage is long-term, persisting inter-annually. Permafrost, which persists for millennia, is an example of long-term storage. Other examples of long-term storage include deep, sub-permafrost aquifers in which water is conveyed very slowly, or the peatlands themselves, that cycle and release water slowly (Morris & Waddington, 2011).

In the discontinuous permafrost region, transient storage in the snowpack dominates the annual hydrograph. The storage capacity of the supra-permafrost layer (combination of active layer and perennially thawed ground overlaying permafrost) is limited because of the shallow soils, and changes throughout the season as thaw occurs (Bonnaventure &

Lamoureux, 2013). The active layer often does not extend all the way from the ground surface to the permafrost table, leaving a confined talik with the capacity to store and transmit liquid water year round sandwiched between the permafrost table and the active layer (Woo, 2012). Confined taliks can form a shallow groundwater flow network, allowing water stored in lakes, fens and connected bogs to move downstream when it would otherwise be confined by ground ice (Bense *et al.*, 2009; Connon *et al.*, 2018). If these taliks penetrate the permafrost in some locations, flow 'windows' open, connecting the shallow groundwater regime with the deep groundwater and allowing for recharge or discharge at the regional scale. This is called an open talik (figure 2.4 (b)). The connection to the deep groundwater system transforms the shallow groundwater flow network from a local, rapid response to precipitation or melt events to a more regional system with slower response to climate forcing (Bense *et al.*, 2009).

2.4.2 Losses

Evapotranspiration (ET) represents the largest water loss in peatland systems because the water table is close to the topographically flat ground surface, and ponded water is abundant (Wright *et al.*, 2008). In the discontinuous permafrost region, ET is limited by incoming solar radiation, mean annual air temperatures, and the dominance of non-vascular vegetation (Wright *et al.*, 2008; Tarnocai, 2009; Swindles *et al.*, 2015; Woo, 2012). Vascular plants, though small in number, can account for up to 80% of the ET losses (Woo, 2012; Whitfield *et al.*, 2009). However, the coniferous canopy that exists in sub-arctic and arctic peatlands does not transpire significantly, and the understory is dominated by non-vascular mosses and lichens which lack the ability to move deeper water stores to the atmosphere (Clymo, 1984). Ponded open water is prevalent because of irregularities in the permafrost which form impermeable depressions, leading to significant open water evaporation (Wright *et al.*, 2008; Shook *et al.*, 2013).

Discontinuous permafrost peatlands do not exhibit typical variable source area behaviour in which increasing water table is linearly related to increasing runoff (Hewlett & Hibbert, 1967; McDonnell, 2003; Woo, 2012). Limits to infiltration and storage caused by ground ice trigger threshold behaviours which are non-linear and hysteretic (McDonnell, 2003; Connon *et al.*, 2015). Spatial differences in frost table elevation define lateral boundaries that act as flow thresholds resulting in abrupt changes in runoff when they are overtopped (Woo, 2012). Permafrost peatlands exhibit fill-and-spill behaviour similar to that described by Tromp-Van Meerveld & McDonnell (2006) on bedrock slopes. Due to the relatively flat topography and lack of hydraulic gradients, fill-and-merge behaviour is also likely to occur when two adjacent wetlands merge before becoming hydrologically

connected with the outlet (Leibowitz *et al.*, 2016). The order in which storage features become connected, and their contributing area, depend on antecedent moisture conditions, pre-existing connections in the landscape, and the local distribution of rainfall (Shook *et al.*, 2013; Connon *et al.*, 2015). Shook *et al.* (2013) showed that flattening the topography increases these hysteretic effects.

Overland flow is prevalent early in the thaw season when the frost table is near the ground surface, leading to local and intermediate flow systems dominated by lateral flows in or over the shallow thawed organic layer (Devito *et al.*, 2005). Discharge shifts to the subsurface as the season progresses and flow paths thaw and deepen. In areas where taliks connect adjacent storage features, there can be simultaneous quick-flow along the top of the frost table and subsurface flow through a talik. An example of the different flow regimes and resulting rating curve can be seen in figure 2.6, though numbers will differ based on particular site characteristics, and have been discussed by Bense *et al.* (2009).

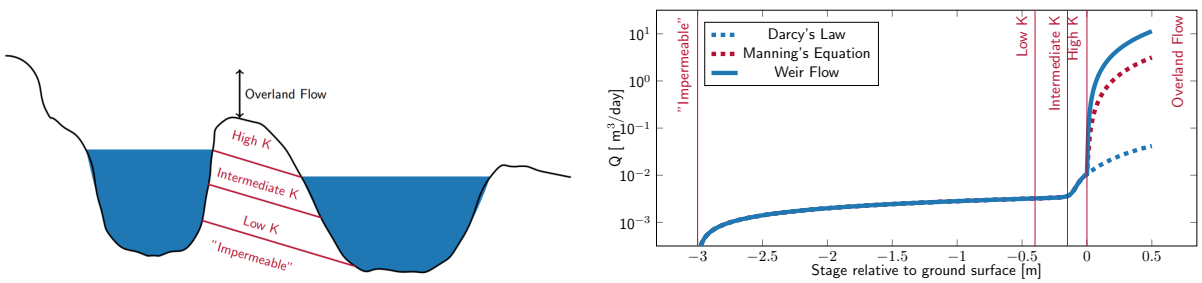

Figure 2.6: Flow regimes and rating curve for flow between two storage features in discontinuous permafrost zone. Subsurface flow rates are depth dependent, and overland flow in this system is rare after the spring freshet.

Subsurface drainage of peatlands is dependent on the underlying substrate, which is given by the topography of the frost table mentioned above (Devito *et al.*, 1997; Wright *et al.*, 2008). Quick-flow along the top of the permafrost table follows a fill-and-spill mechanism in the discontinuous permafrost region, until flow is intercepted by an open talik (figure 2.4) (Yoshikawa & Hinzman, 2003; Sjöberg *et al.*, 2016; Woo, 2012). Open taliks are often found under lakes or wetlands because of increased thermal conductivity in wet regions, but can also exist in clearings where unimpeded insolation increases seasonal thaw. These features allow for surface and ground water mixing (Woo, 2012; Walvoord & Kurylyk, 2016). Increased ground thaw activates deeper flow paths with lower hydraulic conductivity, slowing the lateral movement of water if the water table drops with the permafrost table. When thaw occurs in natural areas of discharge, it can lead to increases

in stream baseflow, and make ephemeral streams flow year-round (Bense *et al.*, 2009). Open taliks can also alter the landscape, draining thermokarst features (wetlands formed by subsidence resulting from thaw) that were once maintained by permafrost boundaries (Bense *et al.*, 2009; Yoshikawa & Hinzman, 2003). This poses a risk to peatlands that formed as a result of water ponding above impermeable permafrost boundaries that no longer exist, as they are likely to dry, resulting in successional change and altered hydrology (Bense *et al.*, 2009).

2.4.3 Contributions to Runoff

A significant fraction of annual precipitation falls as snow in cold regions, and midwinter melt events are extremely rare because of cold winter temperatures (Woo, 2012). In the discontinuous permafrost regime the freshet is the dominant hydrological event, and can account for more than 70 % of the annual water inputs, leading to floods and overland flow (Woo, 2012; Wright *et al.*, 2008). This water input replenishes many storage features that are otherwise disconnected from the rest of the landscape (Woo, 2012). In contrast to the continuous permafrost regime, where the spring runoff is almost exclusively composed of meltwater, Carey & Quinton (2004) found that a significant fraction of spring runoff is composed of 'old water' thought to have been stored deeper in the supra-permafrost layer in the discontinuous permafrost region. In areas without permafrost or where taliks are present, the water table is less likely to follow the surface topography, and follows the regional flow trends instead, resulting in a higher water table near streams (Carey & Quinton, 2004). The combination of the deeper water table and the presence of perennially thawed flow paths enhances the ability of event (snowmelt) water to infiltrate discontinuous permafrost. However limited storage capacity and the high input during a short freshet results in high runoff.

The contribution of ground ice thaw water to streamflow is small when compared to the freshet and the increases in hydrologic connectivity afforded by thaw (Walvoord & Kurylyk, 2016). In the discontinuous regime ground thaw contributes water to baseflow year-round, not only through the water from seasonal ice thaw and permafrost thaw, but also from the deep groundwater that is made available as holes develop in the permafrost. The increase in connectivity due to ground thaw has been observed to increase baseflow and allow some previously ephemeral streams to flow year-round (St Jacques & Sauchyn, 2009). The formation of deep groundwater flow paths due to permafrost thaw in peatlands is important because unlike temperate peatlands that become disconnected from their watersheds when the water table is low, there is no isolating mechanism for permafrost

peatlands after the permafrost thaws. This can eventually lead to widespread drainage of the landscape.

2.5 Thaw Trends

Table 2.1: Representative water balance terms in the continuous (Roulet & Woo, 1986), discontinuous (Wright *et al.*, 2008), and temperate (Lafleur *et al.*, 2005) regions. Note that the temperate regime has significantly more precipitation than the two permafrost regimes. Dashes indicate missing data, (+) indicates input and (-) is loss, and all values report water in mm.

	Continuous		Discontinuous		Temperate	
	Winter	Summer	Winter	Summer	Winter	Summer
Storage ΔS	101	385	99	-99	400	-400
Precipitation	101	134	215	154	490	416
ET	0	-223	0	-280	-90	-350
Runoff	0	99	–	220	–	–
Subsurface	0	-1	–	–	0	0
Snowmelt	0	146	0	215	200	0
Ice Melt	0	230	1	245	0	0

As can be seen in table 1, the overall trend in hydrologic behaviour as permafrost thaws seems to be decreased storage capacity and increased connectivity, however further data should be collected to add certainty to this trend. This results in an increase in baseflow and a deeper water table, and there is potential for increased ET from the system because the deeper water table allows vascular plants to colonize the area (Smith, 2011). The question remains whether or not northern peatlands that developed in conjunction with permafrost will be able to survive after thaw has occurred, or whether the conditions will be too dry, leading to decomposition, an increased chance of fire (observed in northern peatlands recently by Oledefeldt (2016); Tarnocai (2009)), and eventual land-cover change to Boreal forest. This change could result in the emission of significant carbon and methane stores to the atmosphere, which would form a positive feedback cycle between thaw and climate change, potentially changing cold regions and the earth's climate irreversibly.

The current understanding of permafrost peatland hydrology neglects many local-scale thaw processes. It is documented that the landscape is changing, hydrologic connectivity is increasing, and land surfaces are subsiding, but the actual mechanisms and patterns of

this thaw are poorly understood. Taliks have been observed in the vicinity of lakes and fens, but their formation and expansion is generally undocumented, as is their existence in other locations in the landscape, even though they may play a critical role by: acting as pathways for advective heat transfer, isolating permafrost from the atmosphere and preventing permafrost cooling, increasing the hydrologic connectivity of the landscape, and storing liquid water and nutrients which become available to plants when the active layer thaws. This thesis aims to address the gap in our understanding of thawing peatlands systems through the detailed study of talik formation and function in different regions of the landscape. To better understand and predict changes due to permafrost thaw, conceptual and numerical models must be developed and compared to field observations. Current models have not been able to account for all of the hydrologic processes and their interactions in permafrost peatlands, especially at the regional scale.

2.6 Modelling Permafrost and soil freeze-thaw

Modelling is a useful tool to test hypotheses about system function and project possible future system states. In the discontinuous permafrost environment, the appropriate representation of permafrost and seasonal ground ice thaw is essential. The presence of frozen soil strongly affects not only the hydrology, but also the thermodynamics, soil chemistry and ecology of regions experiencing freezing soils, as outlined in figure 2.7 (Hayashi, 2013). Practically, it is essential to accurately model soil freeze-thaw because it controls many important processes including infiltration, the migration of soil moisture to the surface, winter quiescence of hydrological systems, and the destabilization of soils (especially in the permafrost region). Jutras et al. (2009) point out that with an incomplete representation of soil freezing and thawing processes, it is impossible to model multiple seasons (e.g., a poor representation of snow melt refreeze limits the ability to model the spring freshet). Hydrologic models neglecting soil freezing and thawing can therefore only be run seasonally, and are inappropriate for multi-year predictions, or climate projections. To date, models representing discontinuous permafrost have either been 1-D vertical freeze-thaw models, such as NEST (Zhang *et al.*, 2003), or local models (McClymont *et al.*, 2013).

Though both seasonal ground ice and permafrost are under-represented in current models, seasonal ground ice is more commonly incorporated into hydrological models (Goodrich (1978); Craig *et al.* (2020); Semenova *et al.* (2013); Zhou (2014)). These representations are generally not interchangeable as they are currently implemented, as seasonal ground ice only affects the system for a portion of the year, and primarily impacts infiltration (Slater *et al.*, 1998). Permafrost affects infiltration and redistribution, but also acts as an

aquitard, modifying the storage and routing of water in the system (Wania *et al.*, 2009). The few algorithms available to represent these processes (Slater *et al.* (1998), Wania *et al.* (2009), Oelke *et al.* (2003), Hinzman *et al.* (1998)) are primarily designed for the continuous permafrost region. Continuous permafrost process representation is unsuitable for the discontinuous permafrost system as described in literature (e.g., Wright *et al.* (2009), Quinton *et al.* (2009)), in which permafrost-free areas exist adjacent (spatially and temporally) to regions underlain by permafrost, and to regions in which permafrost is degrading both vertically and laterally, and active layer development is non-uniform. Most permafrost models include only vertical thaw (e.g., Hayashi *et al.* (2007); McClymont *et al.* (2013); Kurylyk *et al.* (2014)), neglecting lateral heat transfer. McClymont *et al.* (2013) have however shown that thaw in the discontinuous permafrost region is dominated by lateral heat transfer. This points to a need for computationally efficient multidimensional freeze-thaw models.

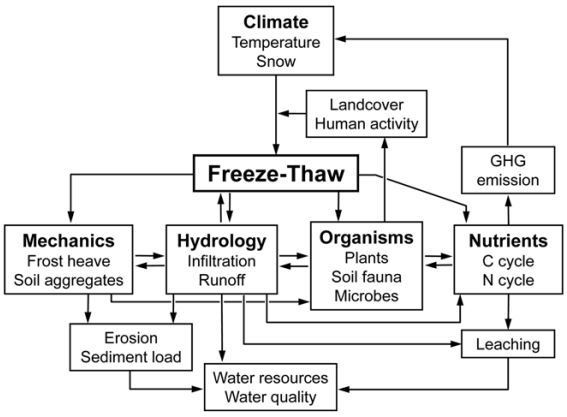

Figure 2.7: Interplay between freeze-thaw, hydrology, and other processes. Arrows indicate the direction of influence, and GHG refers to greenhouse gas. Modified from Hayashi (2013).

The formation of pore ice results in a decrease in hydraulic conductivity, similar to the drying of temperate soils (Lawrence *et al.*, 2008). Models often assume a binary value of hydraulic conductivity (i.e., zero when the soil is frozen) along with a binary freezing function, but this leads to numerical instabilities in a continuum model and is not typically an appropriate physical representation of the system (Lawrence *et al.*, 2008). Three dimensional continuum models, such as SUTRA-ICE, avoid these instabilities through fine discretization, but can only be deployed to simulate these systems at the local hillslope scale, and are not readily applied to larger systems (McKenzie *et al.*, 2007). Continuum models of freeze-thaw, such as those presented by Slater *et al.* (1998), Goodrich (1978), and Hinzman *et al.* (1998), are computationally expensive, and attempts to increase the efficiency of these models represent some processes empirically, neglect latent heat transfer, and invariably make approximations in assigning relatively large model element size rendering them ineffective in the discontinuous permafrost region because of the heterogeneity of the landscape. These

approximations have not been adequately justified through benchmarking and sensitivity analysis, nor are they likely to be effective in the study area.

Entirely empirically-based models of permafrost systems also exist (Oelke *et al.*, 2003). Empirically-based models are generally accurate in the region in which they are developed, and are sufficiently computationally efficient to be applied to large modelling scales (e.g. Hinzman *et al.* (1998); Slater *et al.* (1998)). However, their ability to represent diverse hydrologic response units (HRU) is limited (e.g. Zhou (2014)). Though it is computationally feasible to extend these relationships to represent larger or ungauged areas, the predictions generated are not physically meaningful because the empirical relationships are defined based on measurements in a particular basin, with fixed soil characteristics and hydrological parameters. Therefore, they cannot be reliably extended to regions with differing soil characteristics, vegetation classes, or even channel characteristics, unless these parameters are known, and available to be modified in different regions as in a distributed model (Wania *et al.*, 2009). Even in distributed empirically-based models, the challenge remains that empirical coefficients cannot be derived from data in ungauged basins, and empirical models assume system stationarity, so even if there is basin data, it is insufficient to make predictions of future system states when faced with changes in land-use, climate or any other model parameter(s) (Magnusson *et al.*, 2014). Stationarity is the assumption that historical data is indicative of the system over time, with the implicit assumption that changes in climate or land cover do not occur. This limits the ability of empirically-driven models to make predictions of future system behaviour.

Physically-based models solve the governing equations of heat transfer and moisture migration in the system. These processes are generally described using coupled partial differential equations and an operator splitting approach. Due to the computational demands of solving this coupled system, approximations about the moisture content of the system are often made, commonly assuming a completely saturated soil profile, or a fixed thermal conductivity.

2.6.1 Heat Equation

Heat transport in the porous media is governed by:

$$\left[c\rho + L\frac{dF}{dT}\rho\eta\theta\right]\frac{\partial T}{\partial t} = \left(\frac{\partial}{\partial z}\left(\lambda_b\frac{\partial T}{\partial z}\right) - c_l\rho_l\frac{\partial q_z T}{\partial z}\right) + q_y\rho_w c_w(T_{in} - T) \tag{2.4}$$

in which the parameters c [J kg^{-1}°C], η [-], λ_b [J m^{-1}s^{-1}°C], and q [m s^{-1}] refer to bulk heat capacity, porosity, bulk thermal conductivity and flow rate of liquid water respectively.

The subscripts z [m] and y [m] refer to the vertical and horizontal directions, and T_{in} [° C] is the temperature of water laterally entering the soil column driving advection. Note that water may be supplied laterally to the column via the final q_y term, with the flux given by $q_y = -K(\psi, T)\frac{\partial h}{\partial y}$, where the gradient is fixed for each simulation, and K values reflect the impedance due to ice content. This term is applicable only when the soil column contains a talik connected to a wetland feature. The inclusion of this source term allows the 1-D vertical model to represent lateral water movement in short-term simulations of permafrost evolution. This method is not appropriate for long-term change detection where lateral permafrost thaw is expected.

2.6.2 Unsaturated Richards' Equation

Water movement is governed by the unsaturated Richards' equation (represented in mixed form here, similar to Celia *et al.* (1990)):

$$\left(\frac{\partial \theta_l}{\partial \psi} + S_s\right)\frac{\partial \psi}{\partial t} + \left(\frac{\rho_i}{\rho_l}\theta_i + \theta_l\right)\frac{\partial F(T)}{\partial t} = \frac{\partial}{\partial z}\left(K(\psi, T)\left(\frac{\partial \psi(z, T, \theta)}{\partial z} - 1\right)\right) \tag{2.5}$$

where θ [-] represents water saturation, ψ [m] is soil matric potential, Ss [m^{-1}] is specific storage, t [s] is time, ρ [kg m^{-3}] is density, F [-] is the temperature-dependant ice fraction, T [°C] is temperature, z [m] is vertical distance, and K [m s^{-1}] is hydraulic conductivity. The hydraulic conductivity is given using the van Genuchten model with peat-specific parameters (Van Genuchten, 1980). The hydraulic conductivity is modified by an empirical relationship describing the impedance of ice content to water movement through the partially-saturated soil, as presented by Kurylyk & Watanabe (2013). The subscripts l and i refer to liquid water and ice phases respectively. The less common term $\left(\frac{\rho_i}{\rho_l}\theta_i + \theta_l\right)\frac{\partial F(T)}{\partial t}$ on the LHS is a source/sink term arising from the inclusion of phase change. Vapour flux is not included in this model; Putkonen (1998) deemed it unimportant (especially in wet soils) as compared to the other processes occurring in an unsaturated 1-D freezing or thawing soil column. The main role of vapour flux is to deliver water to the freezing front, which is accomplished instead by the Clausius Clapeyron (CC) relation (Karra *et al.*, 2014). The CC relation is included in equation 2.5 when the temperature is in the freezing range, assumed to be 0 °C to -0.05 °C (equation 2.6). This equation is very similar to the form of the Clausius relationship presented in Kurylyk & Watanabe (2013). The terms g, L and $\Delta\rho^{-1}$ refer to gravity [m s^{-2}], the latent heat of fusion of water [J kg^{-1}] and the change in specific volume associated with the phase change [m^3 kg^{-1}] respectively. Note that ψ yields the combined matric potential and cryosuction as will be discussed further in

chapter 4, while $\psi*$ is the effective matric potential given by the soil characteristic curve at the particular saturation and with an effective porosity reflecting the ice content in the soil as a loss in available porosity.

$$\psi(\theta, T) = \begin{cases} \psi^*(\theta, \eta_{eff}) + \frac{L}{\rho g T \Delta \rho^{-1}} \frac{\partial T}{\partial t} \Delta t & \text{if } T_{res} \leq T \leq 0 \\ \psi^*(\theta, \eta_{eff}) & \text{else} \end{cases} \tag{2.6}$$

$$\eta_{eff} = \eta - \theta_i$$

In the above relation, we note that the cryosuction and matric potential terms are additive, while in literature pressure is attributed to one or the other of these terms Kurylyk & Watanabe (2013). Given the assumptions in the derivation of equation 2.2, we know the free energy of both liquid and solid phases are the same, and given that the energy is continuous, the pressure should also be continuous. This implies that at the initiation of freezing and the residual water content when the CC relation no longer applies, it is expected that the matric potential match the pressure of the mixed phase. Note that the cryosuction term tends to zero at the limits of the freeze thaw range (as the change in density is zero when phase change is not occurring), and thus a sum achieves this goal. Other relations are considered, but there is no justification for an increase in mathematical complexity. Additionally, it is intuitively reasonable to expect that the pressure deficit be greater in freezing dry soils than in freezing soils near saturation. Though literature was consulted, very little was found on this topic, and it ought to be investigated in future studies.

2.6.3 Modelling at Large Scales and in Ungauged Basins

In physically-based models, input parameters describing the soils, vegetation, and other local system characteristics are included to define the physical system. This enables these models to be extended to regions beyond their initial study basin, and to make predictions in ungauged areas, where sufficient land cover and class information exists to drive the models (Goodrich, 1978; Semenova *et al.*, 2013; Craig *et al.*, 2020). Extending the predictive ability of these models to wider areas often requires significant input data, and computational cost. It is often difficult, time consuming or costly to obtain these input data. For this reason, it is desirable to determine the sensitivity of the model to various input parameters, and to propagate the uncertainty in input parameters to uncertainty in modelled output. To accurately characterize uncertainty in parameter values and model

predictions, sensitivity analysis is a useful tool. These analyses, similar to calibration, require multiple model runs, and can be prohibitive for large physically-based models (e.g. Hinzman *et al.* (1998)), though some relatively coarse models of smaller areas employ these techniques to determine the driving processes (e.g. Kuchment *et al.* (2000)).

Current cold region hydrology models generally act at a particular scale, and provide useful predictions for the scale at which they were developed (Lawrence *et al.* (2008), Wania *et al.* (2009), Oelke *et al.* (2003), Slater *et al.* (1998), Goodrich (1978), Frampton *et al.* (2011)). Though separate models are developed at many scales, they lack the ability to simultaneously represent multiple scales. For example, Cherkauer & Lettenmaier (1999) can represent freeze-thaw using a modification of the VIC (Variable Infiltration Capacity) model at the point scale, but is unable to predict streamflow at the scale of the basin as it cannot handle sub-basin heterogeneity or lateral thaw. The problem of scale is well-known and well-documented in hydrology (Bloschl & Sivapalan (1995)), but has not been sufficiently addressed in the representation of soil freezing and thawing. Emergent behaviour at larger modelling scales has been assumed in some cold-region models. For example, Kuchment *et al.* (2000) assume that snow accumulation over a large area can be represented by a log-normal distribution to capture the effects of redistribution in the basin. However the use of emergent behaviour is not widespread, and is often not rigorously tested. Determining and verifying emergent scale behaviours in hydrologic models with field data would be an important and useful contribution to cold-regions hydrology, and may be a byproduct of this work.

Though this discussion has revealed that some work has been completed on the freeze and thaw of peatland soils, a need has been demonstrated to extend this work to physically represent freeze-thaw processes on a regional scale in areas of discontinuous permafrost. Coupling soil pore water state to moisture migration, snow processes and subsurface water movement will identify emergent behaviour, which will be compared to field observations. Significant uncertainty in future system states exists, and leaves room for new process understanding in thawing permafrost systems. The focus of this research will be the efficient hydrological representation of freezing and thawing soils in the discontinuous permafrost region, and then impact of permafrost thaw on hydrology.

Chapter 3

Study Site

Field studies were completed at the Scotty Creek Research Station (SCRS), located approximately 70 km south of Fort Simpson in the Liard River watershed as seen in figure 3.1. This landscape is dominated by discontinuous permafrost peatlands (described in Quinton *et al.* (2018)) . The mean annual air temperature is approximately -3.2 °C, with a mean precipitation of 369 mm as reported by the Environment Canada Climate Normals from 1971 - 2000 for the Fort Simpson weather station (Meteorological Service of Canada, 2012). The climate is described as dry-continental with long winters and short summers. This landscape is nival, and the hydrograph collected at Scotty Creek at Highway 7, of which the SCRS is a headwaters, is clearly dominated by the spring freshet (Water Survey of Canada, 2020). Based on this gauged stream outlet, the Scotty Creek Basin is approximately 140 km^2.

The SCRS was established in 1999, and is ideal for the study of permafrost degradation because it includes permafrost in a variety of stages of degradation including stable permafrost features, features with isolated and connected taliks, and permafrost-free wetland features (Connon *et al.*, 2018). The land cover of the Scotty Creek basin is primarily described as forested uplands with lowland peatlands which are the focus of this study. The peat deposit in the lowlands ranges from 2 m to 8 m in thickness, and overlays clay, silt/clay, and low-permeability glacial till (Quinton *et al.*, 2018). High permeability peat soils drain readily when the water table is below the ground surface, leaving a relatively dry insulating surface peat layer that preserves permafrost underlying peat plateaux (Quinton *et al.*, 2009). Though insulated from high summer temperatures, the permafrost in this discontinuous permafrost site is warm, and a significant portion of it is within the zero curtain (undergoing phase change) as shown in figure 3.2. This figure depicts the upper and lower bound of temperatures measured using deep thermistors installed in two talik

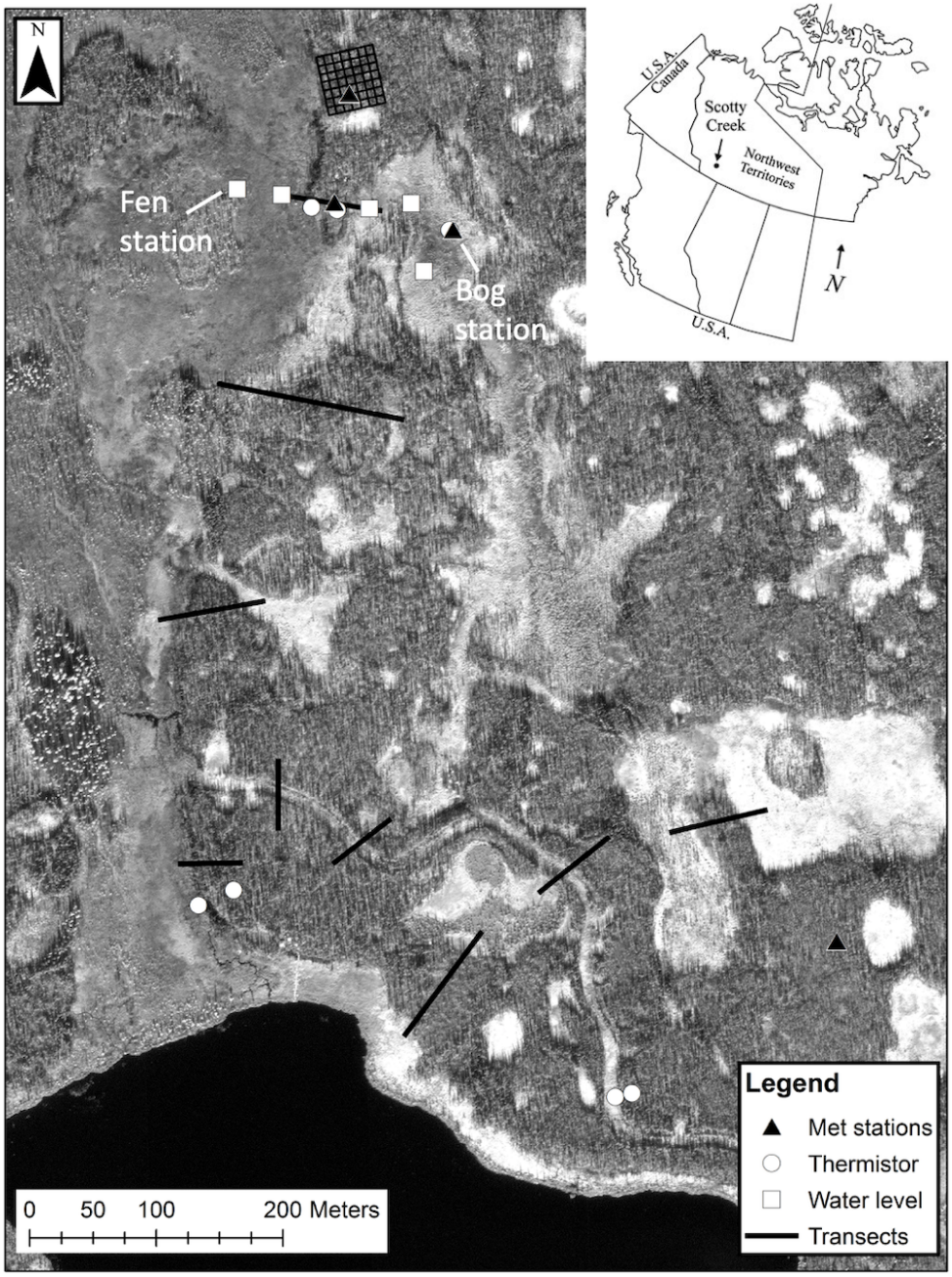

Figure 3.1: Location of field site inset or aerial imagery of study site. Transects and locations of meteorological stations, water level records and thermistors used in this work indicated.

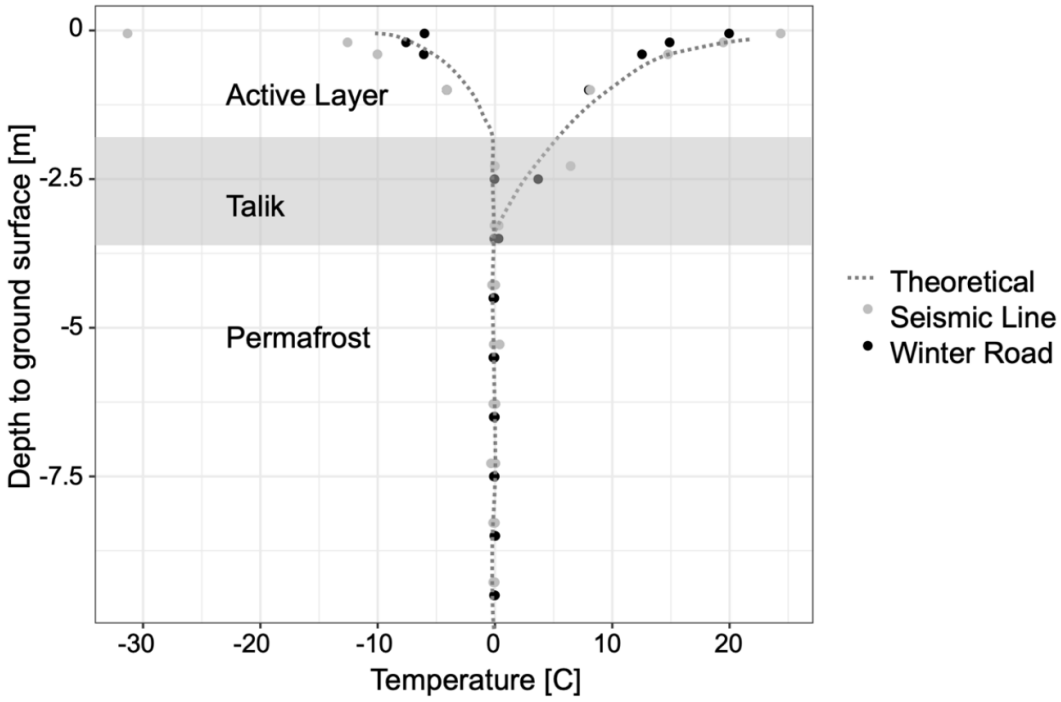

Figure 3.2: Typical subsurface temperature profile at SCRS in a location with a talik. Note that isothermal region at freezing point indicates phase change at depth - this permafrost is likely thawing and contains fractional ice content.

features (along the seismic line and winter road) at the study site. Data is collected from RBR thermistors up to a depth of 9 m.

Within the peatland lowlands, peat plateaux are elevated above the surrounding permafrost-free wetlands due to the subsidence which accompanies permafrost thaw, and the loss of segregated ground ice. Plateaux have a relatively dry vadose zone, allowing them to support a black spruce (*Picaea mariana*) canopy (Quinton *et al.*, 2009). The ground cover is dominated by lichens and mosses, while sparse vascular ground cover persists in some area. These plateaux are surrounded by two wetland types that dominate the landscape. Collapse scar bogs act mainly as water storage features, and are sphagnum-dominated clearings Quinton *et al.* (2009). These features are referred to as bogs in this work, however they do not fit the true ombrotrophic definition of a bog as they may be ephemerally connected to other wetland features either losing or gaining water though narrow channels Connon *et al.* (2015). Channel fens that act as the low-gradient routing feature in this flat, high-storage landscape (Gordon *et al.*, 2016). Fens are sedge-dominated, and contain

hummocky terrain that supports tamarac (*Larix*) stands. These are relatively sparse in comparison to the black spruce on plateaux.The water table is generally found up to 20 cm below the ground surface in the wetland features while it remains between 50 and 70 cm below the ground surface on plateaux. This is also the maximal depth of the active layer observed in this site, where regions with isolated taliks may have deeper permafrost tables and generally collect water Connon *et al.* (2018).

A land cover classification based to a digital elevation model from 2008 categorized the peatland landscape as 39 % treed peat plateaux, 37 % collapse scar bog, and 24 % fen Chasmer *et al.* (2014). This classification can be seen in figure 3.3. Note that there are two types of anthropogenic linear features that can be seen in this figure, which are usually classified as bog (in yellow) unless they are traversing a fen (green). The straight cut lines (the most obvious of these runs SW - NE between the lakes) are seismic exploration lines, while there are also cut lines from a army road (or winter road) established and used in the 70s. The winter road is best picked out along the east side of the small lake in the centre of the map, as well as to the west and between the lakes. These linear features are generally permafrost-free and take on the behaviour of the nearest wetland features.

In this landscape of ephemerally interconnected wetlands, lateral movement of water through the portions of the supra-permafrost layer (usually in areas with a talik) that remain saturated most of the year is common, and may help explain variability in permafrost degradation rates across the landscape (Chasmer *et al.*, 2011). Peat plateaux adjacent to wetland features have been observed to degrade more quickly (both vertically and laterally) than plateaux with isolated taliks (McClymont *et al.*, 2013; Baltzer *et al.*, 2014); it is proposed that lateral advection through the talik plays a considerable role in determining the rate of permafrost degradation. This flow generally happens at depths exceeding 20 cm below ground surface, through peat which is moderately to well-decomposed. This peat has lower hydraulic conductivity (on the order of 0.125 m/day) than the overlaying 15 - 20 cm of undecomposed peat (360 m/day) Quinton *et al.* (2008). The porosity of the living surface peat is near 0.9, while at depth this decreases to about 0.8, though decomposed peat is know to be a dual-porosity material, meaning many of the pores are not connected to a wider flow network and therefore do not fill or drain readily Price *et al.* (2005). The permafrost underlying plateau features is (conceptually) impermeable.

Since its establishment in 1999, many studies have taken place at the SCRS, and a significant data archive has been established. Meteorological stations have been established on each of the land cover types, including measurements of net radiation, temperature, humidity, snow cover, wind velocity and direction, soil moisture and soil temperature profiles as well as ground heat flux. This is augmented by a vast network of pressure transducers recording water levels in wetland features and in depressions on the peat

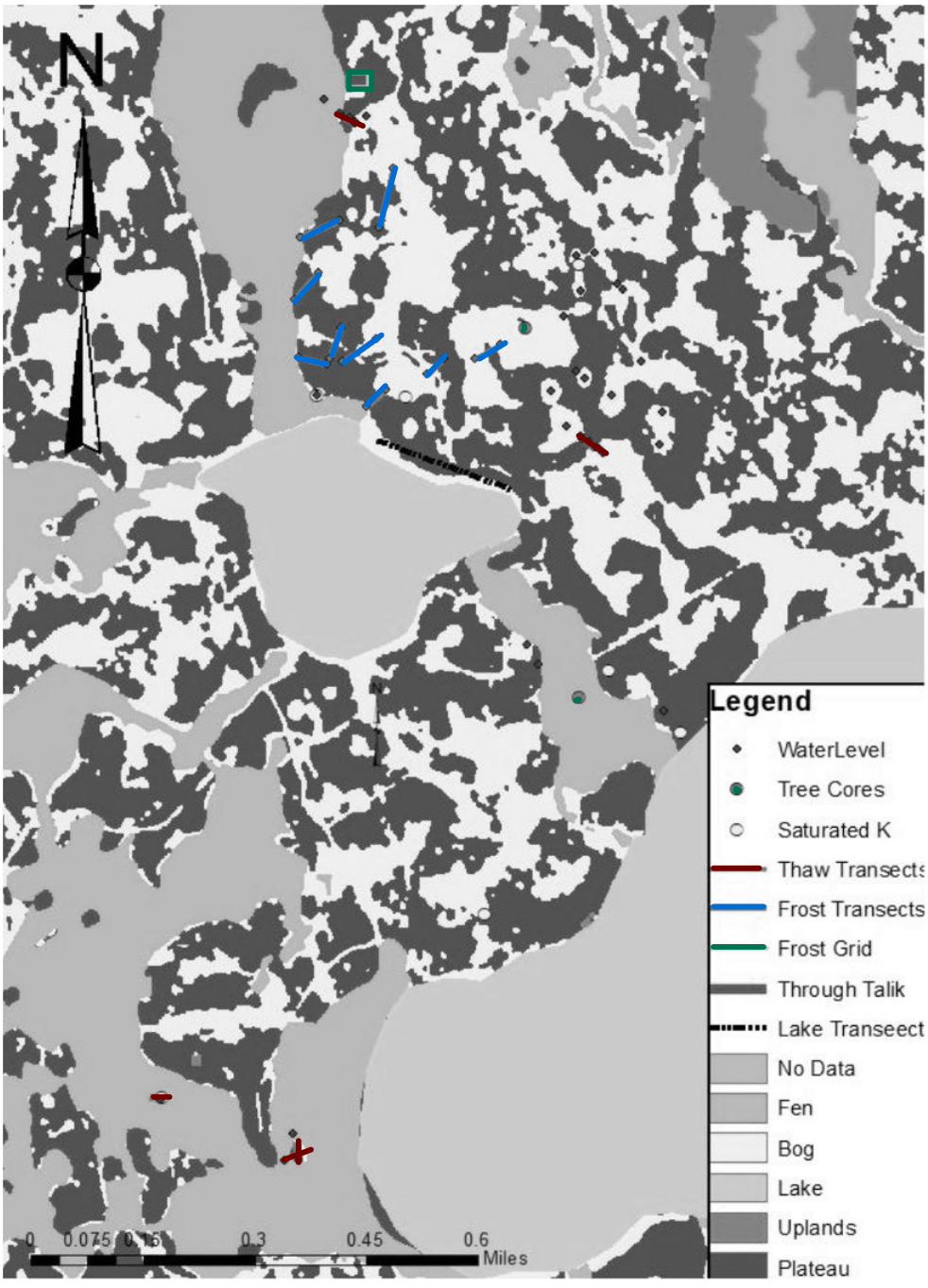

Figure 3.3: Land cover classification of Scotty Creek Research Station with locations of instrumented sites.

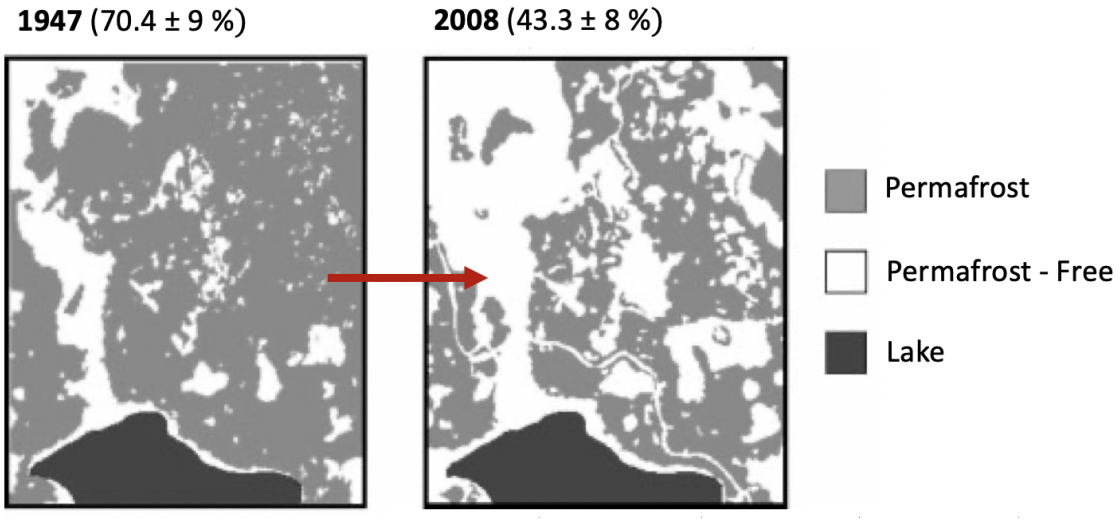

Figure 3.4: Loss of permafrost (grey shaded areas) between 1947 and 2008. Figure modified from Chasmer *et al.* (2014).

plateaux. There are many transects and two grids monitored semi-annually for maximal thaw and refreeze depth. Snow surveys are also conducted annually. Two shielded weighing gauges for precipitation measurement are also located in the study site, one in proximity to each lake feature. The location of measurement points can be seen in figures 3.1 and 3.3. Saturated hydraulic conductivity has also been measured at the yellow markers in figure 3.3. Auxiliary data such as digital elevation models and vegetation surveys are also available for the site. Only a small subset of the data collected was used in this thesis, but all the data collected in support of this work and other studies at the SCRS can be found in the data archive linked in appendix A.

A summary of the evolution of this site over the past two decades of study is presented in Quinton *et al.* (2018), and describes this data in detail, including noting the nonstationarity of each measurement site, as it will be demonstrated that nearly all permafrost in the landscape is at some stage of degradation. A summary of permafrost loss over the past five decades is presented by Chasmer *et al.* (2014), and shows preferential permafrost loss adjacent to existing wetland features (as seen in figure 3.4).

Carpino *et al.* (2020) establish a trajectory of change for this landscape, using a space-for-time approach to outline the phases of permafrost degradation, and the impact of permafrost loss on energy and water balances. In figure 3.5, pane I indicates stable continuous permafrost, but with a change in surface energy flux, often due to an alteration

in canopy dynamics, an isolated talik is formed as seen in pane II. As thaw progresses this thaw feature widens and deepens, potentially thawing through the entire depth of permafrost and becoming a collapse scar bog. Stage IV shows bog capture - the process where a fen or bog adjacent to another wetland feature expands and coalesces with the neighbouring thawed feature. Stages V and VI detail the loss of permafrost generally and the slow drainage of the landscape. Forest establishment (stage VII) may result in the return of permafrost in locations where the climate is favourable for this, while as is noted herein, permafrost is not in equilibrium with the climate at the study site, and permafrost loss is permanent. Though pane I and pane VII appear similar in canopy coverage and carbon storage, the presence of permafrost in the subsurface alters the hydrologic and thermodynamic behaviour of the system notably. This likely has implications on the nutrient cycling in the system, the discharge from the system, and it's response to changes in climate.

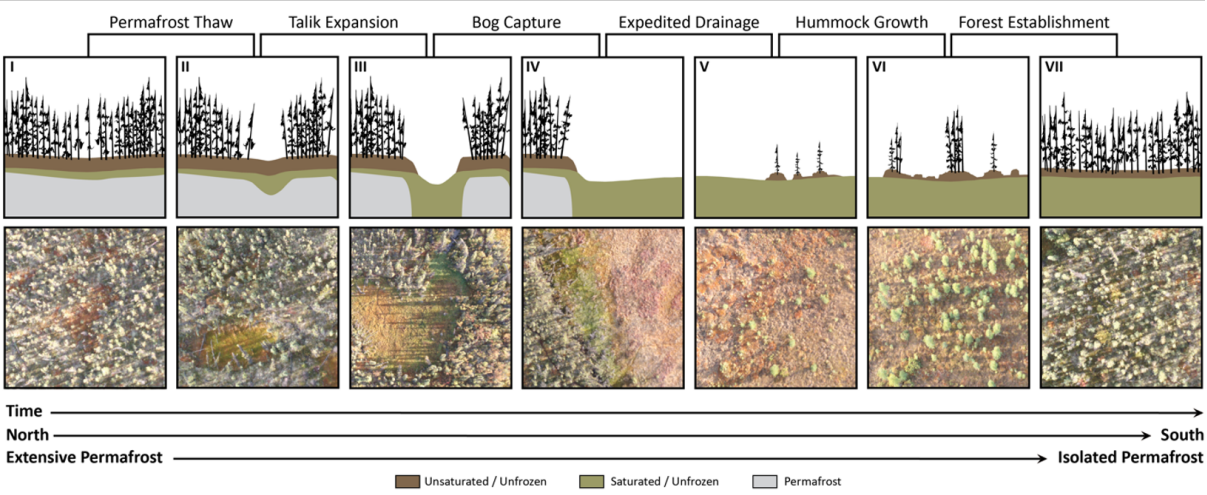

Figure 3.5: Trajectory of change in permafrost environments as presented in Carpino *et al.* (2020).

Chapter 4

Taliks : A tipping point in discontinuous permafrost degradation in peatlands

Statement of contribution

The following chapter is based on the following published manuscript:

Devoie, É. G., Craig, J. R., Connon, R. F., and Quinton, W. L. (2019). Taliks : A tipping point in discontinuous permafrost degradation in peatlands. *Water Resources Research*. DOI: https://doi.org/10.1029/2018WR024488

This paper presents the results of a modelling study in which a 1-D variably saturated freeze-thaw model is applied to soil columns to test the sensitivity of talik development to various conditions. In this paper, I developed the model in Matlab, and collected and aggregated field data from the Scotty Creek Research Station to be used as initial and boundary conditions in the model simulations. I also prepared the manuscript. Dr. Craig provided key insights during model development, benchmarking, and the development of test scenarios. His attention to detail and experience solving PDEs where invaluable in his evaluation of the mathematical formulations and editing the manuscript. Drs. Quinton and Connon provided insight into processes in the field, assisted in design and implementation of field studies and guidance through reviewing the manuscript.

4.1 Introduction

Permafrost regions are very sensitive to changes in climate, especially those classified as discontinuous or sporadic (Stendel & Christensen, 2002; Zhao *et al.*, 2010; Chasmer *et al.*, 2011). Climate warming trends have been shown to cause permafrost degradation and loss, resulting in subsidence, wetland expansion, and landscape transition (Rowland *et al.*, 2010; Walvoord & Kurylyk, 2016; Carpino *et al.*, 2018). One of the mechanisms for permafrost degradation is cited as 'active layer thickening', driven by increases in mean annual air temperature, precipitation, and anthropogenic or natural land cover change or disturbance (Shiklomanov *et al.*, 2012; Bonnaventure & Lamoureux, 2013). This process is indicative of permafrost degradation in continuous permafrost, where the active layer, or layer which freezes and thaws annually, is defined by the late summer maximum depth of thaw (Burn, 1998). However, in areas where permafrost is degrading, especially at the southern limit of permafrost, the active layer can either be determined by the depth of thaw or the late winter refreeze depth if a talik exists between the permafrost table and the active layer (Connon *et al.*, 2018). In the second case, the depth of thaw exceeds the refreeze depth, leaving a perennially thawed region between the base of the active layer and the top of the degrading permafrost body.

Taliks are typically documented beneath or adjacent to water bodies such as wetlands or lakes (Bonnaventure & Lamoureux, 2013; Rowland *et al.*, 2010; Woo, 2012), while the formation and evolution of shallow suprapermafrost taliks hydrologically isolated from wetland features over the winter season (hereafter referred to as isolated taliks) have received relatively little attention. Though briefly mentioned in field literature (e.g., Fisher *et al.* (2016)), the factors controlling the formation of isolated taliks have not been thoroughly investigated in thermal modelling literature. A comprehensive review of current thermal models was completed by (Kurylyk & Watanabe, 2013); talik modelling was not mentioned. This omission is likely due in part to scale, where large scale models do not resolve the relatively local process of talik formation, e.g. Stendel & Christensen (2002).

Freeze-thaw models based on analytic or semi-analytic solutions of the Stefan problem (e.g. Hayashi *et al.* (2007); Hinzman *et al.* (1998); Krogh *et al.* (2017); Semenova *et al.* (2013); Woo *et al.* (2004); Zhang *et al.* (2008b)) are unable to represent the three-tiered system (permafrost-talik-active layer) present in talik formation. These models may be inappropriate for modelling degrading permafrost at the local scale because they assume a linear temperature profile between the soil surface and the (single) freeze/thaw front. Existing continuum models (that do not assume a linear temperature profile; e.g. McKenzie *et al.* (2007); Frampton *et al.* (2013); Daanen *et al.* (2008); Karra *et al.* (2014); Schaefer *et al.* (2009); Jorgenson *et al.* (2010); McGuire *et al.* (2016); Zhang *et al.* (2008b)) have

thus far focused on longer-term lateral permafrost extent, water seepage, carbon storage, permafrost resilience or other processes that do not distinguish controls on isolated talik formation or evolution in peatland environments.

The initiation of an isolated talik has been simulated by Frampton *et al.* (2013); Atchley *et al.* (2016); Yi *et al.* (2014); Endrizzi *et al.* (2014); Rawlins *et al.* (2013); Jafarov *et al.* (2013); Brown *et al.* (2015) and Walvoord *et al.* (2019), where controls on the active layer such as saturation, snow cover, shading, forest fire and ponded water were quantified. These studies shed light on processes governing active layer thickness as defined by maximum thaw depth, but talik formation was not their focus. Nicolsky *et al.* (2017) simulated talik formation by the end of the century in the Alaskan North Slope under RCP 4.5 and 8.5 greenhouse gas scenarios, driven by changes in climate forcing, but moisture, snowpack and incoming radiative effects were not distinguished. Evans & Ge (2017) simulated supra-permafrost layer thickening due only to increased mean annual air temperature in the aim of quantifying the effect of changes in frozen ground regimes on groundwater discharge.

The modelling efforts presented in this paper focus on the formation, evolution and persistence of isolated taliks at the local scale. This work aims to build on existing work in discontinuous permafrost presented by Kurylyk *et al.* (2016) and Langford *et al.* (2020). Kurylyk *et al.* (2016) detail the lateral permafrost thaw and vertical thaw at the bottom boundary of permafrost bodies while Langford *et al.* (2020) simulated a single peat plateau in the research basin. The detailed 3-D modelling work presented in these studies did not address vertical thaw at the top of a permafrost body, or the formation of isolated taliks within permafrost plateaux.

It is proposed here that talik formation plays an important threshold-based (as defined by Grosse *et al.* (2016)) thermodynamic role in the initiation of permafrost degradation at the interior of permafrost bodies in discontinuous permafrost regions, and ultimately the hydrologic evolution of permafrost environments in the peatlands region of the southern Taiga Plains, Canada. The impacts of unsaturated soil conditions, moisture migration due to temperature and pressure gradients, lateral advection, and insulation due to variations in annual snowfall will be considered to explicitly identify drivers for talik formation. The subsequent permafrost degradation rate once a talik is formed is also presented for this ecosystem-protected permafrost environment. The objectives of this study are to (1) use a 1-D model to identify the conditions under which isolated taliks are likely to form, (2) asses the extent and controls on the rate of talik formation, and their consequences for permafrost evolution and (3) evaluate the mechanisms by which talik formation can lead to a 'tipping point' condition at which permafrost recovery becomes unlikely.

4.2 Methods

4.2.1 Field Methods

This study focuses on the application of a 1-D vertical freeze/thaw model informed by boundary conditions and validation data collected at the SCRS to simulate a set of representative soil columns in a discontinuous permafrost environment. Temperature data were measured using Campbell Scientific CS107 or CS109 thermistors or Onset HOBO U12 4-channel thermistors and loggers. These were installed in depth profiles approximately every 5 - 20 cm from a depth of 5 cm to 50 cm, where the observation data used to generate boundary condition were measured at either a depth of 5 cm or 10 cm. Exact measurement depths and spacing varied across the measurement sites.

The permafrost that underlays peat plateaux in the landscape can be classified either as *degrading* or *stable*. The *degrading* boundary condition describes a plateau with an isolated talik that remains perennially thawed. The *stable* boundary condition describes a plateau in which the permafrost is not actively degrading, and there is complete refreeze of the active layer in most if not all years. Figure 4.1(b) shows surface temperature data collected in both conditions from which surface temperature boundary conditions were constructed.

Data to inform the mean and variance of the *stable* temperature boundary condition were collected at five different sites in the area of interest, three of which were located on the same permafrost plateau (Indicated as white circles on figure 1(c)). Sites with moss and lichen ground cover were likewise represented; at least three of the sites developed a talik before the end of the data record. Data up to two years preceding talik development were included in the dataset used to generate boundary conditions for the stable condition. Talik formation was inferred if any one of the thermistors in the vertical profile did not drop below the zero curtain for 5 or more consecutive days. The data after the formation of a talik was combined with temperature data collected along an abandoned winter road (an anthropogenic cut line where permafrost has degraded visible in figure 1(c)) to inform the *degrading* temperature boundary condition (those representing unsteady warming conditions) as observed in figure 4.1(b). Both field data time-series included data gaps due to instrument malfunction, but provided a roughly 10-year data record.

Deep soil temperature data were collected at two sites with degrading permafrost using RBR deep thermistors with one metre spacing from 2 m to 8 m below the ground surface white circles on figure 1(c). The temperature of lateral flow through a connected talik was assigned based on the average daily temperature at 40 cm - 50 cm below the ground surface in wetlands in the landscape. Subsurface temperature data for a bog were only available

for a single sampling location (labelled 'bog station' in figure 1(c)), though these data were consistent over the more than 10 year period of record. Similar data were available for a channel fen (the 'fen station'), though the period of record was only four years, and contained several data gaps. Temperature data collected at three other locations in a fen using HOBO U20 pressure transducers and temperature loggers were consistent with this shorter data series. Lateral advective flow rates (q_y) were estimated based on available hydraulic gradients measured using sets of HOBO U20 pressure transducers installed in adjacent features (shown as white circles in figure 1(a)). Soil moisture boundary conditions were based on measured moisture content at a depth of 20 cm using Campbell Scientific CS 615 and Campbell Scientific CS 616 water content reflectometers located at meteorological station indicated as black triangles in figure 1(a). Probes were calibrated according to the manual using soil samples collected at the SCRS. Model parameters such as saturated hydraulic conductivity, porosity, thermal conductivity, field capacity (to define the pressure-saturation relation), and others listed in table 4.1 were fixed at representative values, either measured in the field, or found in literature (e.g. thermal conductivity of peat), without model calibration.

Validation data included temperature data measured in the same locations as above, but at a depth of 50 cm, as well as frost table measurements along 9 transects and one grid, (black lines and grid in figure 1(c)) documenting lateral and vertical permafrost thaw rates. Monitoring points were located along transects traversing permafrost plateaux and intersecting the border of bogs and fens in order to contrast permafrost degradation adjacent to different wetlands. The transects were established in 2011, and permafrost degradation along these transects has been measured annually since 2015, as described in detail by Connon *et al.* (2018).

In typical stable permafrost environments where the ground annually refreezes to the permafrost table, active layer depth can be measured at the end of the thaw season, but taliks are prevalent at the SCRS, resulting in an active layer depth that can only be determined by knowing the (hard to measure) refreeze depth. In the instance of a talik, the active layer is therefore measured in early spring before ground thaw begins by drilling through the frozen soil to find the base of the frozen layer as detailed in Connon *et al.* (2018).

4.2.2 Modelling Methods

Two coupled differential equations are used here to represent the problem of heat and water transport in freezing soils. These equations are solved in one dimension using an iterative

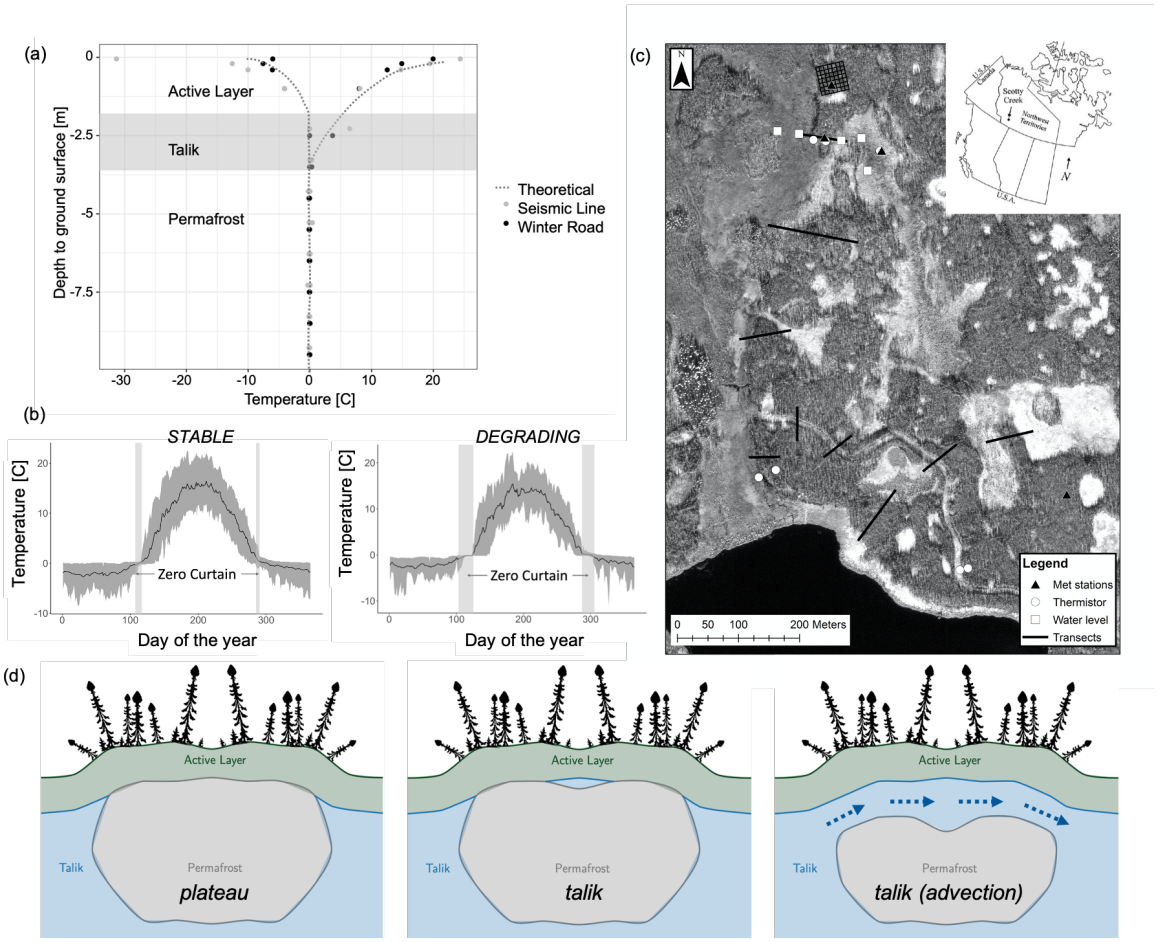

Figure 4.1: (a) Trumpet plot for ground temperatures measured at the SCRS, indicating maximum and minimum soil temperature at various depths. Dashed line illustrates the theoretical curve for this site. Data below the talik sit within the freezing point depression indicating permafrost undergoing phase change. (b) Range of soil temperatures measured on a stable peat plateau (*stable*) and a degrading peat plateau in the presence of a talik (*degrading*) at a depth of 5 - 10 cm below soil surface. Note that the moisture content increases with the formation of a talik, which is reflected in the duration of the zero-curtain periods. (c) Map of study site including frost table transects and grid, thermistor sites where soil temperature is measured in profile, water level recorders used to establish hydraulic gradient and subsurface temperature and meteorological stations monitoring a suite of climate variables including soil temperature and moisture described in Field Methods section. (d) Set of three possible subsurface scenarios - no talik (termed *plateau* in simulations) and *talik* both isolated and allowing flow laterally. (4.2.1).

Crank-Nicolson finite volume solver. Water movement is governed by the unsaturated Richards' equation (represented in mixed form here, similar to Celia *et al.* (1990)):

$$\left(\frac{\partial \theta_l}{\partial \psi} + S_s\right)\frac{\partial \psi}{\partial t} + \left(\frac{\rho_i}{\rho_l}\theta_i + \theta_l\right)\frac{\partial F(T)}{\partial t} = \frac{\partial}{\partial z}\left(K(\psi, T)\left(\frac{\partial \psi(z, T, \theta)}{\partial z} - 1\right)\right) \tag{4.1}$$

where θ [-] represents water saturation, ψ [m] is soil matric potential, Ss [m^{-1}] is specific storage, t [s] is time, ρ [kg m^{-3}] is density (it is assumed the density of ice and water are equivalent for simplicity), F [-] is the temperature-dependant ice fraction, T [°C] is temperature, z [m] is depth below the ground surface, and K [m s^{-1}] is hydraulic conductivity. The hydraulic conductivity is given using the van Genuchten model with peat-specific parameters (Van Genuchten, 1980). The hydraulic conductivity is modified by an empirical relationship describing the impedance of ice content to water movement through the partially-saturated soil, as presented by Kurylyk & Watanabe (2013). The subscripts l and i refer to liquid water and ice phases respectively. The less common term $\left(\frac{\rho_i}{\rho_l}\theta_i + \theta_l\right)\frac{\partial F(T)}{\partial t}$ on the LHS is a source/sink term arising from the inclusion of phase change. Vapour flux is not included in this model; Putkonen (1998) deemed it unimportant (especially in wet soils) as compared to the other processes occurring in an unsaturated 1-D freezing or thawing soil column. The main role of vapour flux is to deliver water to the freezing front, which is accomplished instead by the Clausius Clapeyron (CC) relation (Karra *et al.*, 2014). The CC relation is included in the $\frac{\partial \theta_l}{\partial \psi}$ term and the RHS of equation 4.1 when the temperature is in the freezing range, assumed to be 0 °C to -0.05 °C (equation 4.2). This relation is a modification to the soil characteristic curve that is applied over the freezing range as explained in section 2.6.2. It includes a form of the Clausius relationship similar to that presented in Kurylyk & Watanabe (2013). The terms g, L and $\Delta\rho^{-1}$ refer to gravity [m s^{-2}], the latent heat of fusion of water [J kg^{-1}] and the change in specific volume associated with the phase change [m^3 kg^{-1}] respectively. This relation is derived in section 2.2.

$$\psi(\theta, T) = \begin{cases} \psi^*(\theta, \eta_{eff}) + \frac{L}{\rho g T \Delta\rho^{-1}}\frac{\partial T}{\partial t}\Delta t & \text{if } T_{res} \leq T \leq 0 \\ \psi^*(\theta, \eta_{eff}) & \text{else} \end{cases} \tag{4.2}$$

$$\theta(\psi, T) = \begin{cases} \eta & \text{if } \psi \geq 0 \\ \theta^*(\psi - \frac{L}{\rho g T \Delta\rho^{-1}}\frac{\partial T}{\partial t}\Delta t, \eta_{eff}) & \text{if } T_{res} \leq T \leq 0 \\ \theta^*(\psi, \eta_{eff}) & \text{if } T < T_{res} \end{cases}$$

$$\eta_{eff} = \eta - \theta_i$$

Note that the soil characteristic curve is assumed to govern the matric potential, to which a correction for cryosuction is added peicewise over the freezing range. Summation was chosen to maintain continuity of energy and pressure. In model simulations, an approach similar to that presented in Kurylyk & Watanabe (2013) for unsaturated freezing soils is used. In this approach, the relation for pressure or water content is corrected in the freezing range both for cryosuction as well as for the change in porosity associated with an assumption that pore ice behaves as soil volume and does not convey water.

Heat transport in the porous media is governed by:

$$\left[c\rho + L\frac{dF}{dT}\rho\eta\theta\right]\frac{\partial T}{\partial t} = \left(\frac{\partial}{\partial z}\left(\lambda_b\frac{\partial T}{\partial z}\right) - c_l\rho_l\frac{\partial q_z T}{\partial z}\right) + q_y\rho_w c_w(T_{in} - T) \tag{4.3}$$

in which the parameters c [J kg^{-1}°C], η [-], λ_b [J m^{-1}s^{-1}°C], and q [m s^{-1}] refer to bulk heat capacity, porosity, bulk thermal conductivity and flow rate of liquid water respectively. The subscripts z [m] and y [m] refer to the vertical and horizontal directions, and T_{in} [° C] is the temperature of water laterally entering the soil column driving advection. Note that water may be supplied laterally to the column via the final q_y term, with the flux given by $q_y = -K(\psi, T)\frac{\partial h}{\partial y}$, where the gradient is fixed for each simulation, and K values reflect the impedance due to ice content. This term is used only when the soil column contains a talik connected to a wetland feature. The inclusion of this source term allows the 1-D vertical model to represent lateral water movement in short-term simulations of permafrost evolution. This method is not appropriate for long-term change detection where lateral permafrost thaw is expected.

Both governing PDEs were discretized using an Crank-Nicholson scheme, and solved numerically through matrix inversion. An operator splitting approach was taken in coupling the relations, in which first the unsaturated Richards' equation was solved to determine fluxes in a given timestep, and then these fluxes were applied when solving the heat equation. Change in ice content was then updated before incrementing the timestep and returning to the Richards' equation.

These equations have individually been solved elsewhere, and the uncoupled formulations (i.e. unfrozen Richards' and saturated conductive heat transport) were separately benchmarked against results from Kurylyk *et al.* (2014) and Celia *et al.* (1990). Model benchmarking was performed using parameter values listed in table 4.1, and benchmarking results for the thermal portion of the model are presented in figure 4.2. No existing analytical models are available to benchmark the coupled set of equations. The relationships are coupled using operator splitting, first solving the unsaturated Richard's equation

Table 4.1: Model parameter values used to model a uniform peat soil column. Values were not assumed to change with depth, however changes due to variations in water/ice/air content in the soil matrix were included.

Variable	Description	Value	[Units]	Source
η	Porosity	0.8	-	
Ss	Specific Storage	0.001	m^{-1}	Price *et al.* (2005)
ρ_i	Density of ice	1000	kg/m^3	
ρ_w	Density of water	1000	kg/m^3	
K_{sat}	Saturated hydraulic conductivity	6×10^{-6}	m/s	Quinton *et al.* (2008)
g	Gravity	9.81	m/s^2	
L	Latent heat of fusion	334000	J/kg	
λ_w	Thermal conductivity (water)	0.6	J/(msK)	
λ_i	Thermal conductivity (ice)	2.14	J/(msK)	
λ_a	Thermal conductivity (air)	0.024	J/(msK)	
λ_s	Thermal conductivity (soil matrix)	0.005	J/(msK)	Oriol *et al.* (1978)
c_w	Heat capacity (thawed)	4182	J/(kgK)	
c_i	Heat capacity (frozen)	2108	J/(kgK)	
c_s	Heat capacity (soil matrix)	630	J/(kgK)	Oriol *et al.* (1978)
Q	Impedance factor	11	-	Kurylyk & Watanabe (2013)

and then the heat transport equation in each time step, using an approach similar to Harlan (1973). The specific storage S_s is dependent on ice content, θ_i, which is determined from the temperature T, as is the hydraulic conductivity, K. Moisture migration due to temperature gradients near the freezing temperature is allowed using the CC relationship. The inclusion of this process changed model predictions less than 1% in saturated conditions, but reduced model stability and increased computation time. Bulk parameters are calculated based on the ice/water/air fractions in the soil matrix, where the heat capacity (c) and density (ρ) are calculated using the volumetrically weighted arithmetic mean of saturation values determined by the unsaturated Richards' equation, and the thermal conductivity λ_b is calculated using a volumetrically weighted geometric mean, as suggested by Kurylyk *et al.* (2014) for anisotropic heterogeneous media. The physical properties of the assumed soil column are homogeneous, except those which depend on the water or ice saturation of the profile, which are allowed to vary with soil water or ice content. The omission of depth-dependant parameters most affects the hydraulic conductivity and pore water retention in the top 0.3 m of the soil profile, as the other modelled parameters are relatively constant with depth (Quinton *et al.*, 2008; Gharedaghloo *et al.*, 2018). This may speed the equilibration time of the profile when subject to specified water flux conditions due to higher hydraulic conductivity near the surface, but is not expected to drastically affect model results and still permits the comparison of various drivers of permafrost degradation. The overestimate of pore water retention in the near surface my lead to an overestimate of soil moisture in the near-surface and therefore higher than actual thermal conductivities.

As seen in figure 4.3, the soil column is discretized into 2 cm elements for all simulations. For simulations where the soil column is saturated (i.e. not those investigating unsaturated conditions), a 0.48 h time step is used. In unsaturated conditions this is refined to 0.24 h to ensure convergence, and is further refined when moisture migration due to temperature gradients is included to 0.12 h. In all cases, the thermal operator converged at each time step. In the unsaturated case with moisture migration due to temperature gradients, the moisture operator (equation 4.1 failed to converge no more than 0.5 % of the simulation time. This lack of convergence occurred in the shoulder seasons, when the hydraulic conductivity is modified by ice content and very sharp gradients due to relatively rapid movement of the freeze/thaw front were observed as see in figure 4.1 (b).

4.2.3 Boundary and Initial Conditions

As a peatland, the study site maintains a water table near the ground surface. The water table is found within the top 0 - 30 cm of the soil profile in the wetlands and in

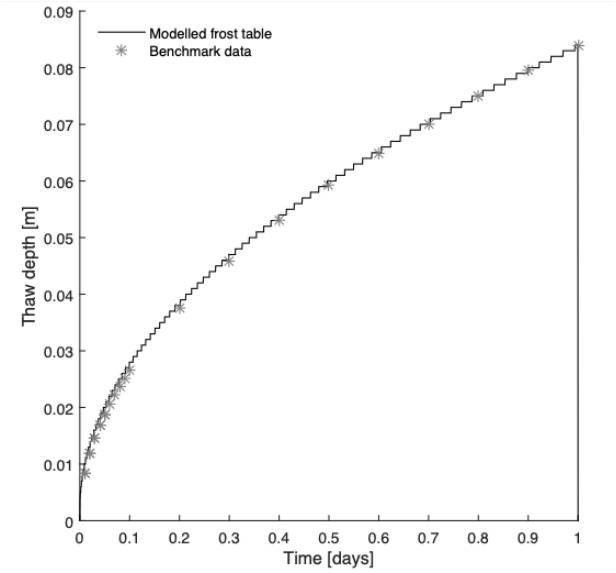

Figure 4.2: Benchmarking of thermal model. Comparison made to Kurylyk *et al.* (2014), using all model parameters for **Suggested Benchmark 1** of that study. The maximum relative error after 24h simulation is 0.3%.

depressions atop peat plateaux. The sloping edges of the peat plateaux are able to drain to adjacent wetlands, and the interior of the plateau can drain to internal depressions. In these locations, the water table is often found just above the frost table at a depth of 30 - 80 cm below the ground surface depending on time of year. A depth of - 50 cm is representative of a well-drained area for most of the thawing season.

The surface boundary condition for the Richards' equation used here is a specified flux condition. Saturated conditions are simulated with a no-flow surface condition imposed on an initially saturated soil column (water table at ground surface). For unsaturated conditions, the average depth to water table of - 50 cm on peat plateaux is used as an initial condition. A constant specified flux condition derived from water level records consists of the removal of 10 cm of water between mid-May and the end of June, and the addition of the same amount of water between mid-August and the end of September. A no-flow condition is imposed at the base of the soil column, where it is assumed that permafrost is always present. A diagram of the model setup including both thermal and water content initial and boundary conditions is included in figure 4.3.

Thermal boundary conditions are given by the ground surface temperature as modified by the presence of the snowpack, generated using a seasonal autoregressive moving average

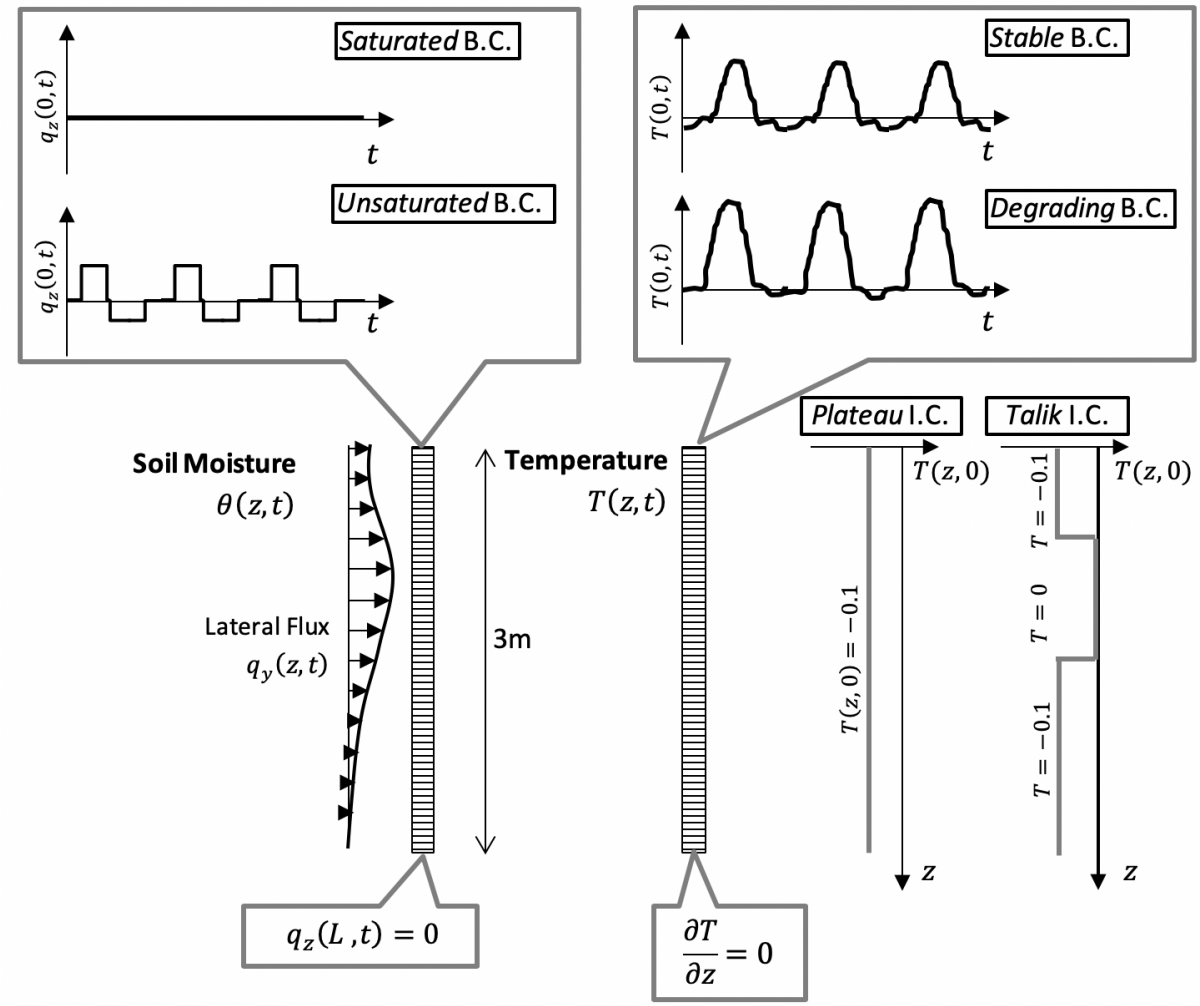

Figure 4.3: Model domain showing boundary conditions and initial conditions for various simulation experiments for both soil moisture and thermal relations.

model following the method outline by Hipel & McLeod (1994) constructed using soil temperatures collected in the field. This allowed to generate multiple independent temperature boundary conditions with the same statistical properties as the collected field data. It was necessary to use a continuous dataset from the same field site to appropriately capture the data covariance. For the *stable* case, only a four year time-series was available for building the autoregressive model. In the *degrading* case, a longer 10 year data set was available, though it had a data gap of approximately six months. Therefore only a four-year subset

was used to generate the autoregressive model, while the entire series was tested for stationarity. Both datasets were tested for stationarity: it was found that a stationary model was sufficient for *stable* permafrost, while a linear trend of + 0.055 °C/year was apparent in the deseasonalized data for the *degrading* case. This positive trend was applied when generating ensemble temperature data for this boundary condition. Boundary conditions realizations for either 5 - year or 10 -year simulations were sampled from the *stable* and *degrading* models reproducing seasonal trends and data variance observed in the field, while incorporating inter-annual variability. The bottom thermal boundary condition is a zero heat flux condition. Field data show that the permafrost is effectively isothermal at 0 °C to a depth of 8 m, and simulations have a maximum vertical depth of 3 m, so the geothermal gradient (of approximately 0.08 W/m^2 (McClymont *et al.*, 2013)) is neglected, see figure 4.1(a). This condition was chosen as opposed to a fixed temperature due to uncertainty in ice content and freezing function - some flexibility to represent various ice contents at the bottom boundary was desired.

Heat flux at the ground surface is a clear direct driver of permafrost degradation (e.g. Walvoord *et al.* (2019)). Changes in tree canopy, surface albedo and ground cover contribute to modified ground heat flux (Quinton *et al.*, 2018). This change is incorporated into model simulations as an increase in soil surface temperature in the summer. It would not be expected that the duration of the summer and winter season or the over-winter temperatures should be affected due to a change in canopy, unless there are changes to the snowpack due to interception. In the winter season, the ground heat flux is controlled by snow accumulation. Snowcover, and inter-annual variability in snowcover, has important implications for the ground thermal regime. End of season snow surveys are conducted annually across all landcover types at the SCRS providing an estimate of snow water equivalent (SWE), or total water stored on the landscape in the form of snow.

Once a talik exists in the soil profile it is possible for it to connect adjacent wetland features. In the case of a connected talik, lateral advection through the talik is parameterized by treating through-flow as a distributed source/sink term in the 1-D energy balance. The lateral hydraulic gradient contributing to q_y in equation 4.3 is specified as 0.002 m/m in the case of a connection to a collapse scar wetland and 0.007 in the case of a channel fen. The gradients are selected based on water level data collected in the field. Actual field data from connected talik features show variations and even reversals in hydraulic gradient over the year, but for simplicity these are omitted in favour of the average observed differences between wetland types. The range of inflow temperatures was derived from measurements in a collapse scar wetland and a channel fen at a depth of 50 cm below the ground surface. Sensitivity to changes in gradient are computed to put this assumption into context. For simplicity, this study neglects any freezing point depression, and a linear freezing function

was applied between 0 and -0.05 °C, while data collected at the field site indicates a very small freezing point depression.

Two sets of initial temperature conditions are used in model simulations: a *plateau* condition and a *talik* condition. These conditions describe (generalized) field observations of mid-winter soil temperatures on a stable peat plateau and a plateau with an isolated talik respectively. The *plateau* initial temperature profile is a uniformly frozen soil column at a constant temperature of -0.1 °C. The *talik* condition is initialized to the same temperature as the *plateau* condition, except from a depth of 0.75 m to 1.5 m which is initialized at a temperature of 0 °C and zero ice content as seen in figure 4.3. All model simulations are summarized in table 4.2.

4.3 Results and Discussion

4.3.1 Model Evaluation

After the model was successfully benchmarked against both thermal and water-content models from literature (Kurylyk *et al.*, 2014; Celia *et al.*, 1990) (figure 4.2), the performance of the model was evaluated in relation to soil temperatures and refreeze depths measured at the SCRS. This ensured that the governing processes in this field site were represented adequately, and the approximated depth-homogenized soil properties were appropriate.

Soil Temperature

The model was first tested by comparing modelled and measured temperatures at depth (40 cm - 50 cm below ground). *Stable* boundary conditions were applied to an unsaturated *plateau* initial condition with water table initially 50 cm below the soil surface to best represent a permafrost plateau. All model simulations are summarized in table 4.2. A contour plot of temperature evolution for the stable peat plateau boundary condition, as well as a comparison of modelled and measured temperatures at approximately 45 cm is shown in figure 4.4 (a) and (b). These results were obtained without model calibration. Modelled soil temperatures adequately represent the zero curtain period both during spring melt and winter freeze up. Measured data at all depths have high variability relative to modelled data because they are aggregated from data collected at 5 different sites over approximately 10 years (with data gaps) including inter-site variability, while simulated boundary conditions are constructed from data collected at a single instrumented site.

Table 4.2: Model boundary and initial conditions for all simulations completed in this study.

Run Name	Thermal BC	Thermal IC	Moisture BC	Moisture IC [m below surface]	Duration [years]	Advection Condition
Spm1	*STABLE*	*plateau*	No flow	Saturated	5	none
Spm2	*STABLE*	*plateau*	Seasonal Flux	0.25 m	5	none
Spm3	*STABLE*	*plateau*	Seasonal Flux	0.5 m	5	none
Spm4	*STABLE*	*plateau*	Seasonal Flux	1 m	5	none
SpmCC1 - SpmCC4	*STABLE*	*plateau*	Seasonal Flux with CC (SpmCC1 No Flow)	as Spm1 to Spm4	5	none
SpT1 - SpT5	*STABLE*, $\mu = 1$ to 5	*plateau*	No Flow	Saturated	5	none
DpT1 - DpT5	*DEGRADING*, $\mu = 1$ to 5	*plateau*	No Flow	Saturated	5	none
SpSWE-t1	*STABLE*, SWE winter 1 = 12.5 cm	*plateau*	No Flow	0.5 m	5	none
SpSWE-t2	*STABLE*,SWE winter 1 & 2 = 12.5 cm	*plateau*	No Flow	0.5 m	5	none
SpSWE-3 - SpSWE+5	*STABLE*, $\mu = 2$, SWE winter 2 = -3 cm to + 5 cm	*plateau*	No Flow	Saturated	5	none
Stm1 - Stm4	*STABLE*	*talik*	Seasonal Flux (Stm1 no flow)	as Spm1 - Spm4	5	none
StmCC1 - StmCC4	*STABLE*	*talik*	Seasonal Flux (StmCC1 no flow)	as Spm1 - Spm4	5	none
St1 - St5	*STABLE*, $\mu = 1$ to 5	*talik*	No Flow	Saturated	5	none
Dt1 - Dt5	*DEGRADING*, $\mu = 1$ to 5	*talik*	No Flow	Saturated	5	none
StSWE-3 - StSWE+3	*STABLE*, $\mu = 2$, SWE winter 2 = -3 cm to + 3 cm	*talik*	No Flow	Saturated	5	none
DtI	*DEGRADING*	*talik*	No Flow	Saturated	5	none
DtB	*DEGRADING*	*talik*	No Flow	Saturated	5	Bog temperature, ∇h 0.002
DtF	*DEGRADING*	*talik*	No Flow	Saturated	5	Fen temperature, ∇h 0.007
DtT0 - DtT20	*DEGRADING*	*talik*	No Flow	Saturated	5	Bog temperature - 1 to Bog + 3, ∇h 0.007
Dtq0 - Dtq20	*DEGRADING*	*talik*	No Flow	Saturated	5	Bog temperature, ∇h 0 to 0.01
Sp1 - Sp20	*STABLE*	*plateau*	No Flow	0.5 m	10	none
Dp1 - Dp20	*DEGRADING*	*plateau*	No Flow	0.5 m	10	gradient 0.002

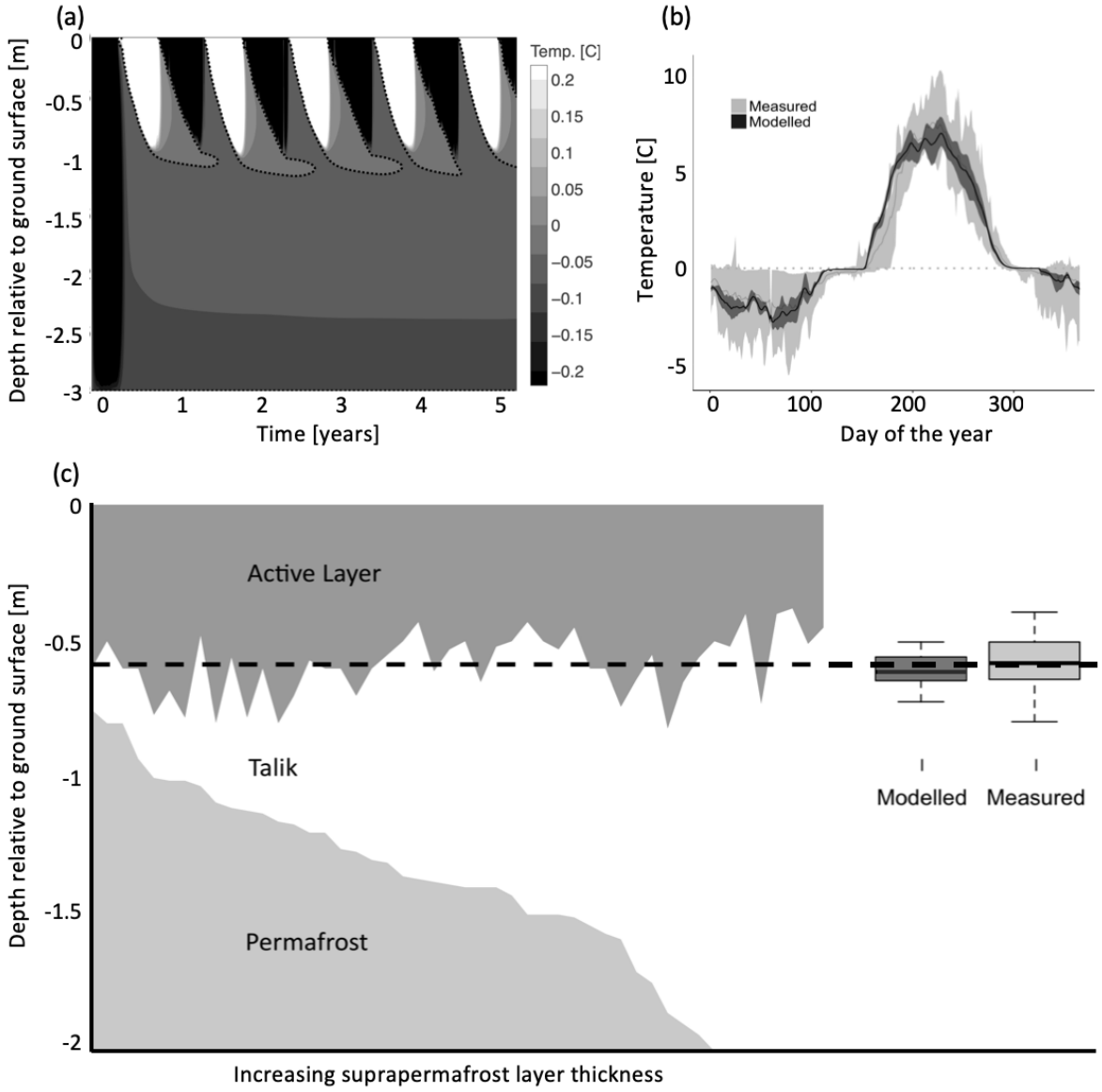

Figure 4.4: Modelled stable permafrost plateau. (a) shows freeze-thaw cycles over 5 year (saturated) simulation. (b) Range of measured and modelled temperatures at 40 cm below ground surface for the soil column, aggregated over 5 year simulation. Data agreement representative of other depths and simulations. (c) Measured refreeze and underlying permafrost [left], sorted by increasing depth to permafrost (n = 48). Dashed line indicates average refreeze (over a talik). Box and whisker plots indicate the measured and modelled variance in active layer (refreeze) depth (n = 12) for all distinct simulation scenarios with a talik.

Refreeze Depth

Though there is good agreement between modelled and measured soil temperature at depth, latent heat represents a large fraction of the system's energy storage and transfer (Hayashi *et al.*, 2007), so the depth of freeze/thaw is also compared to field measurements of active layer (figure 4.4 (c)). Active layer depth in permafrost without a talik is sensitive to measurement timing and given variation in end of season measurements this comparison yielded higher uncertainty. Additionally talik-free active layers are often unsaturated and given the difficulty in achieving model convergence in unsaturated cases the saturated comparison was preferable. Field measurements of maximum thaw depth in the absence of a talik reported 59 ± 4.5 cm (n = 106) and 60 ± 4.1 cm (n = 99) in 2016 and 2017 respectively, while the maximum refreeze with a talik was 58 ± 12.2 cm (n = 120) and 59 ± 11.5 cm (n = 48) in 2017 and 2018 respectively. Numbers in parentheses indicate the number of point measurements. Modelled soil columns with a talik align well with the measured value of refreeze over a talik: 61 ± 6.7 cm (n = 12), while simulations without a talik very slightly under-estimate the maximum thaw depth: 56 ±10.5 cm (n = 15). Given the agreement between modelled and measured soil temperatures and active layer depths, the model was deemed sufficient for the evaluation of controls on talik formation.

The benchmarked and verified model was used to 1) assess the relative influence of controls on isolated talik formation from a continuous permafrost state (section 4.3.2) and, 2) determine how these factors affect permafrost degradation rates once a talik is formed (section 4.3.3).

4.3.2 Controls on Talik Formation

Conditions favourable to talik formation on a permafrost plateau are identified based on the a) soil moisture, b) soil surface temperature, and c) snow cover. All simulations of talik formation were subject to the *plateau* initial condition and (unless otherwise stated) the *stable* boundary condition. Average snow conditions for the study site (115 mm SWE) are used in all simulations except those testing the impact of changes in SWE.

Unsaturated Soil Conditions

To determine the impact of different soil moisture conditions on talik formation, a modelled saturated soil column was compared to three unsaturated columns. For the unsaturated cases, the water table was initially set to a depth of 0.25 m, 0.5 m, and 1 m, and then

subject to a specified flux boundary condition, with and without moisture migration due to temperature gradients.

Figure 4.5 compares the unsaturated (a) and saturated (b) cases. It can be seen by examining the 0 °C isotherm that in the unsaturated case there is complete refreeze of the soil column each winter, while the freezing front penetrates the soil column further than the thawing front. This can be compared to the saturated case in figure 4.5(b), in which a talik forms. The unsaturated surface condition in the summer plays a key role in insulating the permafrost, protecting it from degradation evident in figure 4.5(b) as the expanding region in the zero curtain (between 0 and -0.05 °C).

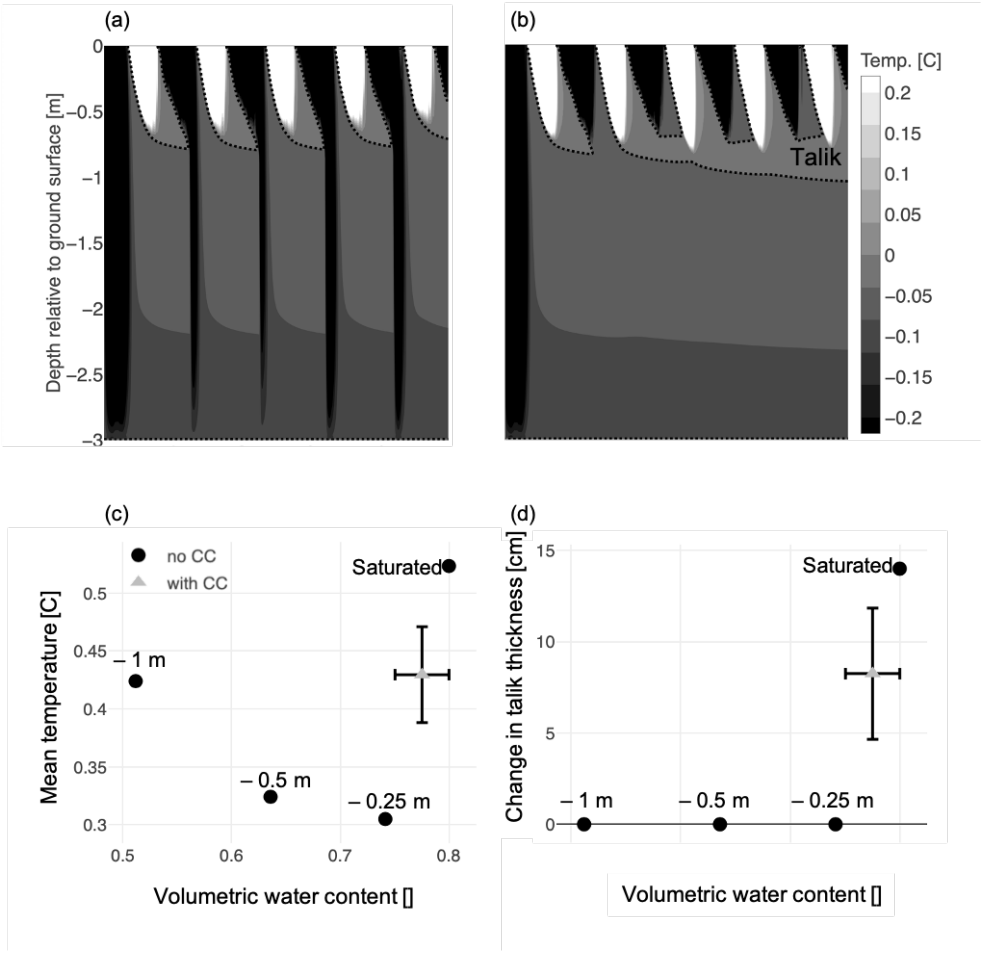

Figure 4.5: Soil temperatures over 5 year simulation with *stable* boundary condition for (a) data-driven unsaturated soil conditions with initial water table 25 cm from soil surface and (b) hypothetical saturated conditions. Dashed line indicates the maximum thaw contour. Panels (c) and (d) present the respective response in mean temperature of near-surface soil and talik thickness to changes in soil moisture (labelled by initial position of the water table below the ground surface).

The response of the mean temperature in the top 1 m of soil, and talik thickness to changes in soil moisture are presented in panels (c) and (d) of figure 4.5. The mean temperature and the volumetric water content are evaluated over the course of the entire 5-year simulation, while the maximum talik thickness is evaluated in the final winter of the simulation. Part (c) of the figure shows that as the moisture content increases, the mean annual soil temperature decreases, likely because more energy is required to heat a wetter soil profile. As the water table moves further from the soil surface, it becomes more difficult to draw the water to the freezing front, insulating the soil column over-winter. The saturated case is drastically different from the unsaturated case because it is not subject to the seasonal water flux at the soil surface. This flux plays an important role in cooling the profile as it increases the thermal conductivity over winter and decreases it during the warmest part of the summer. The inclusion of the CC relation in the simulations (grey triangles) obfuscates the moisture effects because the temperature gradient draws water to the soil surface, bringing the upper soil near saturation. With the CC relation, the applied boundary and initial conditions are not impactful on simulation results, which are shown as an average with standard deviation.

Only the saturated soil column develops a talik without the addition of moisture migration to the freezing front, and though the least saturated case has a warm mean annual temperature, it does not have sufficient heat capacity to offset the over-winter freezing of the soil column. The decreased soil moisture also leads to very low thermal conductivity, limiting the ability of this heat to penetrate the soil column and cause permafrost thaw. The active layer in these simulations is deeper, but is not saturated and stores no more energy than the saturated conditions. In all cases involving the CC relation, a talik was formed. This is thought to be due to the near-saturated conditions induced in the near-surface during both freezing and thawing. The migration of moisture to the thawing front overcomes the imposed summer drying and winter wetting, leading to near-saturated conditions. However, the simulations without the CC relation are consistent with moisture conditions observed in the field and should therefore be considered when understanding the impact of soil moisture on talik formation.

In the field it is thought that taliks are associated with increased soil moisture, and differences in soil moisture are the driving control on differentiating land cover types, where the presence of (dry) lichen indicates higher permafrost stability, as reported by Grant *et al.* (2017); O'Donnell *et al.* (2009) and many others. These simulations seem to confirm this field observation. Other modelling studies have found that soil moisture is less impactful on active layer evolution and talik formation when compared to changes in snowfall, but they do not include the observed seasonality in soil moisture leading to dry summer conditions and wet winter conditions (Atchley *et al.*, 2015). The inclusion of this

seasonality alleviates the competing processes of increasing thermal conductivity due to increasing moisture content, with a concomitant increase in latent heat required to fully freeze/thaw the soil column observed in other modelling studies (Atchley *et al.*, 2015).

Temperature

Summer soil surface temperatures were altered to reproduce changes in heat flux into the ground representative of differences in incoming radiation or surface albedo. Both the *stable* and *degrading* boundary conditions were considered. Results are reported in terms of annual mean surface temperature. Figure 4.6 shows the thickness of talik formed due to changes in mean annual surface temperature. Both responses are near linear, with the *degrading* condition forming a notably thicker talik at cooler temperatures. The shape of the temperature profile drives the *degrading* condition to store more heat despite the same mean annual temperature in both simulations. The *degrading* condition differs most prominently from the *stable* condition in that the zero-curtain period is longer. This delay in freezing and thawing may lead to a net energy gain to the system, where the zero-curtain does not provide a temperature gradient sufficient to freeze the soil in the fall, while the (shorter) spring zero-curtain period occurs earlier than in the stable case, leaving the summer thaw season approximately the same length in both cases.

Snow Cover

It is widely understood that snow is a highly effective insulator due to its large (60-90%) air volume. When there is an early or thicker than usual snowpack, the soil temperatures are warmer than usual (Woo, 2012). Though somewhat data-limited at this field site (established in 2006), figure 4.7 (c) shows that this relationship holds true at the SCRS. The relationship between snow water equivalent (SWE) and soil temperature was used to test the impacts of increased snowfall by uniformly increasing the average overwinter temperature for the *stable* condition where the empirical relation from figure 4.7 (c) was used to determine the impact on winter soil temperatures. An increase in soil surface temperature derived from the linear relationship between SWE and overwinter soil temperature (figure 4.7(c)) was applied to only the first winter (figure 4.7 (a)) and then the first and second winter (figure 4.7 (b)). Though there is no immediate talik development in the first case, it should be noted that the talik formed in the fourth winter is actually due to the additional energy stored in the soil profile from the first high snow winter, as without it, the simulation results in figure 4.4 (a). The second case clearly confirms that increased snow cover can be a trigger for talik formation. These results were also found in the study by

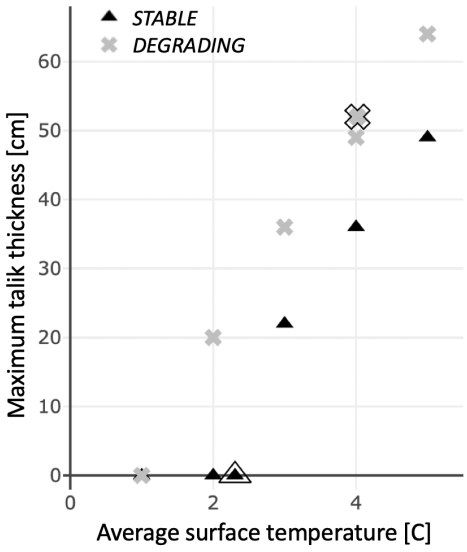

Figure 4.6: Response of talik thickness to changes in mean annual soil surface temperature. Temperature profile derived from the *stable* boundary condition shown in triangles, and *degrading* boundary condition in crosses. The original boundary condition (before summer temperature modification) is outlined in black.

Atchley *et al.* (2015) and Atchley *et al.* (2016), in which it was shown that increased snow cover could lead to talik formation near Barrow, AK. Similarly to that study, increased snow resulted in an extension of the zero-curtain period, and a decrease in the maximum depth reached by the freezing front in high-snow years (Atchley *et al.*, 2015). Some climate change scenarios predict higher snowfall in the study region (Solomon *et al.*, 2007). Snow depth may also be increased locally by talik formation which leads to the development of local depressions where snow will preferentially accumulate, a forward feedback mechanism. These depressions and accompanying increased snow depth have been observed at the SCRS. This is similar to sites with shrub development, where Jafarov *et al.* (2018) have shown that the preferential snow accumulation within shrub patches can lead to the formation of isolated taliks that evolve from closed taliks to through taliks.

The opposite process, in which low-snow years can reverse the formation of a talik is less likely. A decrease in SWE of equal magnitude to the initial increase is required to reverse the formation of a talik. Similarly to other regions in which the overwinter snowpack undergoes transformations such as sublimation and redistribution, the statistical distribution of annual SWE near the study site is skewed. It shows a tail toward high snow years, and a higher probability of just below average low-snow years (Shook *et al.*, 2015). Therefore it is unlikely to see an equal magnitude SWE deficit.

The sensitivity of talik formation to snow cover was tested by modifying the *stable* case with winter temperatures shifted resulting in a mean surface temperature of 2°C as the original saturated *stable* condition resulted in talik formation with no change in SWE. Figure 4.7 (d) indicates the necessary deviation from mean SWE (temperature shift applied only in the second winter) to form a talik is approximately 2 cm.

4.3.3 Talik Evolution

Soil moisture, temperature and snowfall conditions have been identified under which taliks are formed, initiating permafrost degradation. Once a talik is present in the soil column, field observations indicate that it is likely that permafrost will continue to degrade. The sensitivity of this permafrost degradation to the same conditions studied above is presented here. These results are extended to include the impacts of advection through the newly formed lateral flow path. Simulations in the following sections are run with the *talik* initial condition, and (unless otherwise specified) the *stable* boundary condition so as to be directly comparable to the simulations of talik formation. Average snow conditions for the study site are used in all simulations except those testing the impact of changes in SWE.

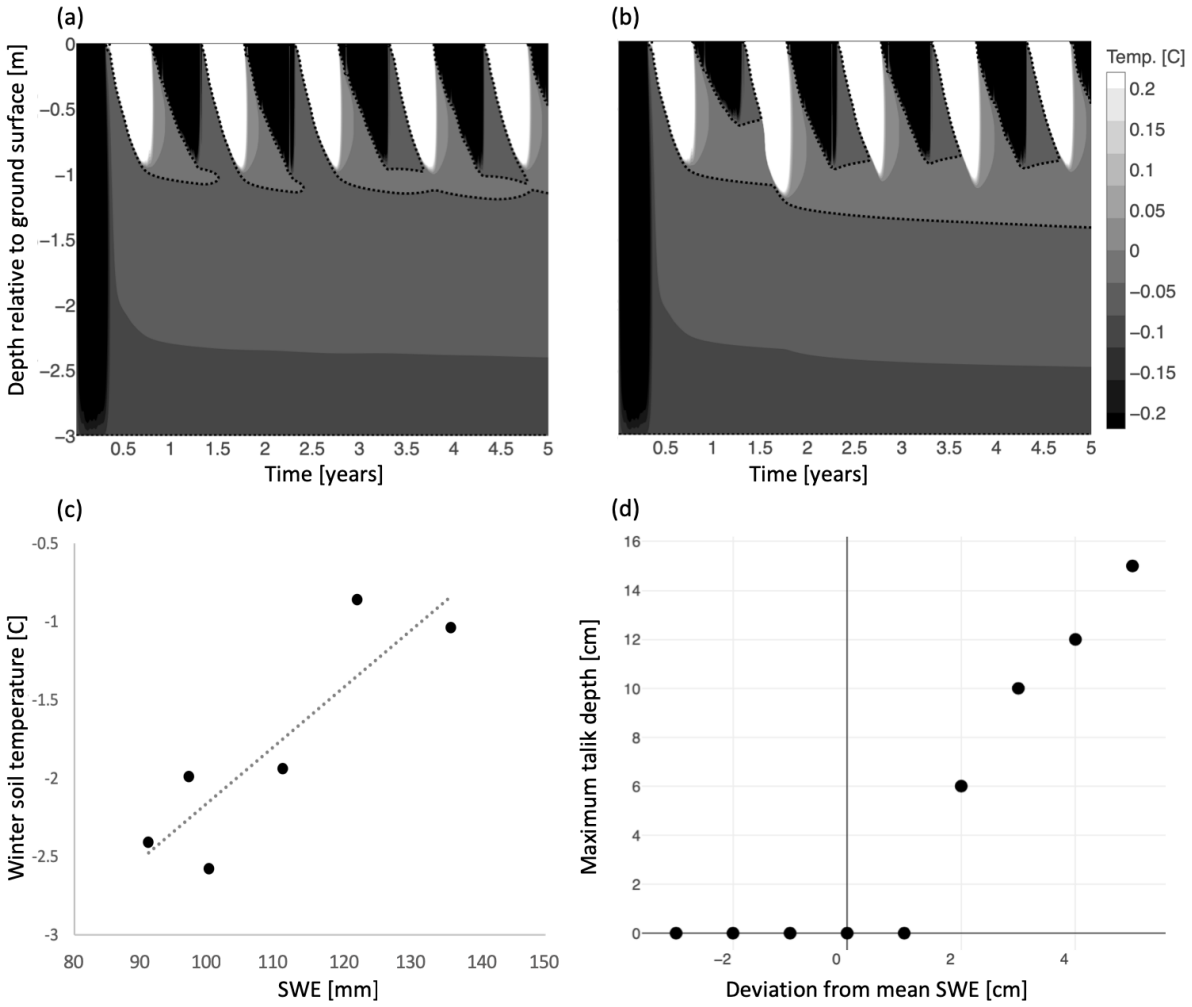

Figure 4.7: Impact of snow accumulation on soil temperatures. (a) One high (SWE =125 mm) snow winter. (b) Two consecutive high snow winters. (c) Average winter (November - April) ground temperature at 5 - 10 cm in relation to maximum snow accumulation. R^2 = 0.77. (d) Modelled talik thickness response to changes in SWE in winter 2.

Soil Moisture

The impact of soil moisture on average temperature in the top 1 m of the soil column is very similar in the *talik* condition and the *plateau* condition, especially when the CC relation is not applied (figure 4.8 (a)). With a talik, there is less temperature-driven movement of

water in near-surface, resulting in similar trends in temperature as the case neglecting the CC relation. In all cases, the mean temperature is higher than without a talik.

The impact of unsaturated conditions on the thickness of the talik is quite remarkable. All unsaturated conditions without the CC relation, and the condition with lowest soil moisture including the CC relation resulted in talik thinning and evidence of permafrost recovery. This contrasts the saturated conditions (and near-saturated conditions with temperature-driven moisture migration) in which the talik thickens over the 5-year simulation.

Temperature

An increase in talik thickness was found in the case initialized with a talik for all surface temperatures above 2° C (Figure 4.8 (c)). A decrease in mean annual temperature up to 1°C did not seem to lead to permafrost recovery as the talik thickness remained constant. Simulated increased summer temperatures result in faster permafrost degradation beneath a pre-existing talik than over a plateau forming a talik.

Snow

The relationship between snowfall and permafrost degradation is very similar before and after the formation of a talik, i.e., small increases in SWE help to insulate the ground leading to increased talik thickness. Though the trend remains the same, an increase in talik thickness is observed in all cases tested, while in the simulation started with the *plateau* condition only showed talik development after a SWE increase of 20 mm (figure 4.8 (d)). Even under low-snow conditions, the talik in the profile is observed to thicken by 4 cm over the course of the simulation, with no evidence of permafrost recovery.

4.3.4 Advection

Here, three hypothetical soil columns with the *talik* initial condition and *degrading* boundary condition are modelled to examine the role of advection: 1) an isolated talik (without advection), 2) a connected talik with a hydrological connection to a collapse-scar wetland, and 3) a connected talik with a hydrological connection to a channel fen. A hydraulic gradient of 0.002 was applied in the case of the bog and 0.007 in the case of a fen, while the isolated talik was not subjected to any lateral flow. Figure 4.9 (a), (b) and (c) shows that although all three simulations result in permafrost degradation, advection accelerates thaw

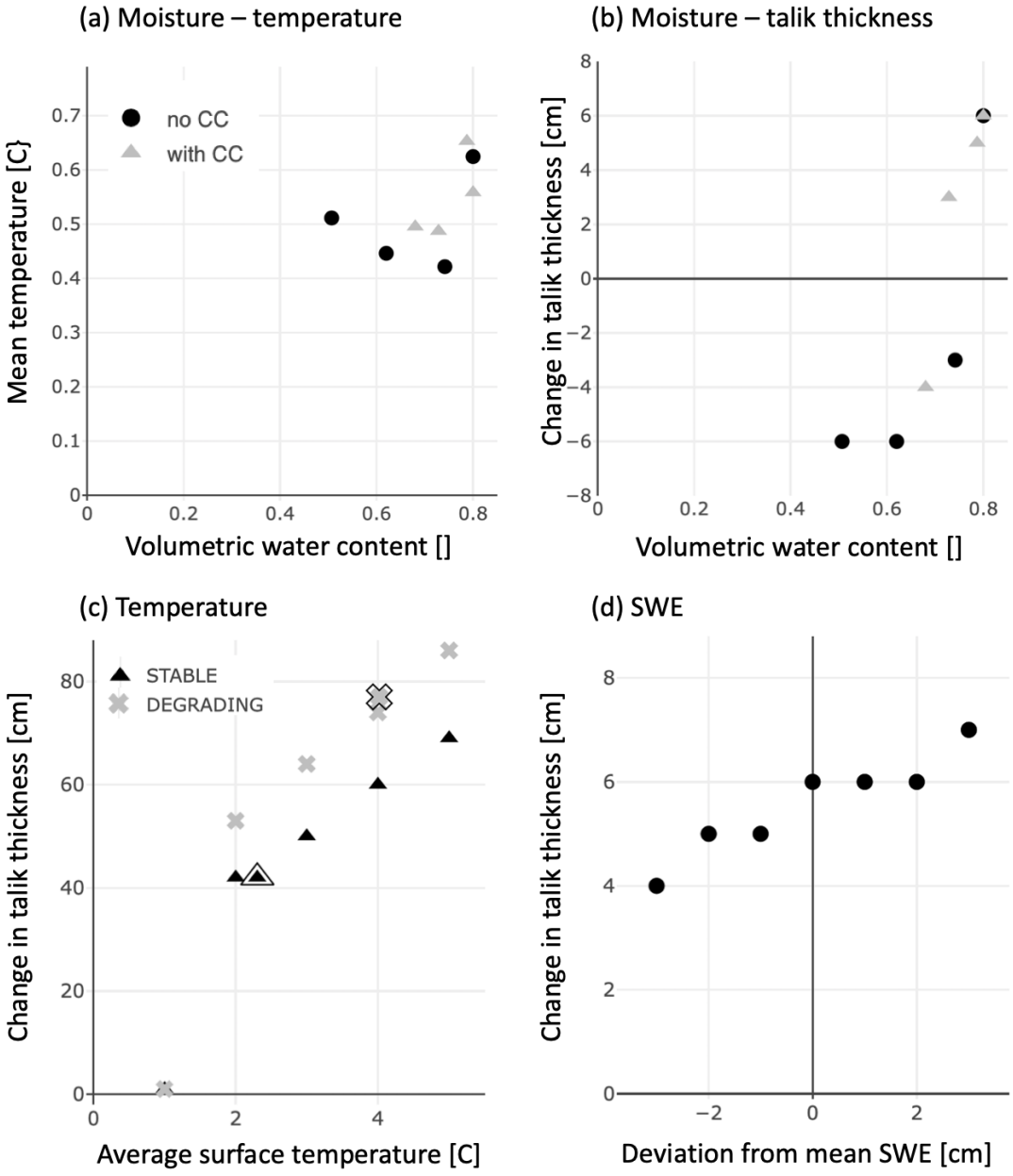

Figure 4.8: (a) Sensitivity of average soil temperature of top 1 m of soil profile (only in the case of soil moisture). Change in talik thickness due to (b) soil moisture, (c) average surface temperature, and (d) changes in SWE for *talik* initial condition.

rates and increases the sensible heat stored in the soil profile. As reported by Sjöberg *et al.* (2016), the abrupt changes in temperature of water flowing through the soil column in a fen observed at the SCRS can have significant impacts on thaw rates because of the high thermal gradients induced. In both cases including advection it is apparent that there is overwinter permafrost thaw in connected taliks adjacent to wetlands, which is not present without advection (see annotations on figure 4.9(c)). This overwinter degradation has been observed in the field in a talik connecting a fen on one side to a bog on the other. Overwinter permafrost degradation can be seen as a tipping point, where permafrost recovery is highly implausible as degradation occurs year-round. No plausible conditions could be identified through modelling that led to permafrost recovery in this case, nor have there been any instances of permafrost recovery observed under these conditions in the field.

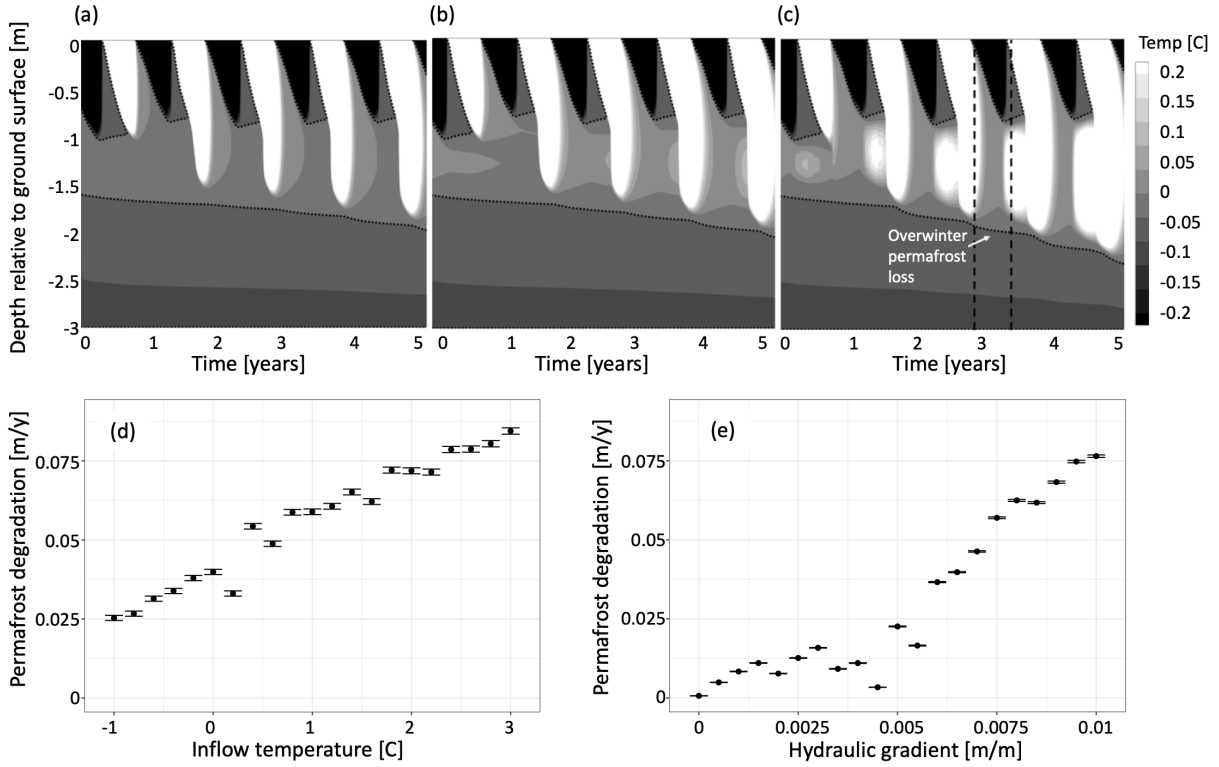

Figure 4.9: Soil temperatures as a result of advection representative of (a) an isolated talik, (b) a connected talik adjacent to a bog, or (c) a fen. Rate of vertical permafrost degradation determined by temperature (d) for a constant gradient of 7×10^{-3}, and hydraulic gradient (e) where the inflow temperature is unaltered from field measurements

The inclusion of plausible advection rates roughly doubles the modelled permafrost degradation rate relative to that with only conductive input (from 9.1 cm/yr to 17.5 cm/yr). McKenzie & Voss (2013) also report that conduction and advection have similar magnitude effects on permafrost thaw rates, though their analysis focused on taliks beneath lakes and groundwater exchanges were the source of (vertical) advection. Lateral flows as the source of advection similar to the ones modelled here were considered by de Grandpré *et al.* (2012), where advection contributed a significant amount of heat to thaw permafrost under a road bed, though the relative contribution of advection was not computed.

The assumption of a constant gradient in the simulations of a bog and a fen neglects the variability in this data. In the case that a talik connects two wetland features, this assumption is reasonable. Though there may be seasonal changes in pressure (especially during the freshet), there is enough water stored in each feature to sustain flow over the winter without large changes in gradient. However, a small isolated talik adjacent to a wetland (with a single connection) likely does not have the storage capacity to sustain flows over winter, so the impacts of advection would be less in these cases. Observed rates of permafrost degradation at the SCRS are slower in these cases.

To better understand the dependence of thaw rate on temperature and rate of advection, 42 simulations with consistent *stable* boundary and *talik* initial conditions were completed for a range of advective flow rates and incoming temperatures. Figure 4.9(d) and (e) shows the change in permafrost degradation rate due to increasing mean advection temperature and hydraulic gradient. Permafrost degradation rate for each simulation was calculated as the slope of a linear fit to the maximum annual depth to permafrost over a 10 year simulation. The inflow temperature was sampled between T_{in} -1 °C and T_{in} + 3 °C, where T_{in} is the mean daily inflow temperature representative of a bog which never drops below 1.2 °C.

Thaw rates are comparably sensitive to changes in hydraulic gradient and advection temperature, where an increase in gradient or temperature leads to a clear increase in permafrost thaw rate, as may be expected from examining equation 4.3. Both relations are linear in the range unaffected by changes in hydraulic conductivity due to partial ice saturation. As seen in figure 4.9(e), at low flow rates, pore ice formation limits the hydraulic conductivity and thus the impact of hydraulic gradient on thaw rate is suppressed (up to a gradient of approximately 0.005). In the field, this decrease in hydraulic conductivity may lead to a resulting increase in hydraulic gradient as water movement becomes limited, pushing advection out of this non-linear, low-flow region. Increases in hydraulic gradient may also be expected during the freshet when ice and snow prevent overland flow and result in ponded water on the landscape, though many flow pathways would be clogged with frozen pore water. Such complicated interplay between partially frozen soils and

groundwater flow is similarly documented in de Grandpré *et al.* (2012), and can aid in explaining the anomaly in linearity of response to increasing hydraulic gradient. The deviation from the linear relation may also be attributed to a *talik* initial condition with *stable* boundary conditions and so some error in equilibration may be expected for relatively low flow rates and temperatures.

4.4 Synthesis

4.4.1 Drivers of Talik Formation

A comparison of figures 4.5, 4.6 and 4.7 indicate that soil moisture conditions and changes in SWE have effects of similar magnitude on the formation of taliks over the expected range of parameter values observed in the field. The magnitude of the resulting change in talik thickness is similar to that observed for a change in ground surface temperature of 0.5 °C. This suggests that with projected climate warming in Northern Canada (Solomon *et al.*, 2007), talik formation is likely regardless of changes in soil moisture and SWE regimes.

Model simulations indicate that small variability in forcing even over a single season can lead to permafrost degradation and talik formation. This sensitivity to perturbation is not unique to the SCRS, where the permafrost can be classified as ecosystem protected, as defined by Shur & Jorgenson (2007). Robinson & Moore (2000) describe how changes to the surface layer of peat due to wildfire can lead to permafrost degradation, but other disruptions to it such as an abnormally wet summer, the removal of a tree canopy, or anthropogenic compaction of the surface layer are also very likely to lead to talik formation (through the process shown in figure 4.5).

Though soil moisture, ground heat flux and SWE are thought to be the main drivers of talik formation, there were other factors which should receive attention. One such factor is the timing of the snow-covered period as a control on the refreeze process. Though not simulated here, it is anticipated that a prolonged delay between the onset of freezing conditions and the arrival of substantial snowfall would result in enhanced refreeze depths as the absence of snow would not only increase the conductive heat transfer through the soil surface, but would also leave the bare surface exposed to convective heat transfer. Measurements and simulations by Zhang *et al.* (2008a) confirm this, showing earlier and deeper refreeze in a year with late snow onset. This is observed in the field as the sloping edges of channel fens which are scoured by wind in early winter generally exhibit refreeze about 10 cm deeper than other, more protected, areas in the landscape.

4.4.2 Talik Formation as a Tipping point

Modelling results from section 4.3.3 demonstrate that once a talik is present in the soil column, only decreases in soil moisture (with seasonally dry summers and wet winters) are able to initiate permafrost recovery in the studied discontinuous permafrost peatlands environment. The other cases including cooler mean annual surface temperatures and decreases in SWE (within ranges observed at the SCRS) did not lead to any talik thinning, though would lead to permafrost recovery if allowed to exceed the likely range at the field site. Comparing results presented in sections 4.3.2 and 4.3.3 leads to the generalization that changes in mean annual temperature results in increased permafrost degradation rates once a talik is formed. Changes to soil moisture and SWE caused slower talik thickening after talik formation due to the increased soil column depth, but did show more sensible heat storage.

Advection modelling tests (section 4.3.4) showed that lateral flow through a connected talik significantly increases thaw rates which has been verified by field observations. Such flow pathways are permanently active year-round and can contribute significantly to permafrost thaw in a manner that is likely irreversible, since advection can only supply energy to frozen ground. McClymont *et al.* (2013) document advection as a dominant control on permafrost thaw, but in this work, as in others (e.g. Walvoord & Kurylyk (2016)), advection is the result of flows along the edges of peat plateaux, along channel fens, or in the moat of collapse scar bogs. Here it is proposed that advection through a talik connecting wetland features (i.e. a bog connected to a fen via a talik) would also lead to thermal erosion of permafrost at the top of a permafrost body. This has the potential for a much higher hydraulic gradient and subsequent flow rate than may be expected in a channel fen in this low-relief landscape (with a typical gradient of 0.0032, Stone (2018) as compared to a gradient of 0.01 measured between features connected by a talik), especially over winter when ice and snow-load can increase subsurface pressure in the landscape.

Given the drivers of talik formation and evolution identified above, the model was applied using observed field conditions to predict likely changes in permafrost in different parts of this landscape. These conditions are the *plateau* initial condition with *stable* boundary condition (Stable Plateau) and *talik* initial condition with *degrading* boundary conditions (Degrading Talik).

Stable Plateau

None of the 20 realizations of surface boundary conditions constructed using the seasonal autoregressive model of the *stable* condition discussed in section 4.2.3 with an initial water

table at a depth of 0.5 m below the surface resulted in the formation of a talik in the 10 years modelled. The simulations did however show potential for active layer thickening, as reported in Shiklomanov *et al.* (2012). There was an increase in maximum thaw depth (with complete refreeze) of approximately 0.3 cm/year over the entire 10 year simulation, with the same average rate in only the last 5 years of simulation for the stable condition. Figure 4.10(a) shows the distribution of rates of permafrost degradation for this *stable* boundary condition on the left for the entire 10-year simulation (grey), and then only for the last 5 years of simulation (black). Agreement between these supports an appropriate selection of initial conditions. The small annual loss of permafrost in a 10 year simulation indicates that the current condition of peat plateaux results in permafrost degradation. Given long enough periods forced with these consistent boundary conditions, it is expected that the permafrost will begin to degrade, as discussed for this field site in Quinton *et al.* (2018). This is analogous to results found by Briggs *et al.* (2014) who shows that though permafrost aggradation has been observed in draining lakes, this phenomenon is only transitional as the permafrost is an artifact of the groundwater regime and shading from shrubs, and it is expected to thaw within the decade.

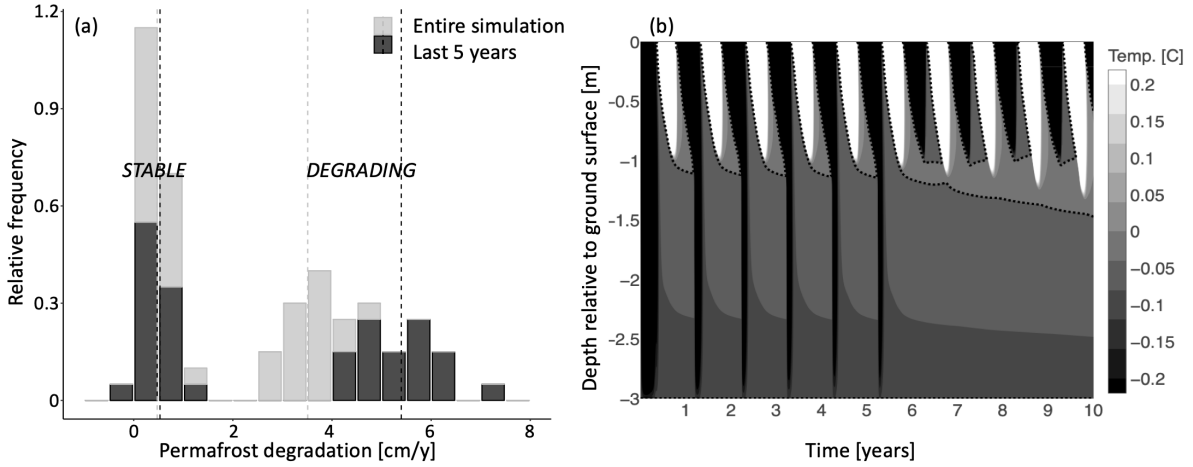

Figure 4.10: (a) Stacked relative frequency distribution of permafrost degradation rates modelled with *stable* boundary condition (left) and *degrading* condition (right). Vertical dashed lines indicate the mean permafrost degradation rate for the entire simulation (10 years) or for only the last 5 years of simulation. (b) Talik formation (for the *degrading* boundary condition) shown as a temperature contour plot. Note that the incomplete refreeze in the sixth winter initiates the formation of a talik, which then provides a previously absent pathway for advection.

At the SCRS there is clear evidence of degrading permafrost. Evidence of aggrading permafrost is sparse and unconfirmed, suggesting that permafrost formation may not be possible in the current climate unless significant dewatering of the landscape occurs. Though sections of permafrost peat plateaux appear stable, they are extremely vulnerable to change as the underlying permafrost is not in equilibrium with the current climate. Given the slow rate of permafrost degradation identified from models with the current boundary conditions, it is only a matter of time before this ecosystem protected permafrost degrades even without the additional mechanisms discussed above. Using tree canopy as a proxy for permafrost (Carpino *et al.*, 2018), aerial imagery from this study site was compared from 1947 to 2008, showing a 38 ± 8 % decrease in permafrost coverage (Quinton *et al.*, 2011), indicating that this degradation is already underway. This is echoed in the findings of Kwong & Gan (1994) describing a northward moving southern limit of sporadic and discontinuous permafrost due to increases in mean annual temperature.

Expanding Talik

Figure 4.10 (a - *degrading*) shows the response of an initially talik-free system to the *degrading* boundary condition. The formation of a talik increases permafrost thaw rates, while also increasing the variability in thaw rate. The variance in simulated thaw rates is significantly greater in the case with a talik for two possible reasons: 1) These simulations include the formation of the talik, as shown in figure 4.10(b), which is sensitive to changes in boundary conditions; and 2) The formation of a connected talik allows for advection which is further modified by the presence of ice in the soil column affecting the permeability. It is not appropriate to compare the permafrost degradation rate in the stable case directly to the talik case as the boundary conditions in each scenario differ. The impact of talik formation on permafrost thaw can, however, be discussed by focusing only on the talik condition simulations.

An example of talik formation can be seen in figure 4.10(b). The first five winters of this simulation involve complete refreeze and subsequent cooling of the underlying permafrost. As soon as a talik is formed in year six, the underlying permafrost remains near the measured freezing point depression and above the temperature at which the freezing function used in the model reaches residual unfrozen saturation. This simulation aptly demonstrates that permafrost degradation clearly accelerates once a talik forms, as can be seen to the right of figure 4.10 (a - *degrading*). This is anticipated for three reasons: 1) the activation of an advective flow pathway, 2) a reversal of the temperature gradient, and 3) (in the case of field measurements) subsidence of the ground surface, resulting in a positive feedback leading to increased soil moisture.

The presence of a talik with a temperature at or above the zero-point depression alters the ground temperature profile such that the surface of a permafrost body always experiences a positive (or zero) temperature gradient (Connon *et al.*, 2018). The permafrost at or below the freezing point depression is always colder than the overlaying thawed talik, and consequently gains thermal energy year-round. This can be seen in figure 4.1(a), which shows the (co-linear) maximum and minimum annual temperatures measured over a talik. The talik is apparent in the figure as the region (in grey) that never cools below the zero point depression, but is warmed in the summer. Below this region, the permafrost is essentially isothermal in the zero curtain, indicating that it is undergoing phase change and is unable to lose energy to the atmosphere. In combination with advection, this can lead to the overwinter permafrost thaw observed in the SCRS. One such connected talik feature connecting a bog and fen has exhibited 21 cm of thaw between August 2016 and May of 2017 and 13 cm of thaw between September 2017 and April of 2018.

In the field, the positive feedback of permafrost degradation after talik formation is furthered by an increase in soil moisture due to ground surface subsidence. As shown in section 4.3.2, this increase leads to slightly enhanced thaw rates, but increased soil moisture also counteracts the only realistic modelled conditions able to promote permafrost recovery - an unsaturated soil column. More energy is able to reach the permafrost table both due to the increased thermal conductivity, as well as a thinning canopy as the black spruce (*Picea mariana*) suffer from water-logging of their root networks (Quinton & Baltzer, 2013). The depressions formed allow for preferential accumulation of snow, which was shown to trigger permafrost thaw. In this sense, the formation of a talik can be seen as a tipping point leading to accelerated permafrost thaw rates with little chance of recovery.

4.4.3 Permafrost Degradation in the Landscape

Given the impacts of soil moisture, advection and the existence of taliks on permafrost degradation rates, it is expected that the rates of permafrost degradation should differ across landscape features. Sjöberg *et al.* (2016) suggest that the relative importance of thaw mechanisms including conduction and vertical or lateral advection vary both seasonally and across different peatland landscape features. To better capture thaw in each part of the landscape, a final modelling experiment was undertaken. In this experiment, advection was forced with temperatures based on profiles observed in a bog and a fen at the SCRS, similar to the simulations used to generate figure 4.9(a), (b) and (c). Temperature boundary conditions were consistent with the stable condition for the plateau landscape type, while the three talik conditions (isolated, connected bog and connected fen) used the a boundary condition constructed using the autoregressive model constructed for the talik condition.

Modelled thaw rates are compared to thaw measured as change in end-of-season depth to permafrost using a frost probe at different locations in the landscape. This comparison is shown in figure 4.11, where field data were categorized according to the type of talik. Note that the high variance in measured thaw rates in connected taliks adjacent to fens and bogs is likely due to variations in flow rate and temperature at different monitoring locations. The modelled thaw rates for taliks assume a saturated soil column. This explains the slight over-estimation of thaw rates in isolated taliks, which are generally wetter than the surrounding stable plateau, but are rarely completely saturated in the field. Permafrost degradation is incrementally faster as advection rates and temperatures increase in bogs and fens, as demonstrated in figure 4.9.

The slow but positive thaw rate observed on a 'stable' plateau is indicative of a system in disequilibrium with the climate. The gradual permafrost loss either as active layer thickening or as talik formation points toward an eventual near-complete loss of permafrost from the system. Once a talik is formed, the rate of permafrost degradation is notably more rapid due to the combined effects of higher thermal conductivity, advection, canopy degradation, thermal storage in taliks, and ground surface subsidence.

At the landscape scale, permafrost loss is likely to emanate outward from existing wetland features, especially fens that have higher flow rates and temperatures, while preferentially forming the hydrologic connections between wetlands where the hydraulic gradient is greatest, as documented by Connon *et al.* (2015). Not only will the edges of permafrost cored peat plateaux be eroded, but depressions are likely to grow into isolated taliks which will expand and interlink, leaving small isolated hummocks of permafrost as described in Quinton *et al.* (2017). These isolated permafrost features are documented in the sporadic permafrost region by Woo (2012).

The long term evolution of discontinuous permafrost is complex and influenced by additional influences not included in the boundary conditions used here, hence the simulation duration was limited to a decade. Such influences include gradual wetting of the soil profile due to subsidence, increase in surface temperature because of canopy loss, increased snow accumulation due to depression formation, and lateral flow rates and inflow temperatures that may vary based on upstream conditions. Under these more complete conditions, long-term simulations may be more meaningful, but it is likely that the positive feedbacks associated with talik-influenced permafrost thaw presented here would still play a critical role. Further work is needed to better quantify the role of isolated and connected taliks at a longer time scale, and it is anticipated that multi-dimensional modelling may be necessary to inform a more complete understanding of talik influence on long term permafrost evolution.

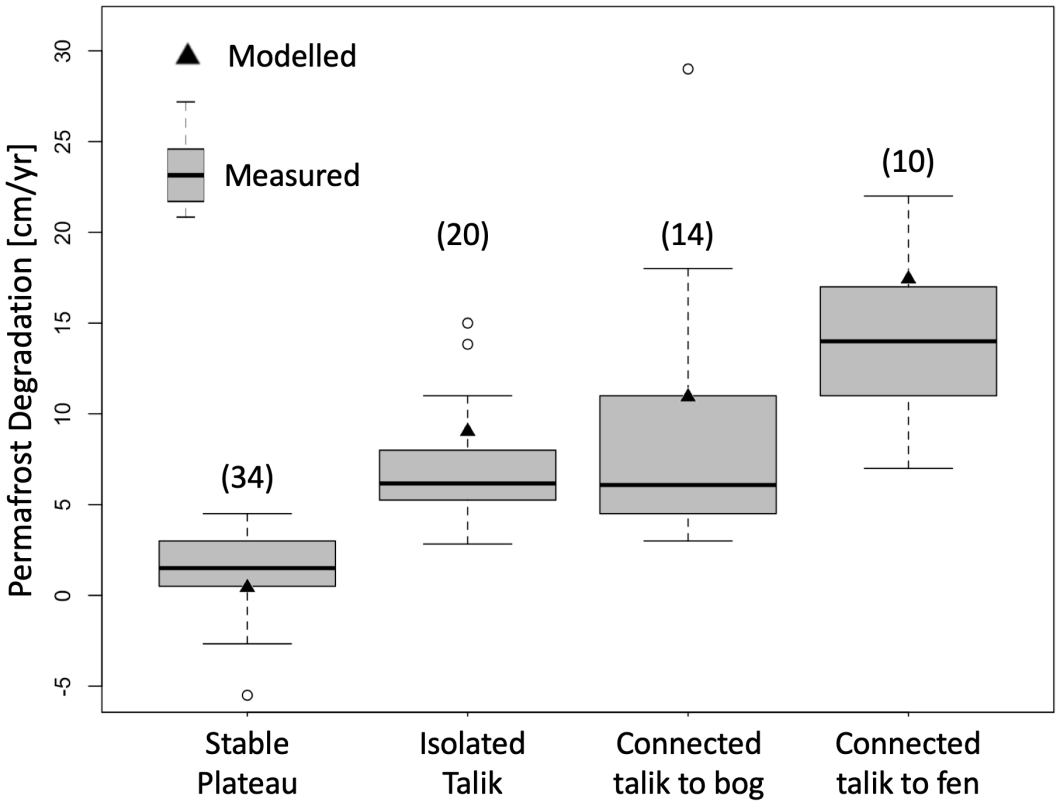

Figure 4.11: Comparison of permafrost thaw rates in different portions of the landscape. Box and whisker plot shows spread in measured talik development data, while triangles show average modelled value for each type of talik. A total of 78 locations were measured semi-annually over the course of 8 years to generate the permafrost degradation rate data. Note that points fall outside of 1.5 times the interquartile range, the upper bound of the whiskers.

4.5 Conclusion

This study used a combination of extensive field data and 1-D modelling to investigate the formation of isolated taliks beneath the active layer. A freeze-thaw model was developed that reproduces temperature data and refreeze depths in discontinuous permafrost peatlands. This model was used to provide a rigorous evaluation of the controls on isolated talik formation, which is prevalent in discontinuous permafrost environments and can be driven by soil moisture, snow accumulation, and/or seasonal temperature trends. Soil moisture, ground heat flux, snowcover, and advection were all found to affect the formation of taliks in different contexts. It was deemed difficult to identify which factor is dominant as they often occur simultaneously and are inter-dependent. However, wet conditions, deep snow, and warmer soil surface temperatures were found to increase the probability and rate of isolated talik formation. Isolated talik formation was shown to be a tipping point in permafrost degradation, leading to accelerated permafrost thaw which is unlikely to recover once the talik is formed. Once a talik is formed, permafrost degradation can be accelerated by subsurface flows through the talik (especially if it forms a pathway between wetland features), increased soil moisture, increased ground heat flux, and snow accumulation due to a critical lack of energy loss from the permafrost to the atmosphere overwinter. Only unsaturated conditions (highly unlikely in permafrost degrading within a wetland system) were found to lead to permafrost recovery, resulting in accelerated and potentially irreversible permafrost thaw in this environment. It may therefore be pertinent to consider talik formation in models of other permafrost environments, especially at larger scales where these processes are often neglected, but may lead to significantly different permafrost conditions.

Chapter 5

Passive flux meters as a measure of water movement in low-gradient, variably-saturated cold regions landscapes

Statement of contribution

The following chapter is written based on the following article:

Devoie, É. G., Craig, J. R., Connon, R. F., and Quinton, W. L. (2020). Passive flux meters as a measure of water movement in low-gradient, variably-saturated cold regions landscapes. *Hydrological Processes* DOI: https://doi.org/10.1002/hyp.13900

This paper presents the results of a field study implementing passive flux meters in a low-gradient permafrost peatland landscape. In this paper, I compare the current Darcy-flux approach to computing subsurface flow in the system to data collected using these instruments. I prepared the field methodology, and performed the data analysis. I also prepared the manuscript. Dr. Craig provided key insights during manuscript preparation. Drs. Quinton and Connon assisted in implementation of field studies and provided feedback on the manuscript.

5.1 Introduction

Field estimates of saturated lateral subsurface fluxes are typically determined through the application of Darcy's law, which depends on a characterization of the spatially and temporally variable hydraulic gradient and hydraulic conductivity. This method is subject to several sources of uncertainty. Measurement of fluxes in variably saturated porous media using the Darcy-Buckingham equation is even more uncertain, as local gradients may dominate and conductivity varies dramatically with saturation (Winter, 1983). Though methods exist to determine the unsaturated hydraulic conductivity (e.g. Ankeny *et al.* (1991)), the water table position evolves over time, making the cross-sectional area of the saturated profile hard to predict. Additionally, water retention curves are known to demonstrate hysteretic behaviour which affects the hydraulic conductivity (Naasz *et al.*, 2005). Lastly, in cold regions, hydraulic conductivity is also sensitive to partial and complete freezing in soils (Lebeau & Konrad, 2012), while the measured hydraulic gradient is affected by temperature gradients, ice-capping and snow accumulation on wetland features, making over-winter flux predictions unreliable.

Annable *et al.* (2005) proposed a novel method for measuring temporally averaged subsurface flow using Passive Flux Meters (PFMs). This method deploys a tracer-impregnated, activated charcoal filled cartridge into a well or piezometer. Subsurface flow through the meter causes the de-soprtion of multiple tracers at (different) known rates, allowing the user to determine the flux of water through the cartridge given the period of installation (Hatfield *et al.*, 2004, 2002). These PFMs have predominantly been used in contaminant monitoring as they contain activated carbon, allowing contaminants to be sorbed while the known tracers are de-sorbed (Haluska *et al.*, 2018; Desormeaux *et al.*, 2019; Klammler *et al.*, 2007; Kunz *et al.*, 2017; Lee *et al.*, 2007; Hatfield *et al.*, 2004). Not only are these instruments capable of reporting mass transport of many diverse contaminants and nutrients, but they provide reliable time-integrated subsurface flux measurements.

PFMs have mainly been used in relatively high flux groundwater studies, and have not yet been deployed under freezing conditions. Though they have been used in a glaciated watershed to determine fluxes in various soil zones (Benton *et al.*, 2018), the study was of short duration, and did not include the freezing season. The use of PFMs in low hydraulic gradient wetlands subject to permafrost and seasonal freeze-thaw is considered here as a means of estimating otherwise highly uncertain water fluxes through variably saturated, variably frozen soils. Results from the PFMs (with uncertainty bounds) are compared to gradient-based measurements for the thawed season, and unsaturated and over-winter data are presented for this novel method.

5.2 Study Site

This study was undertaken at the Scotty Creek Research Station (SCRS) located approximately 70 km south of Fort Simpson in the Northwest Territories, Canada, as described in Section 3 (Quinton *et al.*, 2017). Subsurface flow through talik features is determined by the seasonally variable hydraulic gradient between the wetlands. Understanding the magnitude and direction of subsurface flow is critical in defining the water balance in this flat landscape. Three talik sites were selected, two between a bog and a fen, and one between two bogs, where subsurface flow was suspected based on permafrost thaw rates and measured hydraulic gradients.

5.3 Methods

Five 1.2 m long passive flux meters (Hatfield *et al.*, 2002) were installed in the three sites described above, where two instruments were installed at each site except one bog-fen connection. The exact location of installation was chosen such that the permafrost table was approximately 1.2 m below the ground surface, such that the PFM recorded flow through the entire supra-permafrost layer, as shown in schematic figure 5.1. For smooth installation, a 2" pilot hole was augured to the permafrost table before the PFM was installed in a slotted PVC well slotted from its base to approximately 15 cm below the ground surface. Due to the known high hydraulic conductivity of peat, it was assumed that the PFM would not act as a preferential flow path, and should therefore not alter the subsurface fluxes. Additionally, a flow divergence calculation similar to that presented in Hatfield *et al.* (2004) was computed to find $\alpha = 2$, indicating mild flow convergence, and indicating results may be a slight over-estimate of actual flow. This is due to an average saturated peat hydraulic conductivity of 1.6 m/d, and the given properties of the PFM. The top of the casings were sealed against vertical water inputs from precipitation. All PFMs were installed within two days of August 23, 2018.

The passive flux meters were left over winter, and two were removed within two days of April 10, 2019, while the remaining instruments were retrieved at the end of the thawing season, within two days of September 19, 2018. In order to remove the PFMs in the spring (while the ground was still frozen) small resistance heater strips were affixed to an aluminum rod that was inserted into the central tube of the PFM and left for 24-48 hours attached to a marine cycle battery and a solar array. This sufficiently thawed the cartridge to allow it to slide out of the well. Once removed, the PFMS were sub-sectioned into two segments in the spring, and five segments in the fall. Sections were evenly spaced along

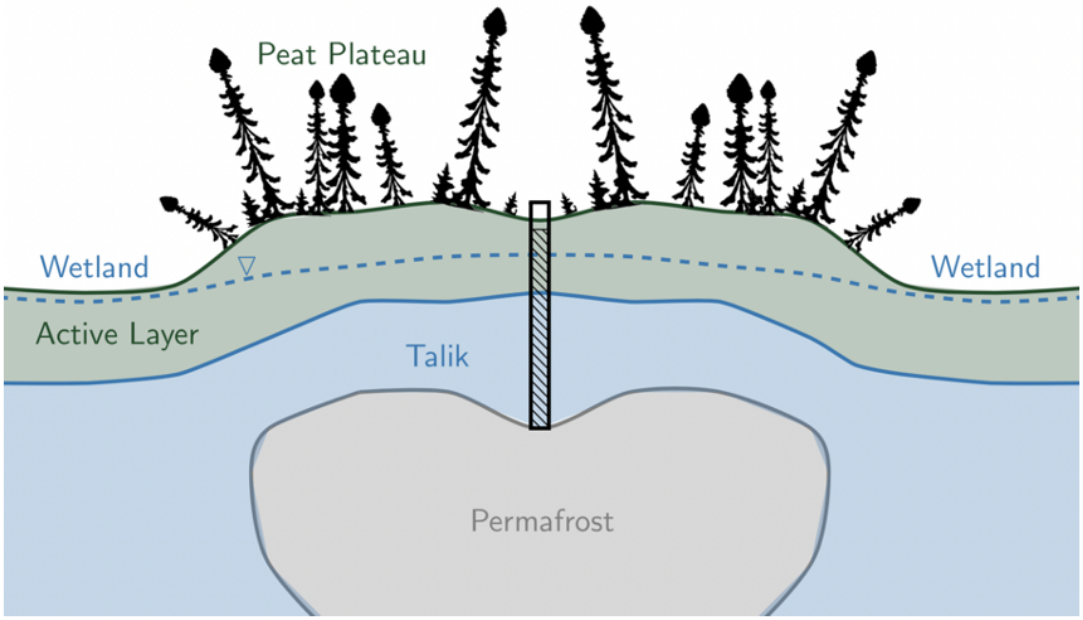

Figure 5.1: Schematic figure describing installation setup of PFM in connected talik features.

the PFMs, resulting in two 60 cm long sections for the over-winter measurements, and five 24 cm sections for the fall measurements. Sorbent from each sampling depth was well mixed, sub-sampled into 500 mL containers, and carefully packaged for analysis, using the methodology set forth by Hatfield *et al.* (2004). Once the samples were collected, they were shipped to the PFM manufacturer EnviroFlux for tracer analysis to determine the total flux through the meter over the period of installation.

Flux measurements were compared to the current standard approximation of groundwater flow - an application of Darcy's law. The hydraulic gradient for this approximation is determined using pairs of HOBO UL20 pressure transducers which report water level in adjacent wetland features, and the saturated hydraulic conductivity. Pairs of water level recorders (WLRs) were installed at each study site up-gradient and down-gradient from each PFM to determine the gradient. Water level was recorded at half-hour intervals for the entire study period. Saturated hydraulic conductivity was determined at different depths and in different locations in the study basin using slug tests and falling head tests. For these tests, a pressure transducer recording at 1 s intervals allowed for high resolution water table position tracking in the drive-point piezometer. These data were augmented

with Guelph permeameter tests in the high-conductivity near-surface peat, as reported by (Quinton *et al.*, 2008).

5.4 Results

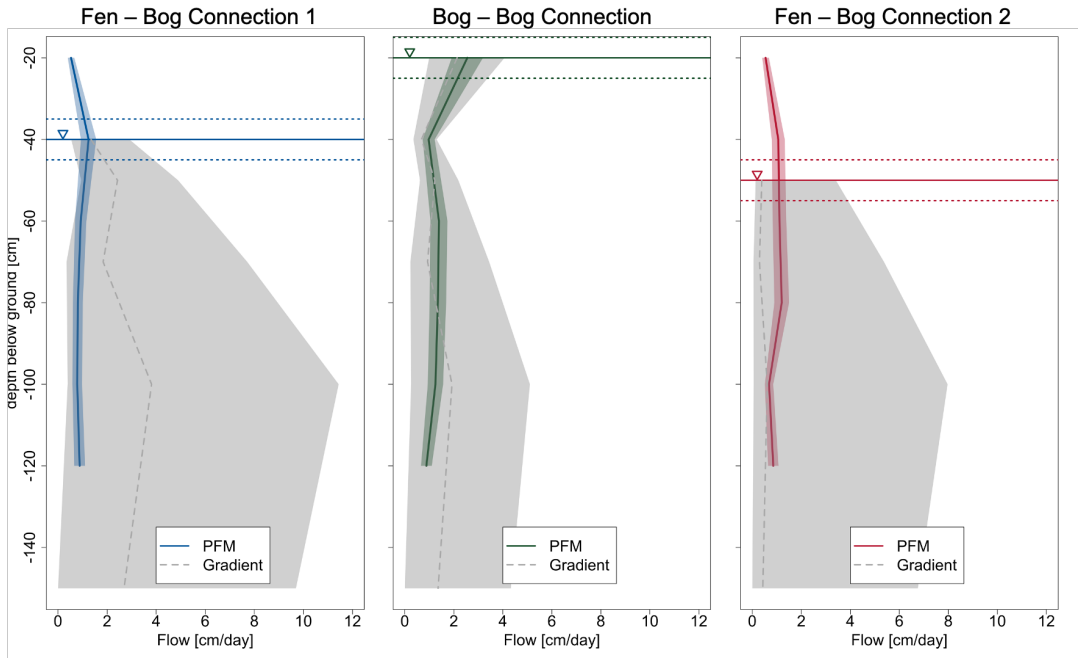

Figure 5.2: Comparison of summer flux at three sites using PRMs (coloured lines) and the K_{sat} & ∇h technique (dashed grey lines and shaded region). Average water table at each site indicated with a horizontal line, note that this water table is not Representative of the wetlands but rather the plateau features separating them.

Figure 5.2 compares the average summer flux measured using PFMs and the gradient-based approach at all three study sites. The estimated uncertainty in the passive flux meter readings based on error bounds supplied by the manufacturer (with maximum shown

as the shaded coloured region) is small compared to the combined uncertainty in the measured hydraulic gradient and saturated hydraulic conductivity (shown as shaded grey regions in figure 5.2). The uncertainty in measured gradient combines the sensitivity of the WLRs, and the Differential Global Positioning System (DGPS) elevation data and separation resulting in up to 2% error. The hydraulic conductivity is much more uncertain as measurements vary spatially and temporally (due to ice content in the subsurface). In order to capture the spread of values observed at the SCRS, all of the data collected using in-situ slug and pump tests, as well as laboratory analyses were combined by depth, and for each depth the range between the maximum and minimum hydraulic conductivity reported at that depth was used as a measure of uncertainty. A combination of these two uncertainties results in the grey shaded region in figure 5.2.

The seasonal PFM data is shown in figure 5.3, indicating that 28% of annual flow occurring over-winter at Bog-Fen Connection 1, and 13 % at the Bog-Bog Connection. The winter flux and summer flux in the saturated region are similar between sites, indicating relatively low spatial variability in time-integrated flux. The over-winter data are not compared to the gradient-based method because the over-winter gradient is unreliable due to pressure artifacts in which vertical moisture movement to the freeze/thaw front caused by near-freezing temperatures (induced by the Clausius-Clapeyron relation, (Kurylyk & Watanabe, 2013)) and snow loading, and there was no hydraulic conductivity data available for either unsaturated, partially frozen or completely frozen profiles.

5.5 Discussion

The gradient-hydraulic conductivity method of estimating flow uses a spatially integrated gradient and point measurement of (saturated) hydraulic conductivity, though this could be spatially averaged given data availability unavailable at this study site. This results in high measurement uncertainty when compared to the PFM method which reports a temporally averaged point measurement. The PFM manufacturer suggests an error of up to $\pm 25\%$ due to uncertainty in sorption/de-sorption rates, spatial variability of hydraulic properties and flow paths and well geometry (shown as coloured shaded region in figures 5.2 and 5.3), thought the error may be as low as 5 %, depending on the degree of de-sorption (Hatfield *et al.*, 2004). These error estimates were provided by the PFM supplier, and may not include specific effects due to ice formation and de-saturation of the profile. Figure 5.3 compares the summer flows for all three study locations. Below the water table, these measurement ranges are overlapping indicating that the spatial variability of flow at each site is likely captured within the error bounds placed on the measurement.

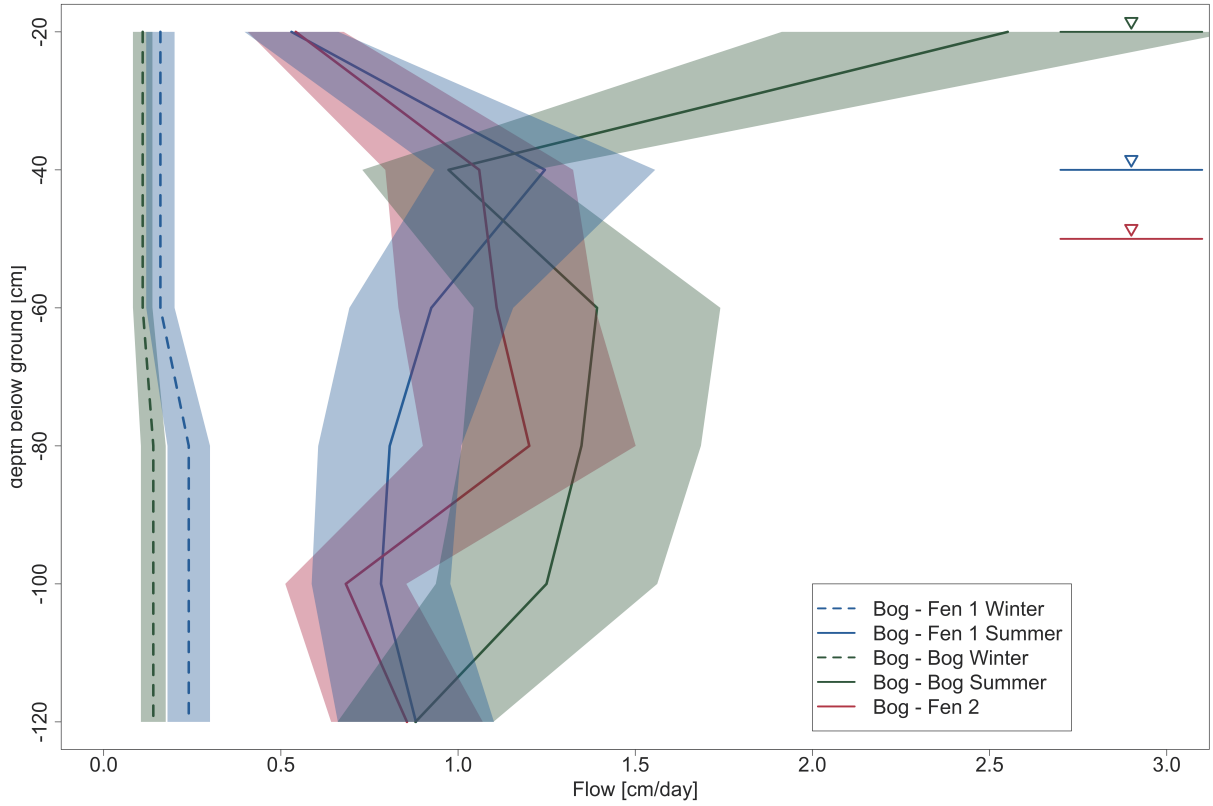

Figure 5.3: Comparison of mean PFM-estimated summer flux at all sites and winter flux for two of the three instrumented sites.

Significantly more sources of measurement error are present in the gradient-based estimation. Firstly, the measurement of the gradient is subject to measurement errors stemming from pressure transducer accuracy and barometric pressure correction as well as DGPS accuracy in both elevation and euclidean distance between sensors. Additionally, the over-winter gradient provided from the sensors is unreliable due to near-freezing temperature induced changes in pressure, ice cover in the wetland where wells were installed and snow load. The hydraulic conductivity is also subject to measurement error. It is made as a point measurement in both space and time, and is known to be highly spatially variable. Not only are slug tests and pump tests susceptible to multiple sources of measurement error due to well screen placement and geometry, boundary effects and well-skin effects (Hyder *et al.*, 1994), but hydraulic conductivity known to be highly spatially vari-

able (Lewis *et al.*, 2012; Sudicky, 1986; Gupta *et al.*, 2006), and repeated measurements made under identical conditions can report highly varying values depending on antecedent conditions (Chappell & Lancaster, 2007). The available data is only applicable to a strictly saturated and thawed soil. It is therefore a gross underestimation of uncertainty in unsaturated or partially frozen systems. Finally, as freezing occurs, the area available for flux shrinks at some unknown rate due to reduced (and unknown) hydraulic conductivity in frozen soils. Gradient-based flow estimation is therefore not only subject to higher uncertainty, but it is unable to provide flux estimates in unsaturated and/or frozen conditions.

Figure 5.3 shows that the PFMs have the potential to address both of the shortcomings of the gradient-based approach. The summer data from the bog - bog connection aligns very well with the gradient-based calculation in figure 5.2. This location maintains a water table near the soil surface, however, the other two sites have an average water table position at a depth of 40 cm or more (figure 5.2), and the surface flux cannot be estimated using the saturated soil properties. In these sites, the near-surface flux reported by the PFMs is significantly lower, but cannot be compared to an estimate using the gradient-based approach. Note that the flows above the water table may be artificially inflated due to seasonal fluctuations in water table as well as the measurement resolution of the PFM - flux was interpolated between the measurement depths that were spaced at least 20 cm apart. The measured flux through the PFM may be affected by the capillary barrier effect, as described by Stormont & Anderson (1999), where preferential flow may occur within the activated carbon of the PFM due to its low porosity compared with the peat. That being the case, Price & Ketcheson (2009) discuss the importance of moisture wicking in unsaturated peat as a mechanism for vertical water transfer, and Quinton *et al.* (2009) discuss the structure of peat which lends itself well to unsaturated vertical water transfer, and may therefor limit the effect of boundary flow. Diffusive effects may also lead to errors in PFM flow estimates, especially for low-flow conditions. Hatfield *et al.* (2004) demonstrated using the Peclet number that fluxes of 0.7 cm/day were the lower limit that could be measured using PFMs without considering diffusive effects. Figure 5.3 shows that the reported fluxes over the summer months are greater than this limit. More work needs to be done using PFMs in unsaturated environments to better characterize unsaturated fluxes.

Instruments do exist that allow for the measurement of soil tension and unsaturated hydraulic conductivity, though estimates of unsaturated hydraulic gradient are extremely uncertain due to soil heterogeneity (strongly affected by pore size distribution which is not spatially homogeneous) (Richards, 1941; Hayashi *et al.*, 1997; Hallett *et al.*, 2004). Tensiometers capable of reporting unsaturated soil tension are however confounded by the freeze/thaw process due to its impact on pressure gradients (Kurylyk & Watanabe,

2013), as well as potential freezing damage to the instruments (Fredlund *et al.*, 1991). Due to fluctuations in water table position, variability in unsaturated hydraulic conductivity depending on soil material, and hysteretic behaviour based on antecedent conditions, the PFMs are a valuable alternate method to estimate near-surface horizontal flux.

Over-winter mean fluxes measured using the PFMs are reported as dashed lines in figure 5.3. This flux cannot be calculated using gradient-based methods, but aligns well with theory. The refreeze depth at Bog - Fen Connection 1 is 52 cm, and is 56 cm at the Bog - Bog connection. This is reflected in the near-zero flux reported at the surface. Bog - Fen Connection 1 thawed earlier than the Bog - Bog Connection due to the presence of warmer fen water, resulting in the higher winter flows reported in this site. Higher flow rates at depth confirm suspected over-winter talik flow, as near-surface flows are higher during the thawed season. Additional evidence for this flow exists in the form of over-winter permafrost degradation observed at Bog - Fen Connection 1, where 21 cm of thaw were observed between August 2016 and May of 2017 and 13 cm of thaw between September 2017 and April of 2018. The ability to quantify over-winter flux through talik connections will allow to better quantify the role of advection in driving permafrost degradation, as outlined in Devoie *et al.* (2019); Walvoord & Kurylyk (2016); McClymont *et al.* (2013).

Prior applications of PFMs show that the main shortcoming of these instruments is that long-term measurements are subject to more error as the tracer concentrations may be depleted below the linear tracer elution limit (Hatfield *et al.*, 2004). The presence of flow reversals while a concern for contaminant monitoring (Hatfield *et al.*, 2004), it is not a concern for flux measurement as total flow through the subsurface is the quantity of interest, and the direction of the flow is not relevant for calculations of advective heat transport etc..

5.6 Conclusion

PFMs are shown to provide measurements of subsurface flux consistent with current field measurement techniques, while reducing measurement uncertainty. This technology can estimate flux rates in variably saturated and variably frozen soil columns, whereas the gradient-based technique is likely to fail under these conditions. Though results are presented for discontinuous permafrost peatlands, they may be transferable to other wetland landscapes in which high measurement precision is desired, soils are variably saturated and/or variably frozen. This work is the first known application of PFMs for evaluating subsurface hydrologic fluxes in cold regions.

Chapter 6

A Semi-Analytical Interface Model of Soil Freeze/Thaw and Permafrost Evolution

Statement of contribution

The following chapter is written based on the following article:

Devoie, É. G., and Craig, J. R. (2020). A semi-analytical interface model of soil freeze/thaw and permafrost evolution *Water Resources Research* DOI: https://doi.org/10.1029/2020WR027638

This paper presents a model for freeze/thaw of variably saturated soil. The model is semi-analytical in nature, numerically stable, and provides a non-equilibrium solution to the heat equation. It has clear advantages in computational efficiency when compared to equivalent finite volume models. I derived the governing equations and implemented the model in Matlab. I also prepared the manuscript. Dr. Craig initially suggested the idea, and played a key role in model development and validation. He also revised the manuscript before publishing.

6.1 Introduction

The presence of frozen soil strongly affects not only the hydrology, but also the thermodynamics, soil chemistry and ecology of regions experiencing freezing soils (Hayashi, 2013). Practically, it is essential to accurately model soil freeze-thaw because it controls many important processes including infiltration, the migration of soil moisture to the surface during freezing, winter quiescence of hydrological systems, and the destabilization of soils, especially in the permafrost region (Gray *et al.*, 2001; Harlan, 1973; Stähli *et al.*, 1999; Woo, 2012; Hinkel *et al.*, 2001). To date, the most accurate models representing freeze-thaw processes in porous media have been continuum models such as SUTRA-ICE which solve the coupled governing energy and water balance equations on a finely resolved grid (McClymont *et al.*, 2013; McKenzie *et al.*, 2007). Due to the presence of sharp wetting fronts and phase interfaces, such models are challenged by stability issues and often require very fine temporal and spatial discretization.

Though these models can often adequately represent non-equilibrium processes of soil freeze thaw, and have the ability to simulate multiple thawing fronts in complex domains, they are notoriously numerically expensive, particularly for higher dimensional problems (Slater *et al.*, 1998; Frampton *et al.*, 2013; Harlan, 1973; McKenzie *et al.*, 2007; Li *et al.*, 2010; Romanovsky *et al.*, 1997). This can make them inappropriate for large-scale modelling, sensitivity analysis, uncertainty analysis or hypothesis testing, and leads to the desire to use more efficient 1-D vertical freeze-thaw models, such as NEST and many others (e.g. Atchley *et al.* (2015); Goodrich (1978); Zhang *et al.* (2003)). Though these models solve the heat equation only in one spatial dimension, they can be coupled through source/sink terms to approximate important lateral fluxes (e.g. Hinzman *et al.* (1998)). A study site can be broken into hydrological response units (HRUs) representing zones with soil or vegetation properties, allowing for semi-distributed freeze-thaw modelling. A comprehensive review of current thermal models was completed by Kurylyk & Watanabe (2013), and found that existing models vary widely, especially in their treatment of partially frozen and partially saturated soils. These 1-D models are also still computationally demanding and conditionally stable (Kurylyk *et al.*, 2014), which can deter use in sensitivity analysis, uncertainty analysis or for simulating long timeframes and large geographic expanses.

In an effort to solve the freeze-thaw problem more efficiently, often for integration into land surface schemes, a variety of analytical or semi-analytical solutions have been proposed. These solutions make simplifying assumptions so that it is possible to solve the heat equation directly. These simplifications include neglecting sensible heat (Hayashi *et al.*, 2007), and assuming an equilibrium temperature profile (Woo *et al.*, 2004), using time-invariant soil properties (Semenova *et al.*, 2013), tracking only one freeze/thaw interface

(Krogh *et al.*, 2017; Kurylyk & Hayashi, 2016) and/or simplifying surface boundary conditions (Woo *et al.*, 2004). Freeze-thaw models based on analytic or semi-analytic solutions of the Stefan problem -boundary value problem which tracks interface in a homogeneous medium undergoing phase change- (e.g. Hayashi *et al.* (2007); Hinzman *et al.* (1998); Krogh *et al.* (2017); Semenova *et al.* (2013); Woo *et al.* (2004); Zhang *et al.* (2003)) can also track a single freezing front by assuming homogeneous saturated soil conditions. These models may be inappropriate for modelling degrading permafrost at the local scale because they assume a single (often linear) temperature profile between the soil surface and the (single) freeze/thaw front and neglect the buffering effect of an unsaturated zone. This poses a problem because it is thought that the formation of lateral taliks confined between the active layer and permafrost (perennially thawed soil in permafrost environments) is a critical component of discontinuous permafrost degradation (Connon *et al.*, 2018), while lateral talik representation requires the tracking of multiple freeze/thaw interfaces. The representation of lateral perennially thawed zones (taliks) requiring multiple freeze-thaw fronts is noted to be important in the mobilization of permafrost carbon (Walvoord *et al.*, 2019), as well as the representation of groundwater flow in permafrost environments (Wellman *et al.*, 2013).

The aim here is to develop, assess, and demonstrate the application of a computationally efficient, physically-based semi-analytical model of active layer evolution and permafrost thaw capable of simulating permafrost degradation through lateral talik formation. This robust solution to the soil freeze-thaw problem does not place constraints on temperature boundary conditions, allows multiple and dynamic freeze/thaw fronts to be tracked simultaneously, tracks only a small number of state variables, allows for non-equilibrium temperature profiles, and does not neglect sensible heat. It also allows for unsaturated near-surface soil conditions. This model is proposed as a stable and efficient component of hydrological models to describe seasonal frost, active layer and permafrost evolution.

6.2 Methods

The proposed interface model represents the ground using up to five representative domain elements, depending on the season and soil column history. A domain element consists of a frozen or unfrozen soil layer which is permitted to be saturated or unsaturated, but is distinct from the layers above or below, such as the thawing active layer in the summer, or a lateral talik sandwiched between the active layer and top of permafrost in the winter. The number and size of these elements is allowed to vary according to mass and energy balance constraints. Porous media is treated here as spatially homogeneous with properties

dictated by the pore volume occupied by ice and liquid water. The seasonal progression of a soil column is conceptually represented in Figure 6.1(a).

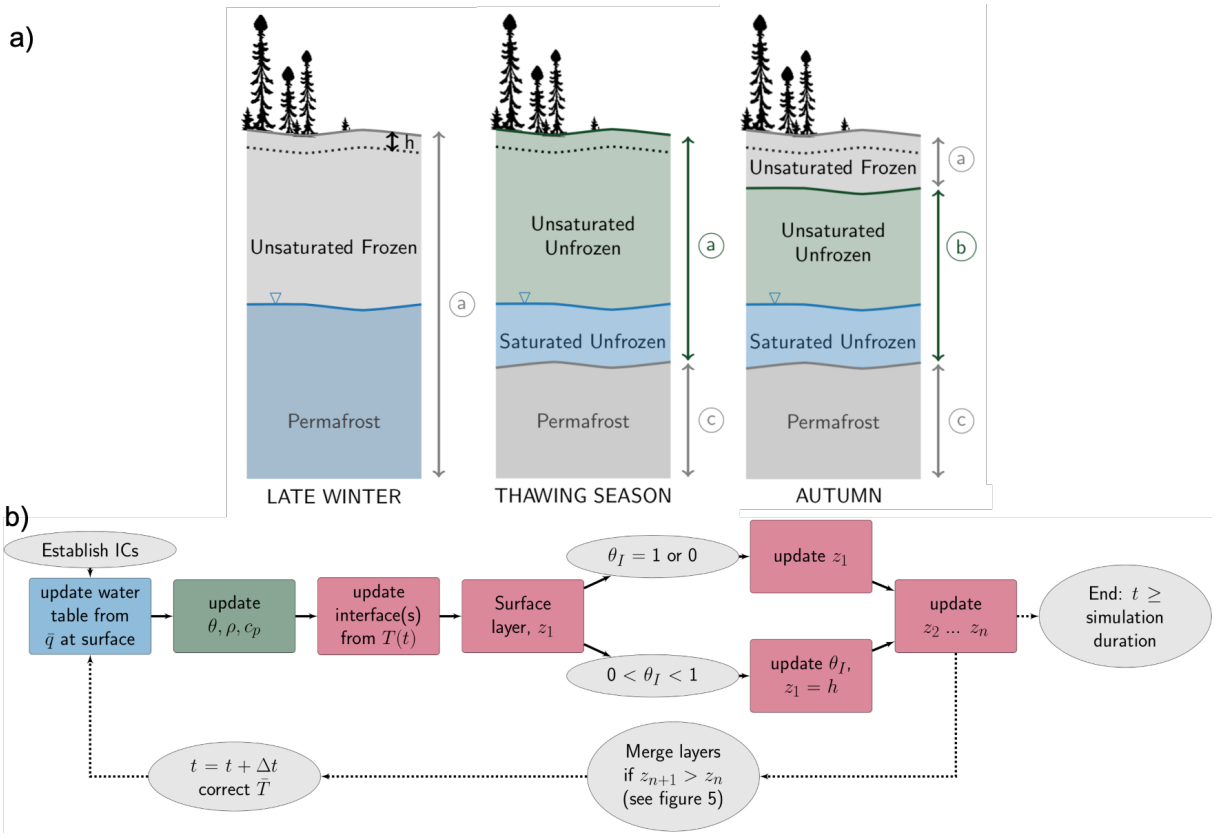

Figure 6.1: Seasonal transition in soil profile elements of the interface model representing permafrost environment, forced with surface temperature, and assuming a freeze/thaw front located at the 0° isotherm in pane (a). Letters indicate set of governing equations defining thermal regime of layers further discussed in sections 6.9: a) surface free boundary problem, b) confined problem, and c) linear problem. Flow chart representing model configuration in pane (b)

In order to simulate the model domain, 5 assumptions are made:

1. The interfaces between frozen and unfrozen elements are updated driven by an energy balance performed on the interface consistent with applying the Stefan condition.

2. The water table elevation is determined through a mass balance on the unsaturated zone including infiltration and evaporation from the soil surface, and percolation to the water table.

3. The temperature gradients at element interfaces are obtained through transient analytical solutions to the heat equation; these are used to drive the energy balance. The mean temperature is also tracked as a proxy for energy content in each element for energy conservation.

4. Under unsaturated conditions, a mass balance is applied to track the water table position and water content of the soil column, which is used to determine the bulk thermal parameter values. However, the differential equations describing the temperature profile are solved in an element which may include an unsaturated and a saturated portion.

5. In order to avoid the creation of many infinitesimally thin soil layers due to surface temperature oscillations, a single buffer layer of fixed height h (approximately 10 cm) is maintained at the surface and allowed to be partially frozen and partially saturated.

These assumptions lead the mass and energy transport in the soil column to be expressed using a set of up to nine coupled differential equations: four defining the temperature profiles in the soil column (including the buffer layer), three defining the freeze/thaw interface positions, one defining ice content of the partially frozen buffer layer and one defining the water table position. This can be compared to 100 coupled equations required for a coarsely discretized 50-layer soil column in a continuum model. The interfaces in the model domain are updated using mass and energy balance equations which are described in sections 6.2.1 and 6.2.2. These depend on the analytic solution to the heat equation which is solved for the three different thermal domain elements in section 6.2.2. The problem is then solved through an operator-splitting technique in which 1) fluxes are calculated based on the energy content and domain length of the current analytical solution, 2) these fluxes are used to update the interface positions, and finally 3) the analytical solution is updated to conserve energy in the new domain length through a dilation process discussed in section 6.2.2, as outlined in figure 6.1 (b). This method does not solve the PDE in equation 6.9 exactly, but uses a box model informed by local solutions to the PDE to evolve the system through time while conserving mass and energy.

Symbol	Units	Definition
α	[m^2/s]	Thermal diffusivity, $\kappa/\rho c_p$
η	[-]	Porosity
κ	[J/° Kms]	Thermal conductivity
λ_f	[J/g]	Latent heat of fusion
ω_n	[1/m]	Eigenvalue in analytical solution, $n\pi/L$
ρ_b	[g/m^3]	Bulk density
ρ_w	[g/m^3]	Density of water
θ	[-]	Total water content
θ_I, θ_w, θ_{res}	[-]	Ice, liquid water and residual saturations
$\bar{\theta}$	[-]	Mean water content
a_n	[-]	Coefficients in analytical solution, $2/n\pi$
$c_{p,b}$	[J/g]	Bulk specific heat capacity
$c_{p,w}$,$c_{p,w}$	[J/g]	Specific heat capacity of water and ice
e	[J/kg]	Specific internal energy
ET	[m/s]	Evapotranspiration
h	[m]	Buffer layer depth
I	[m/s]	Infiltration rate
K	[m/s]	Hydraulic conductivity
L	[m]	Profile depth
P	[m/s]	Precipitation
q	[m/s]	Water flux
t	[s]	Time
Δt	[s]	Time step
T	[° C]	Temperature
T_s	[° C]	Surface temperature
T_f	[° C]	Freezing temperature
$\bar{T}$	[° C]	Mean temperature
U	[m]	Depth to water table
z	[m]	Freeze/Thaw interface depth

Table 6.1: List of all symbols, unis and their definitions

6.2.1 Mass Transport

The movement of moisture in the profile can be reduced to fluxes between representative elements. Instead of analytically solving the unsaturated Richards' equation in each element, a simplified near-equilibrium solution is assumed. In this relation, the flux is based on the total moisture content and depth of the element.

The surface flux is first applied and separated into infiltration/evaporation (I [m/s]) and runoff, based on the moisture deficit of the soil and its infiltrability. Infiltration is determined by the unsaturated hydraulic conductivity (including impedance due to ice) and a unit gradient, as it is assumed that the pressure relationship is in equilibrium. Runoff occurs when the infiltrability of the soil is exceeded, or when the moisture deficit is satisfied.

If $P - ET > 0$

$$I = \min \begin{cases} (P - ET) \\ K(\theta_w, \theta_I) \\ (\eta - \theta_w - \theta_I)U/\Delta t \end{cases} \tag{6.1}$$

otherwise

$$I = \max \begin{cases} (P - ET) \\ -K(\theta_w, \theta_I) \\ -(\theta_w - \theta_{res})U/\Delta t \end{cases} \tag{6.2}$$

where P [m/s] is precipitation, ET [m/s] is evapotranspiration, Δt [s] is the length of the time step, K is hydraulic conductivity, dependent on mean soil moisture content in the unsaturated element, θ_w and ice content θ_I which is dependent on temperature, T [°C]. η is the soil porosity, θ_{res} is the residual saturation, and U [m] is the depth to the water table.

The water table position is then updated based on the flux in order to achieve an equilibrium moisture content, given by the soil characteristic pressure saturation relation, $\theta(h)$, where h [m] is the hydraulic head, as depicted in figure 6.2. This equilibrium assumption is consistent with the assumption of a hydrostatic pressure distribution in the unsaturated zone. Given the high hydraulic conductivity of peat soils near saturation, and the timescale of simulations (days to years, not seconds to minutes) this assumption is representative of reality. Given the water table position, U, the mean water content of the surface layer of depth L is given by:

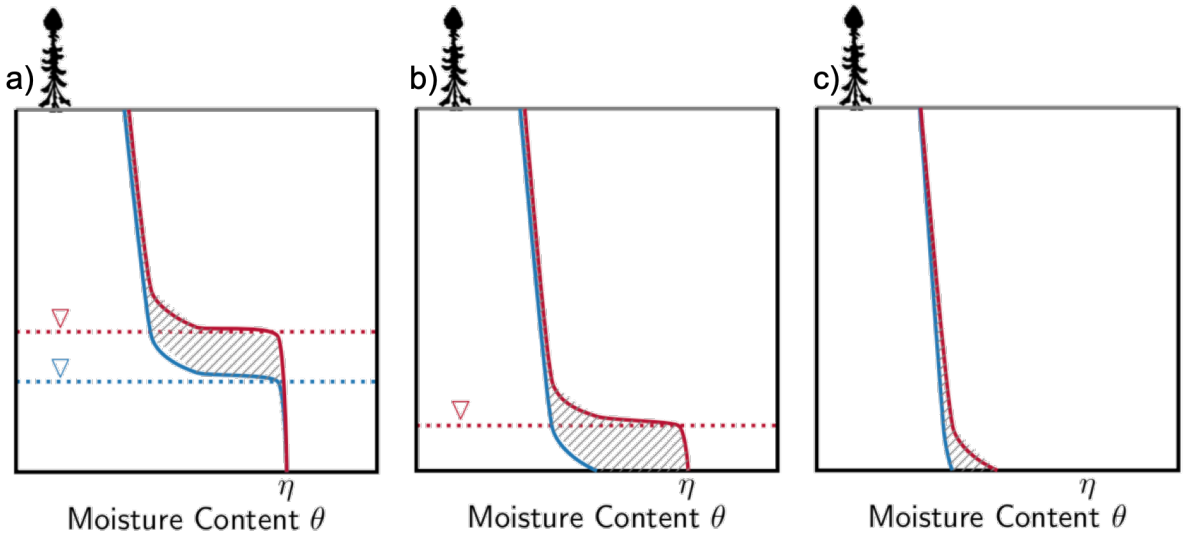

Figure 6.2: Depiction of three possible results of infiltration: a) increase in water table within thawed layer; b) formation of a water table in a previously unsaturated profile and c) change in hydrostatic pressure due to infiltration of water without the formation of a water table.

$$\bar{\theta}(L,U) = \frac{1}{L}\left[\int_0^{\min(L,U)} \theta(h + \max(U-L,0))dh + \eta * (\max(L-U,0))\right] \tag{6.3}$$

This same relation can be used to calculate the water content of any element, replacing 0 with the top of the element, and L with the bottom. For an infiltration rate of I over a time step Δt, the incremental change in water table position, ΔU, from an initial position U can be found from the following relation:

$$I\Delta t = L\left[\bar{\theta}(L(t+\Delta t), U(t+\Delta t)) - \bar{\theta}(L(t), U(t))\right] \tag{6.4}$$

this relation can be iteratively solved to find the new position of the water table ($U(t+\Delta t)$) and simplified using a lookup table. It is assumed that there is no flow through a frozen saturated layer.

6.2.2 Interface Update: Freeze-Thaw

In order to track the thermodynamic evolution of the system, it is necessary to know the energy stored in each element. The energy balance for a single element, where $\dot{Q}$ is heat transfer rate, $\dot{m}$ is mass flow rate and e is specific internal energy is as follows:

$$\begin{aligned} \frac{dE}{dt} &= \dot{Q_{in}} - \dot{Q_{out}} + \dot{m_{in}} e_{in} - \dot{m_{out}} e_{out} \\ Lc_{p,b}\rho_b \frac{\partial \bar{T}}{\partial t} + L\bar{T}\frac{\partial c_{p,b}\rho_b}{\partial t} &= \kappa \left(\frac{\partial T}{\partial z}|_{top} - \frac{\partial T}{\partial z}|_{bottom} \right) + Ic_{p,w}\rho_w T_{precip} - q_{bottom} T_{bottom} \rho_w c_{p,w} \end{aligned} \tag{6.5}$$

where the thermal conductivity κ [J/° K m], and bulk specific heat capacity of the inputs and outputs, $c_{p,b}$ [J/kg], are dependent on the ice content θ_I and the degree of saturation, θ_w. The bulk density ρ_b is dependent on the saturation, while the densities of ice and water are assumed to be equivalent so as to be comparable with other models. Bulk parameter values are computed using a weighted arithmetic mean of each component, the arithmetic mean was selected to facilitate benchmarking against existing models. The specific heat capacity of water is specified by $c_{p,w}$, while q_{bottom} is nonzero when there is vertical water transport in the profile. This is computed using the change in mean water content using equation 6.3 evaluated over the element at the beginning and end of the timestep, where the change in water table position is computed based on surface flux conditions, and then subsurface water content is updated using the soil characteristic curve. $\bar{T}$ is the mean temperature in the element, which can be computed from the specific internal energy, e as follows:

$$\bar{T}(e) = \begin{cases} \frac{e-\lambda_f}{c_{p,i}} & e < -\lambda_f \\ 0 & -\lambda_f < e < 0 \\ \frac{e}{c_{p,w}} & e > 0 \end{cases} \tag{6.6}$$

Note the distinction between the frozen and thawed heat capacities, $c_{p,i}$ and $c_{p,w}$. The internal energy is relative to pure liquid water at 0 °C, and λ_f is the latent heat of fusion. The ice content is also directly related to the internal energy:

$$\theta_I = \begin{cases} \theta - \theta_{res} & e < -\lambda_f \\ \frac{-e}{\lambda_f}(\theta - \theta_{res}) & -\lambda_f < e < 0 \\ 0 & e > 0 \end{cases} \tag{6.7}$$

Finally, the temperature gradients at element interfaces must be known in order to calculate the heat flux across these interfaces. In order to approximate this gradient, an analytical solution to the heat equation (without phase change as this process only occurs at the interface) is used in each domain element. There are three such distinct profiles for each type of element, as depicted in figure 6.3. These solutions are outlined in the following three sections.

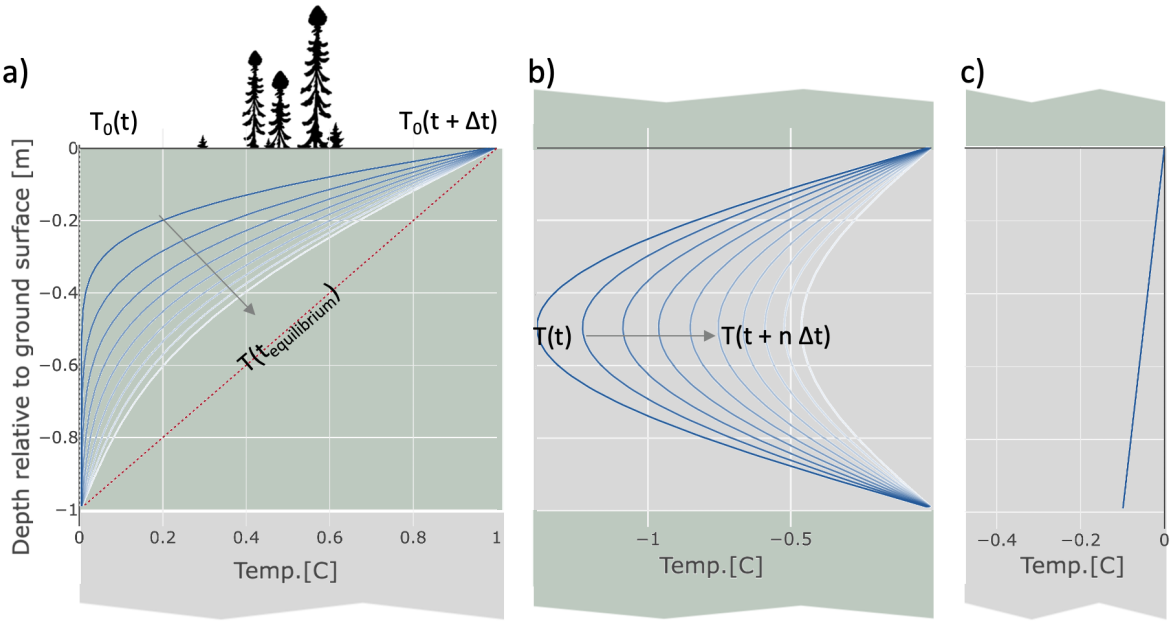

Figure 6.3: Depiction of three local temperature solution types drawn from model simulation data: 1) surface layer in which there is one fixed (bottom) temperature boundary and one boundary allowed to vary arbitrarily; 2) confined problem with two fixed temperature boundaries and 3) steady temperature profile which exist in permafrost elements with an equilibrium temperature profile.

The movement of the (sharp) interfaces is determined by the fluxes based on temperature gradients and thermal conductivity. The change in interface position (z_i) is given

by:

$$\begin{aligned}\frac{\partial z_i}{\partial t} &= \frac{1}{\lambda_f(\theta_w - \theta_{res})\rho_w}\Delta q|_{z=z_i} \\ &= \frac{1}{\lambda_f(\theta_w - \theta_{res})\rho_w}\left(\kappa^+\left(\frac{\partial T}{\partial z}\right)_{z=z_i^+} - \kappa^-\left(\frac{\partial T}{\partial z}\right)_{z=z_i^-}\right)\end{aligned} \tag{6.8}$$

where z is depth, and $\kappa^{\pm}$ is the thermal conductivity of the element above (+) or below (-) the interface.

Surface free-boundary problem

The temperature of the surface element, whether thawed or frozen, is governed by the heat equation (equation 6.9) assuming no advection and an arbitrary, time-dependent boundary condition, $T_s(t)$:

$$c_{p,b}\rho\frac{\partial T}{\partial t} = \kappa\frac{\partial^2 T}{\partial z^2} \tag{6.9}$$

Let $\alpha = \frac{\kappa}{\rho c_{p,b}}$, $\omega_n = \frac{n\pi}{L}$ and $a_n = \frac{2}{n\pi}$, where $c_{p,b}$ is the bulk specific heat capacity of the soil, dependant on ice content and saturation. The solution to this equation in a fixed domain with thickness L and fixed boundary conditions $T(0,t) = T(L,t) = 0$ is given by (Carslaw & Jaeger, 1959):

$$T(z,t) = \Sigma_{n=1}^{\infty} a_n \sin(\omega_n z)e^{-\alpha\omega_n^2 t} \tag{6.10}$$

From this solution, it is possible to find the solution to the heat equation with fixed boundary conditions, $T(L,t) = 0$ and $T(0,t) = T_s$, or more generally $\Delta T_s = T_s^{i+1} - T_s^i$, where T_s is the surface temperature condition (Carslaw & Jaeger, 1959). Using the principle of superposition, it is possible to generate the solution to the steady state problem and perturbation due to a change in temperature at the ground surface:

$$T(z,t) = \sum_{n=1}^{N}\Delta T_s^n\left(1 - \frac{z}{L} - \sum_{j=1}^{\infty} a_j \sin(\omega_j z)e^{-\alpha\omega_j^2(t-t^n)}\right)_n \tag{6.11}$$

Superposition can be repeated for consecutive arbitrary perturbations in surface temperature, allowing the underlying layer to respond directly to the history of applied surface forcing temperatures. Note that this relieves the need to track the entire temperature profile in this surface layer, as we need only the mean temperature (energy content) and the gradient at the base of the layer to compute the heat flux at the interface and consequently the change in thickness L, and the change in mean temperature.

This solution is exact for a domain of fixed length L when an infinite number of terms are retained. Truncating the sum to 200 results in relatively small error given the high thermal conductivity of water and high porosity of near-saturated peat soils. In order to account for changes in domain length as the interface moves, a linear stretching/scaling of the profile is applied, which would result in an over-estimate of the energy contained in the profile without correction. Therefore, mean temperatures are corrected such that there is no net change in energy content in the profile beyond that used in phase change using the following relation:

$$\bar{T}^{n+1} = \frac{\bar{T}^n L^n}{L^{n+1}} + \Delta t \frac{q_{surface} - q_{base}}{\rho_b c_{p,b} L^{n+1}} \tag{6.12}$$

The imposition of this stretching/scaling is the primary source of error in solving the governing equation 6.9; this error is minimized when interface movement is slow. The interface position is therefore updated every timestep. Note that this applies both in the frozen and thawed case, where the difference lies only in the values of thermal conductivity and specific heat capacity.

If the soil column is partially saturated, bulk thermal parameters are used instead of treating an unsaturated profile as a two-layer system with an unsaturated layer sitting on top of a saturated layer. This was tested using a continuum model for various soil properties, and it was found that for all reasonable combinations of porosity, thermal conductivity, density and specific heat capacity, there is no sharp change in the temperature profile at the water table for a wide range of parameter values. The diffusivity of saturated and unsaturated soil samples differs by at most a factor of 10, which does not result in sufficiently sharp changes in parameter values to be detectable in the temperature profiles. The soil parameters for several standard soils are included in table 6.2.

Confined Conditions

In the cases when a confined layer of unfrozen soil exists between the frozen surface and the underlying permafrost (e.g. during Autumn in Figure 6.1), the heat equation is subject to

Soil	η [-]	ρ $[kg/m^3]$	$c_{p,b}$ $[J/kg°C]$	κ $[W/m°C]$	α Saturated $[m^2/s\ ]$	α Unsaturated $[m^2/s]$
Peat	0.8	250	630	0.05	1.6×10^-6	1.6×10^-7
Sand	0.4	2650	732	8.4	7.2×10^-6	1.3×10^-6
Mixed Mineral	0.35	2650	732	2.9	2.3×10^-7	5.2×10^-7
Mixed Organic	0.45	1300	1925	0.25	2.2×10^-7	1.2×10^-7

Table 6.2: Summary of porosity, density, specific heat capacity, thermal conductivity and diffusivity for various realistic soils under saturated and unsaturated conditions.

isothermal boundary conditions at the freezing point. It is assumed that the temperature profile in the domain of length L can be approximated by a sinusoid. Between thawed or frozen layers, the soil temperature is governed by a decaying sinusoid, where α is dependent on phase as defined above, and T_f is the freezing point:

$$\bar{T}^{n+1} = (\bar{T}^n - T_f)\frac{\pi}{2}e^{-\frac{\pi^2\alpha}{L^2}\Delta t}\sin\left(\frac{\pi z}{L}\right) + T_f \tag{6.13}$$

Similarly to the previous case, the energy balance must be preserved during dilation and shrinking of the domain. The same solution (equation 6.13 is applied to a confined frozen layer, but with $\bar{T} < 0$.

Permafrost Interface

A zero or a linear gradient is assumed in the underlying permafrost, with some constant temperature defined at the bottom boundary, and the surface of this layer at the freezing point, as shown in figure 6.3 c).

6.2.3 Buffer Layer

When conditions for phase change at the soil surface (surface temperature drops below zero in the case of a thawed profile, or rises above zero in a frozen profile) are present, the top h cm of the soil profile is allowed to have a fractional ice content. The soil properties of this buffer layer are updated based on ice content, water content and temperature of this soil layer using the mass and energy balances discussed above. It is assumed that the heat flux from the surface element at the interface at fixed depth h below the soil surface is zero until

phase change in this element is complete, and this interface is fixed at the freezing point T_f. Heat flux from the element below is calculated as in section 6.2.2, depending on the conditions, and referred to as q_{base} in this section. The energy flux at the ground surface is based on a linear temperature gradient determined by the current surface temperature, the mean temperature, the depth h and the bulk thermal conductivity of the buffer layer:

$$q_{surface} = \kappa_b \frac{2(T_s - \bar{T^n})}{h} \tag{6.14}$$

where the thermal conductivity κ_b is calculated using a weighted harmonic mean of the frozen and thawed soil components (which are calculated as above using an arithmetic mean). The mean temperature of the element is based on the surface temperature, T_s^n, and the ice content as follows:

$$\bar{T^n} = \begin{cases} \frac{1}{2}(T_s^n - T_f)\theta_I & T_s^n < T_f \\ \frac{1}{2}(T_s^n - T_f)(1 - \theta_I) & T_s^n \geq T_f \end{cases} \tag{6.15}$$

Figure 6.4(a) depicts the initial temperature profile in the buffer layer when it is formed (in black), the correction to this temperature profile (in red), and its response to changes in surface temperature in part (b). The initial unmodified temperature profile resulting from the free-boundary surface problem is non-physical as it neglects phase change in the buffer zone. Equation 6.15 must be used to correct the mean temperature and ice content to reflect the more physical red curve in figure 6.4 a). Once the temperature of the surface element and the flux at the surface are known, it is possible to calculate the change in ice content as follows:

$$\theta_I^{n+1} = \theta_I^n - \frac{\Delta t(q_{surface} - q_{base}) - c_{p,b}\rho_b h\left(\bar{T}^{n+1} - \bar{T}^n\right)}{\theta \rho_w \lambda_f h} \tag{6.16}$$

where the term $\Delta t(q_{surface} - q_{base})$ represents the energy transfer across the buffer layer boundaries, and the second term in the numerator accounts for the energy used to change the sensible heat of the profile, $\bar{T}$. Once the ice content reaches 1 or 0 depending if the profile is freezing or thawing, then the interface is assumed to be sharp and is updated as detailed above. If the ice content exceeds 1, or is less than zero, the excess is translated into moving the sharp interface. Including this partially frozen buffer layer avoids the formation and tracking of many very thin layers in shoulder seasons when thaw occurs daily and freezing occurs every night.

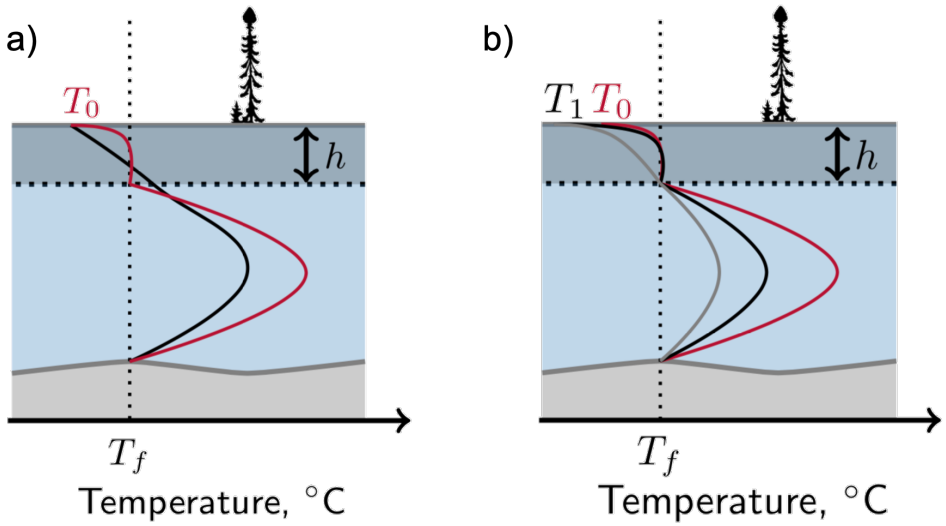

Figure 6.4: Temperature profile in the buffer layer. (a) shows the initial temperature profile in black, and the corrected profile after phase change is accounted for in an initially thawed profile subject to below zero surface temperatures in red. (b) shows the temporal evolution of this profile as the surface temperature cools further. The temperature profile for one time interval is shown in black, while that for two time intervals with the same fixed surface temperature T_1 is shown in grey.

The choice of h should depend both on the soil surface temperature and the subsurface temperature observed in the field as well as the timestep chosen for the simulation. In the model benchmarking, a value of 10 cm was chosen and adjusted through trial and error to be the thinnest layer to provide adequate buffering against the formation of thin freeze/thaw layers. When considering the field data, the depth at which most temperature oscillations occurred in the shoulder seasons was also very close to 10 cm. It is recommended that this parameter be selected based on any known data from the field site where the model is applied and adjusted to the minimum thickness such that daily temperature oscillations do not cause the formation of many thin layers.

6.2.4 Change in number of interfaces

Four general cases when interfaces are generated or merge in the profile are shown in figure 6.5. The layers are formed from the surface when freezing conditions change to thawing conditions or vice versa, while the loss of layers occurs when an intermediary

layer in the profile pinches out. Figure 6.5 shows the change in indexing when layers are formed/removed. The mean temperature is also updated when a layer is formed or pinches out. In the case of pinching out (panels (a) and (b) of figure 6.5), the mean energy is updated as follows:

$$\bar{T}_i^{n+1} = \frac{c_{p,i}^n \bar{T}_i^n (z_{i+1}^n - z_i^n) + c_{p,i+2}^n \bar{T}_{i+2}^n (z_{i+3}^n - z_{i+2}^n)}{c_{p,i}^{n+1} (z_{i+1}^{n+1} - z_i^{n+1})} \tag{6.17}$$

where the parameters are described in figure 6.5, but are evaluated when the layer is pinching out. In the case of layer formation, the temperature of the underlying layer remains the same, that is to say $\bar{T}_2^{n+1} = \bar{T}_1^n$, while the formed freezing/thawing layer is initialized and evolved as described in section 6.2.3.

When two elements are merged, or a new element is formed, there is an abrupt change in the temperature profile as the temporal history of the profile is no longer relevant. In these cases, the new temperature profile is initialized with an equilibrium temperature profile based on the boundary conditions, and with energy content satisfying the conservation of energy, as detailed in equation 6.17.

6.2.5 Model Limitations

The proposed interface model was conceived for homogeneous peat soils under near-saturated conditions. Low hydraulic conductivity soils in which the saturation is rarely at equilibrium cannot be represented using this mass balance approach. Even highly variable discharge-recharge events may be misrepresented using this model as the soil moisture history and hysteresis are neglected. Additionally, bulk parameter values are used in each soil layer, which may not be representative of an unsaturated soil with significant differences in diffusivity between the saturated and unsaturated states.

The choice of buffer layer should be informed by data representative of the modelled soil column. Making this layer too thin results in multiple unrealistic freezing and thawing fronts caused by oscillations above and below the freezing point in the surface temperature boundary condition. Assuming a buffer layer that is too thick delays the advance of the freezing front until this layer is completely frozen, resulting in poor resolution of freezing and thawing fronts during the shoulder seasons. The alternative to incorporating the partially frozen buffer zone would be the use of a sharp interface. However, this sharp interface is not typically observed in the field, where large portions of the soil column may be partially frozen at any given time.

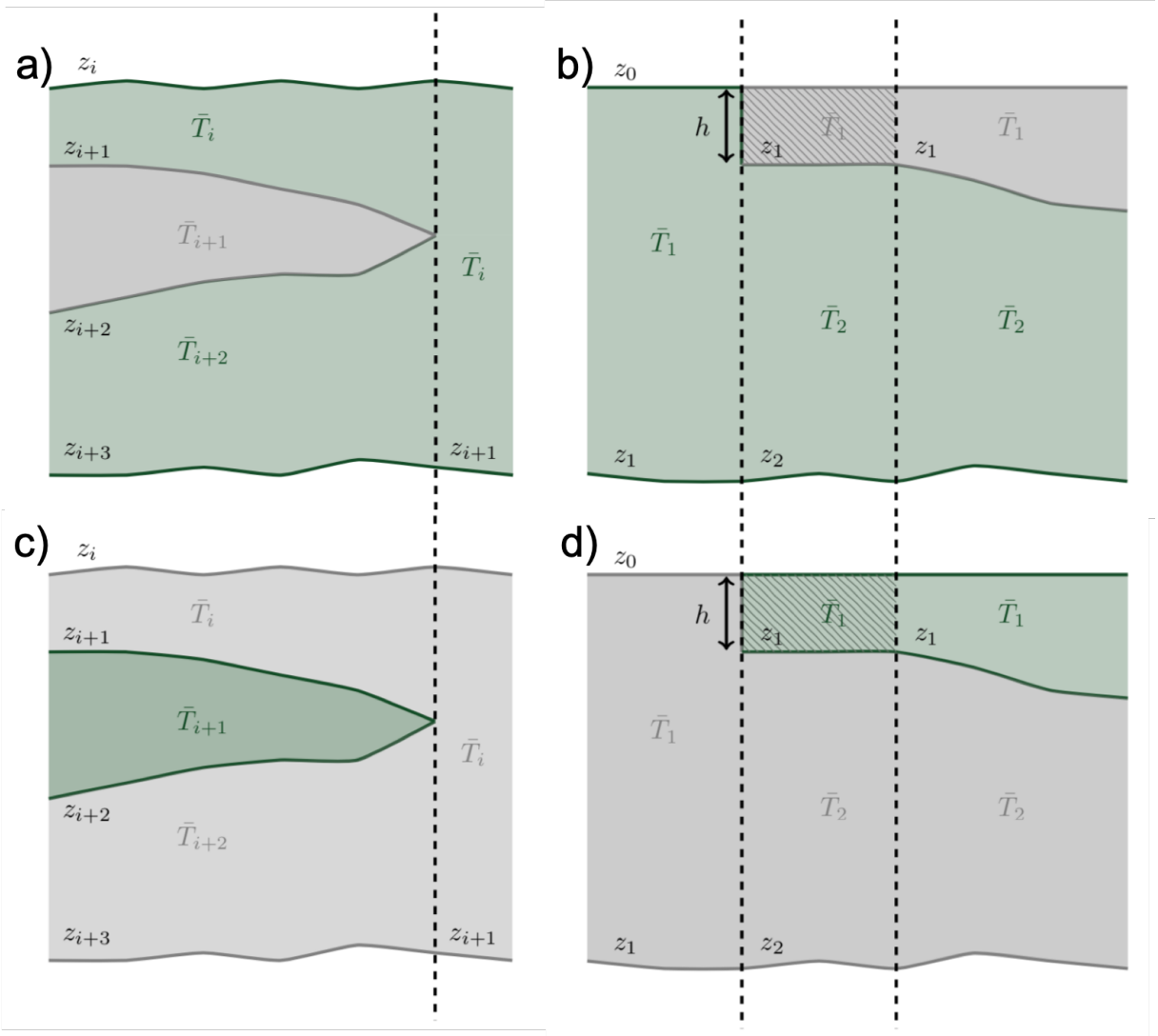

Figure 6.5: Depiction of loss of intermediary frozen or thawed layer (a) and (c) or formation of frozen or thawed layer in (b) and (d). Vertical dashed lines represent transition in profile. All temperatures are time-dependant. Note the hatched area in figures (b) and (d) represents partial ice content.

The focus of this model is on the near-surface seasonal freeze-thaw and shallow lateral talik formation and evolution as these processes affect hydrology on the annual to decadal scale. The interface model is consequently accurate on the short to moderate-term sim-

ulations, by design. It has not yet been configured for application to a system in which permafrost degrades completely. This would require a different bottom boundary condition; such a condition is generally amenable to handling by the methodology described herein, but was not treated here.

6.3 Results and Discussion

Several benchmarking exercises are presented to validate the model. First the free boundary problem solved in the surface element is compared to the classical Stefan solution (Solomon, 1979) and the expanding confined layer solution is benchmarked against an analytical computation. The coupled unsaturated model is then compared to a full finite volume solution to the coupled heat equation and unsaturated Richards' equation presented in Devoie *et al.* (2019). This 1-D continuum model uses operator splitting to couple the solutions to the unsaturated Richards' equation and the heat equation with phase change in a vertical soil column, reporting soil temperature, ice and water content at each node for the duration of the simulation. The utility of the interface model is demonstrated by comparing the computational efficiency of the interface model and the continuum model. Finally, the model is applied to observed field data describing continuous permafrost, and a soil column containing a talik.

6.3.1 Stefan Solution Benchmark

The interface model solution is first compared to the full analytical solution to the classical Stefan problem for thermal properties of pure water with an initial temperature of 0°C and an imposed surface temperature of 5°C shown in Figure 6.6 (Solomon, 1979). The error in thaw depth approximation was approximately 0.5 cm over the course of the 100-day simulation, and over a 1000-day simulation the error grew to approximately 1 cm. This comparison reports the error associated with the inexact operator-splitting approach, showing that the choice of length dilation is appropriate.

6.3.2 Talik Expansion Benchmark

A talik expansion benchmark is developed to evaluate the accuracy of the interface model under confined conditions. A fully saturated 3 m domain initially at 0°C, except a 1 m slice from a depth of 1 m to 2 m which exhibits a sinusoidal temperature profile with

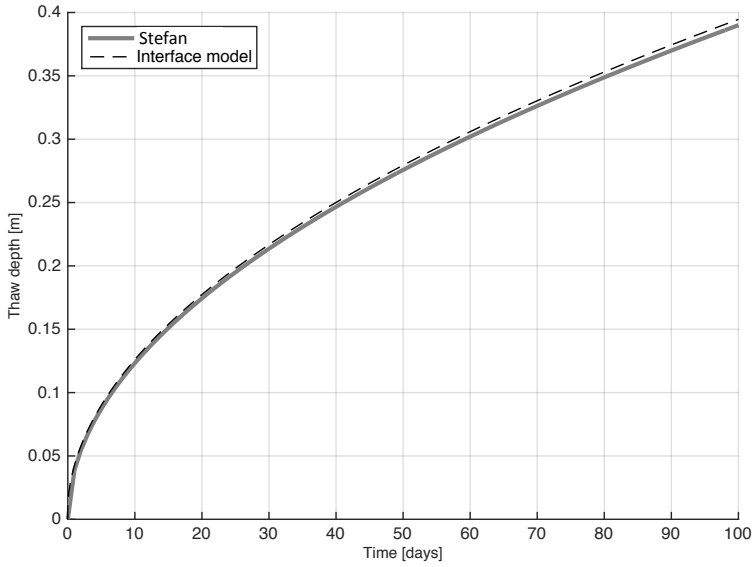

Figure 6.6: Stefan solution benchmark, interface model subject to constant temperature boundary condition as in Stefan problem.

(nonphysical) amplitude of 50°C. Both ends of the profile are fixed at the freezing point, and the profile is allowed to evolve such that the energy stored in the talik gradually thaws the frozen soil above and below. The expected thaw over the course of the 100 day simulation is shown in Figure 6.7, where the solid red line represents the thaw over time in the interface model, and the dotted line is the theoretical maximum thaw. After 100 days, the modelled solution reproduces 99.8 % of the predicted thaw. Predicted thaw was computed using an energy balance assuming that all of the energy stored in the talik of initial length z_0 and temperature T_0 would be used for phase change, resulting in an equilibrium solution with uniform temperature (at the freezing point, T_f) and thawed domain of length $z_0 + \Delta z$:

$$(T_0 - T_f)\, c_{p,b} \rho_b z_0 = \theta \lambda_f \rho_w \Delta z \tag{6.18}$$

Note that $c_{p,b}$ and ρ_b refer to the bulk parameters for the frozen soil, while ρ_w is the density of pure water, which occupies θ volume fraction of the soil matrix. In this figure, results from a benchmarked continuum model were also compared to the results of the interface model. The continuum model was subject to the same initial and boundary conditions, and

was run with 2 cm element size and 2 minute timesteps. Note that the equilibrium thaw is slightly different from the interface model and the analytically predicted thaw because freeze-thaw occurs between -0.01 and 0 °C in the continuum model, and some sub-zero soil therefore has ice content below the residual saturation. This figure does however show very similar timing in thaw for both models, validating not only the energy balance, but also the magnitude of the heat fluxes.

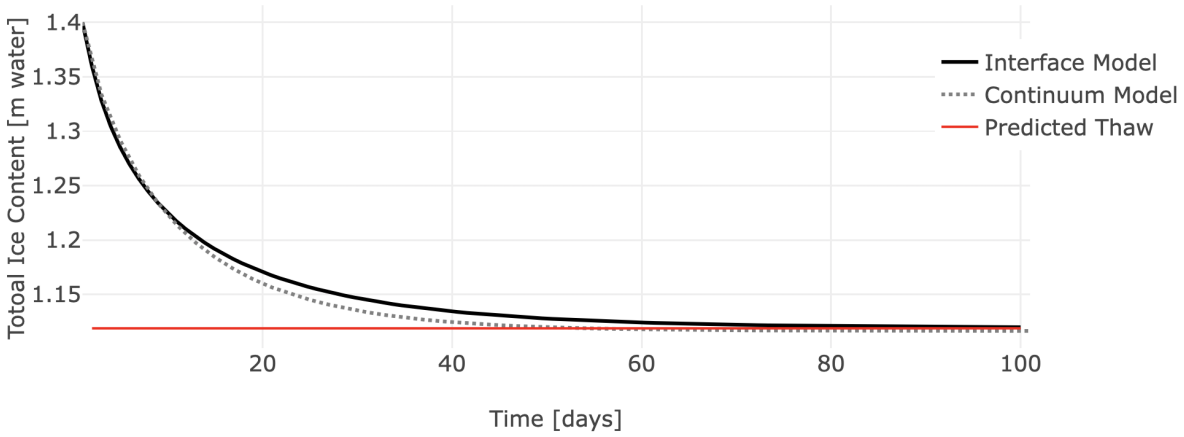

Figure 6.7: Benchmarking confined problem for a 100 day simulation, interface location of interface model (solid line) compared with theoretical maximum thaw from equation 6.18.

6.3.3 Field Condition Benchmark

The final benchmark is the direct application of the model to a realistic domain subject to representative initial and boundary conditions. Two scenarios are considered for comparison between the finite volume method and the interface model, first a stable plateau, and second a profile containing a talik and degrading permafrost. The stable case is initialized as a completely frozen profile with uniform temperature of -0.1°C. The case with a talik is initialized to a similar temperature profile, but with a thawed region from 0.5 m to 1.5 m, with an initial temperature of 0°C (with zero ice content), and a linear gradient between the talik and the surrounding -0.1°C. The domain height is 3 m for all models and all scenarios and a fixed temperature (-0.1°C) is imposed at the base of the soil profile. The surface temperature was based on two time series constructed from data collected at the Scotty Creek Research Station (SCRS, a field site located in discontinuous permafrost peatlands approximately 70 km south of Fort Simpson in the Northwest Territories,(Quinton

et al., 2018)), the first representative of a stable peat plateau, and the second a degrading permafrost body with a lateral talik. The water table was initially at a depth of 10 cm below the ground surface, and mass flux at the surface was applied seasonally, with an average ET rate (-1.728 x 10^{-3} m/d) applied in spring/summer and an average recharge rate (2.076 x 10^{-3} m/d) in the fall. The net mass flux was zero annually.

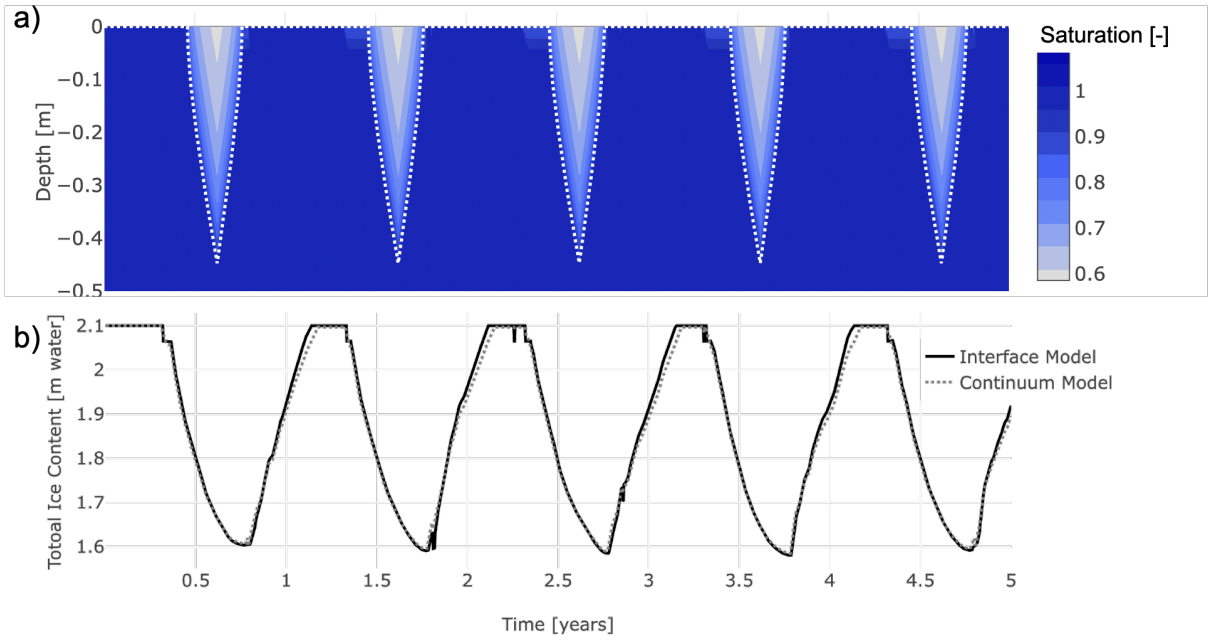

Figure 6.8: (a) Comparison of water table positions in interface model (dashed line) and continuum model (contour plot), (b) comparison of total ice content (integrated over the soil column) for the same two simulations. Note that the sharper changes in water content in the interface model occur when the buffer layer is formed resulting in more abrupt changes than the continuum model.

Consider first the stable plateau condition. The interface model was compared to the continuum model discussed above first in terms of water table position. Figure 6.8(a) shows a favourable comparison between the simulated water table using the interface model and the contour plot of water content in the profile. Because the interface model assumes an equilibrium water content profile, and the continuum model considers the unsaturated Richards' equation, the small deviations in water content (less than 0.1 % difference in average water content over the duration of the simulation) between the models is expected, especially as they occur predominantly when changes in surface boundary conditions occur,

and the equilibrium assumption is less accurate.

The total ice content of the profile was then also compared between the continuum model and the interface model in figure 6.8(b). Similarly to the water content, the ice content was integrated over the entire domain. The maximum possible ice content is 2.1 m, representing a completely frozen soil profile (with residual water content of 0.1) in both model scenarios. The interface model and continuum model are in excellent agreement, except perhaps when the buffer layer is formed (similarly to the case above). This results in some sharp changes in ice content for the interface model when the water flux at the soil surface changes, or when the buffer layer is added or removed. There is also evidence of an over-estimate of refreeze rate using the interface model when approaching a fully frozen soil profile when compared to the continuum model. The maximum difference in ice content between the two models is 6 cm (occurring at one of the changes in buffer layer), while the mean difference in ice content over the entire simulation is 0.33%.

Finally, the freeze-thaw interface was compared between the interface and continuum models for a stable permafrost case (figure 6.9(a)) and a the profile containing a talik in figure 6.9(b). The simulations were run with identical boundary conditions, initial conditions with the same energy and water content (identical temperature profiles were not possible due to model configuration) and with a 1 hour timestep. The interface (shown as a dotted line) lies within the -0.05 to 0 °C contour, indicating excellent agreement between models, as it is the freezing range of the continuum model. There is a tendency for the interface model to under-estimate phase change in a confined profile, likely because the continuum model allows for partial ice content, as can be seen in figure 6.9(b), where the interface sits within the 0 to 0.05 °C contour. The equilibrium profile for the continuum case would therefore have a large partially frozen component, which clearly extends beyond the sharp interface. The largest difference between the interface and continuum models occurs in the talik case near the beginning of the simulation. This is a reflection of the differences in model structure given a sharp interface and a slushy zone, it was not possible to assign identical equilibrium initial conditions to both models, though mass and energy were consistent. After the first simulated year, the models recover from the initial model setup and show significantly better agreement.

6.3.4 Model efficiency and stability

The computational efficiency of the interface model and the continuum model were compared for the saturated, and unsaturated cases with and without taliks. The comparison is shown in table 6.3. It is clear that the semi-analytical method is significantly faster

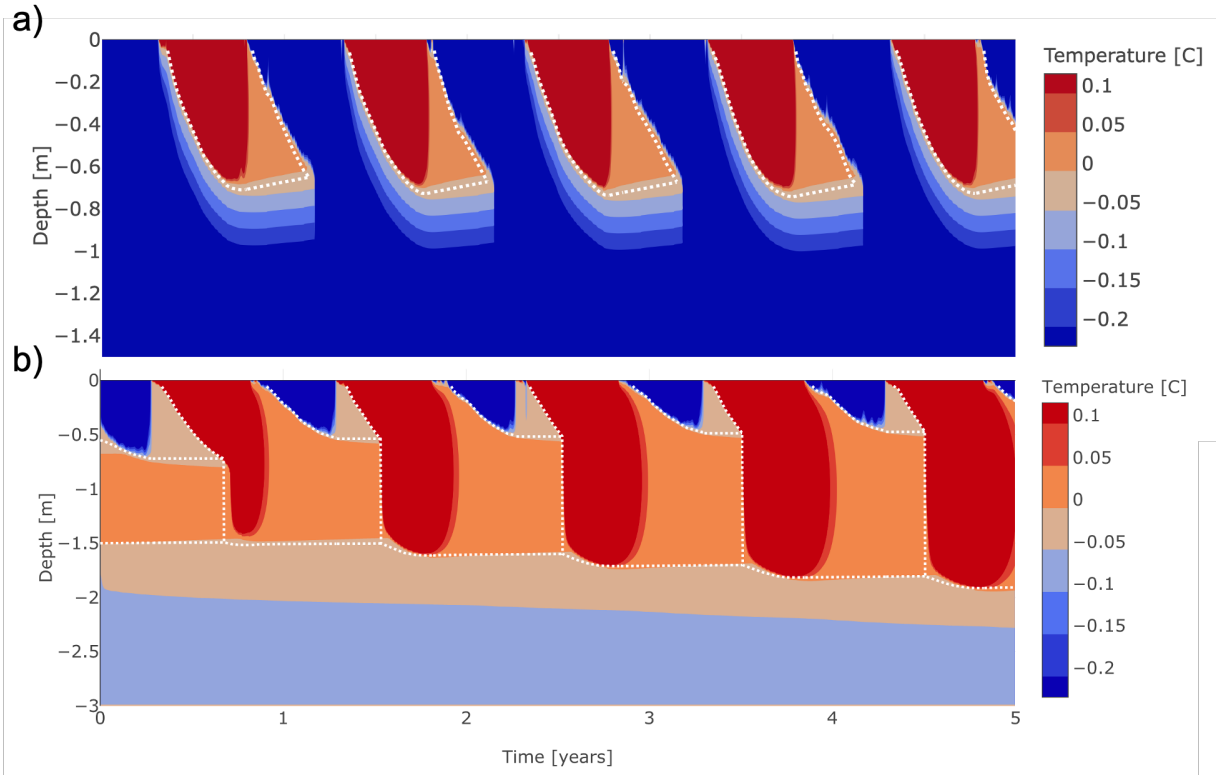

Figure 6.9: Contour plot showing subsurface soil temperature for continuum model of unsaturated freeze-thaw problem overlain with lines showing interface position modelled using interface model with a one hour timestep. Panel (a) shows a stable permafrost condition, and panel (b) shows degrading permafrost with an expanding talik.

than the finite volume solver, however this speed-up is drastically improved by the choice of larger timestep due to the stability of the interface model solver. In order for the finite volume solver to converge to a (realistic) solution, timesteps were limited to no larger than 2 hours, while the interface model converged for any choice of timestep, which was eventually limited at 5 days due to concerns of information loss. The aggregation from hourly to daily and 5 day average data resulted in the difference shown in figure 6.10. For the purpose of long-term hydrological simulations, the accurate timing, but 1.7% error in maximum frost depth prediction between the hourly and 5-day simulation is acceptable given the improvement in simulation duration. Larger than five-day timesteps are possible, however at this scale of aggregation, the information loss begins to affect model simulation results, and this coarse resolution is not considered in the model comparison as it is due

Table 6.3: Model run times for various model configurations. For each scenario, model results compared favourably between the interface and continuum model, even when the interface model timestep was increased to one day instead of one hour.

Model Type	Finite Volume	Interface	Interface
Timestep	1 h	1 h	24 h
Saturated	317 s (5.3 min)	51 s	3 s
Unsaturated	1275 s (21 min)	63 s (1 min)	4 s
Unsaturated with Talik	1695 s (28 min)	84 s (1.4 min)	5 s
Unsaturated with Talik 10m domain	10246 (2 h 51 min)	84 s (1.4 min)	5 s

to averaging effects in the boundary conditions and not model limitations.

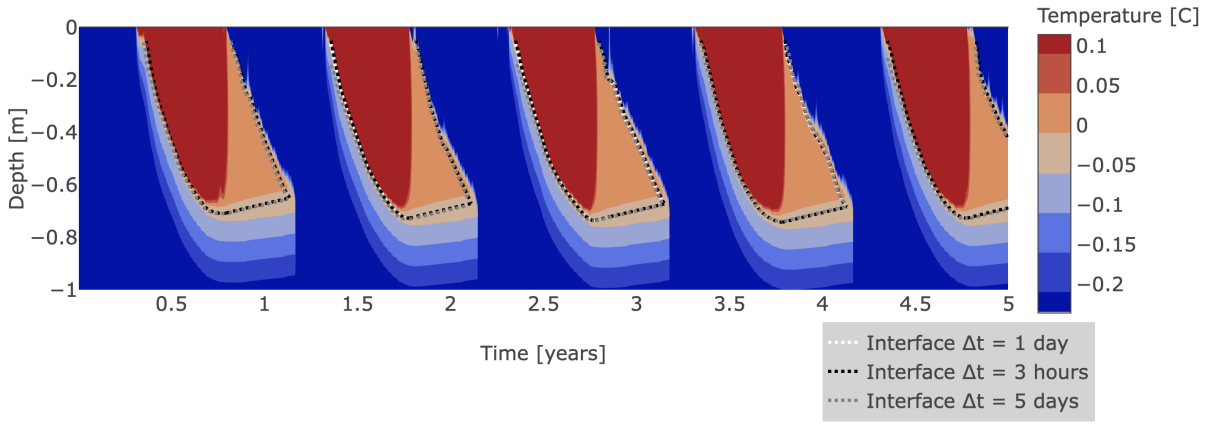

Figure 6.10: Comparison of interface model for various timesteps with continuum model. Note that the interface model simulations are almost indistinguishable due to insensitivity to timestep.

One appealing feature of this model is that computational cost is a function of the number of interfaces (which is fixed by the model) and not the model domain size. However, finite volume methods require significantly longer simulation durations for larger domain sizes, especially when a uniform grid spacing is used. Simulations with a larger model extent are also reported in table 6.3, demonstrating the scale invariance of the interface model.

Changes to simulation timestep and domain are possible because the interface model is numerically stable. The semi-analytic nature of the model means that it will converge regardless of the smoothness of boundary conditions, timestep size, or size of model

domain/element size. The model is however incapable of representing more than five freeze/thaw domain elements, so if oscillatory data is provided leading to the formation of multiple stacked frozen and thawed layers, the model will produce an error. This condition is not expected to be physically possible in any realistic simulation, though the constraint can be lifted if needed for certain applications given some modifications to the model code.

6.3.5 Model Application

Due to the model efficiency, it was relatively easy to run multiple scenarios to compare modelled permafrost degradation rates to those measured in the field. Surface temperature boundary conditions were drawn from field data collected at multiple sites for varying time periods. Surface temperature data was drawn from four different stations at the SCRS. Over the course of the (discontinuous) up to 10 year data record, data was categorized according to location and presence of lateral taliks, and then used as input to seasonal autoregressive integrated moving average (SARIMA) forecasting method to generate statistically homogeneous temperature boundary conditions. Further details on boundary and initial conditions for model simulations can be found in Devoie *et al.* (2019). Each ensemble of boundary conditions was used as input to the interface model which was run in one of two configurations: a stable permafrost system, and the formation of an isolated talik. The model was initialized as a completely frozen soil column with uniform initial temperature of -0.1°C, but the boundary conditions were constructed from temperature data collected at different sites, which either did or did not exhibit a talik.

Though 1000 temperature time series were generated for each simulation, some were considered non-physical because the boundary conditions generated using the SARIMA model resulted in the formation of many alternating thin (less than 5 cm) frozen and thawed layers near the soil surface. This is usually due to diurnal or multiple day temperature oscillations when the air temperature is near the freezing point. Up to 0.5% of generated boundary conditions were discarded due to this behaviour. Similar oscillations were not observed in the original field data.

Each ensemble of modelled permafrost and active layer systems was used to determine the rate of permafrost degradation - measured as the change in depth to the top of the permafrost table year over year. These values are favourably compared to measured changes in permafrost depth from the field in figure 6.11. Though the sampling experiment was repeated 1000 times for each simulated scenario, the variation between these simulations was negligible, indicating that the statistically homogeneous samples resulted in near-identical permafrost degradation. The variation within the samples drawn from any of the four locations is less than 1 mm.

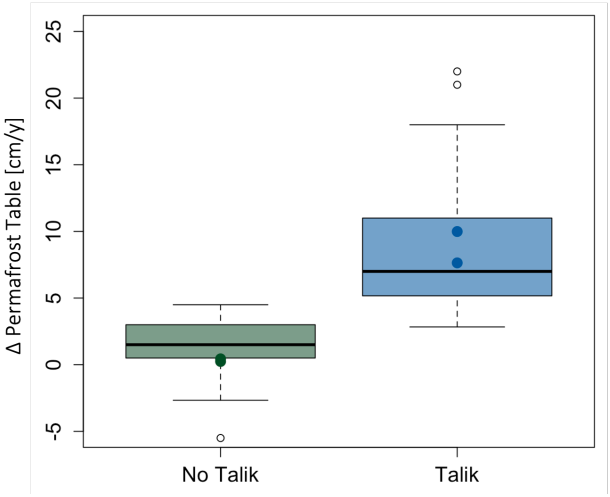

Figure 6.11: Box and whisker plot showing permafrost degradation rate (increase in supraperamfrost layer depth) as measured in the field in each landscape type. simulated permafrost degradation rates shown as circles (with standard deviation which is smaller than marker size) for boundary conditions sampled from similar field conditions.

6.3.6 Proposed Model Applications

The aim of the development of this model is to advance the current state of hydrologic and climate modelling through improved representation of permafrost and frozen ground in large-scale simulations. Semi-distributed, process-based hydrologic models such as Raven (Craig *et al.*, 2020) or SWAT (Arnold *et al.*, 1998) may be extended to incorporate the freeze/thaw process representation, which is likely to improve flow predictions not only in areas underlain by permafrost, but also in simulations including seasonal ground ice. The interface model can provide means to update multiple frozen and unfrozen soil horizons for better representation of near-surface processes. The addition of this process to a model like SWAT may alleviate the shortcomings of the current approximation of permafrost as an impermeable layer (improving the poorly represented overwinter flows) (Fabre *et al.*, 2017). The issue of freeze-thaw representation is also present in large-scale modelling projects, and the interface model is sufficiently efficient and stable to provide an alternative to current permafrost representations in GCMs, which currently demonstrate high levels of uncertainty in their representation of permafrost, (Koven *et al.*, 2013) but also incur significant computational burden when trying to represent these processes using discrete freeze-thaw models.

Though this work focused on the representation of a thawing discontinuous permafrost landscape, the same set of relations can readily solve the analogous problem of seasonally frozen ground. Such an extension of the model would make it possible to have seasonally-varying soil properties represented in large and small scale hydrological and global circulation models to reflect the impact of freezing and thawing soils. In large scale models, even those representing the impact of climate change on runoff such as Chen *et al.* (2012); Shen *et al.* (2018), and even in models explicitly investigating permafrost dynamics such as those in the CMIP5 project (Koven *et al.*, 2013) seasonally frozen ground is not considered. The frost penetration into thawed soils drastically affects their hydrologic characteristics, and the exclusion of seasonally frozen ground in temperate environments is arguably more impactful than in permafrost environments. Several studies investigating large-scale freeze-thaw processes exist, but in order to make predictions at this scale, they are often limited to equilibrium lumped approaches (e.g. Gelfan *et al.* (2017); Obu *et al.* (2019)) and the proposed modelling strategy here may improve predictions where heat and moisture fluxes could be considered as 1-D, especially in high organic soils and in areas with low diffusivity and resulting long temperature memory.

6.4 Conclusion

A unique moving interface model of soil freeze/thaw in saturated/unsaturated systems was developed and benchmarked against a continuum model. The proposed interface model is adequate for the simulation of permafrost degradation and annual freeze-thaw. Results agree well with analytical solutions and a benchmarked continuum model, though the interface model demonstrates up to a 2000-fold increase in computational speed. This tool can be applied to better understand the condition of discontinuous permafrost in northern peatlands, allowing for sensitivity analysis, uncertainty analysis, and calibration to be feasible. The model can easily be extended to represent seasonal ground ice and different soil types. Next steps in model development include the representation of lateral flow through the thawed soil column, seasonal ground ice, as well as segregated ice development and their impacts on hydraulic conductivity and pore volume.

Chapter 7

The hydrologic and thermodynamic function of isolated taliks

7.1 Introduction

Permafrost thaw is driven by climate warming which is amplified in arctic and sub-arctic regions (Pörtner *et al.*, 2019). Observed thaw rates are strongly dependent on land cover types, where ecosystem protected permafrost beneath organic soils tends to persist even after the climate is not favourable for permafrost development (Bonnaventure & Lamoureux, 2013). This contributes to heterogeneity in permafrost degradation at the continental scale, while there are also factors that lead to field-scale heterogeneity in permafrost degradation. Focusing on discontinuous permafrost peatlands, thaw rates over the last five decades show significant permafrost losses, especially adjacent to wetland features (Chasmer *et al.*, 2011). It has also been determined that subsurface heterogeneity in soils, soil moisture, and freezing function lead to variations in observed thaw rates, and explain some of the patterns of talik formation (Amiri & Craig, 2019). Taliks are perennially thawed layers overlaying permafrost, and it is thought that their formation is often the first stage of permafrost degradation and loss in permafrost peatland environments (Devoie *et al.*, 2019).

The modelling work presented in Devoie *et al.* (2019) (chapter 4) focuses on vertical permafrost degradation. In this work, two mechanisms for heat transfer driving thaw are proposed: conduction and advection. In cases where water movement is not observed in the thawed or thawing soils, it is thought that conduction is the dominant mechanism for heat transfer. Conduction is governed by Fourier's law (Fourier, 1878):

$$q = -k\frac{dT}{dz} \tag{7.1}$$

where q [w/m^2] refers to the conductive heat flux, k [kJ/kg°C] is the thermal conductivity of the media (soil in this case), T refers to the temperature [° C] and z is the vertical depth [m]. Much of the heterogeneity in thaw arises from heterogeneity in thermal conductivity, k, which is a function not only of the soil properties which are often spatially variable, but also depends strongly on soil moisture. Soil moisture is temporally variable and linked with topography and vegetation (Yi *et al.*, 2018). In addition, it has been observed that talik formation often leads to local subsidence, which provides a location for water to collect, ponding if surface water is present. This increase in soil moisture and subsequently increases the thermal conductivity of the soil, and forms a positive feedback (Connon *et al.*, 2018). This positive feedback is only strengthened by the thermal gradient which is highly dependent on talik presence. In the summer, the thermal gradient is directed downwards, conducting heat deeper into the soil, while in the winter months the gradient is reversed, such that freezing is a result of heat export from the soil. However, after the formation of a talik, there is no occasion for this gradient reversal at the interface between the talik and the permafrost table, as the talik is always above the freezing point, and the permafrost is at or below the freezing point if it is frozen (Connon *et al.*, 2018). This denotes a tipping point in permafrost thaw which is only accelerated by advection.

Advection is governed by the advection equation, which describes heat transfer rate, q [W/m^2], from a moving fluid with velocity v [m/s], density ρ [kg/m^3], specific heat c_p [kJ/kgK], and temperature difference ΔT between the inflowing and outflowing water:

$$q = vc_p\rho\Delta T \tag{7.2}$$

In the 1-D case of vertical thaw, this advective movement of energy is taken to be in the x-y plane while thaw occurs in the z direction, as permafrost is often assumed to be impermeable, precluding vertical advection (Quinton *et al.*, 2003). Advection is only a driver of vertical permafrost thaw when taliks provide a flow conduit between features with different hydraulic heads, driving flow with a velocity v. This is a relatively rare occurrence in discontinuous permafrost, though it has been observed in cascading bog series documented at the Scotty Creek Research Station in the southern Northwest Territories (Connon *et al.*, 2015).

Advection is much more likely to play a role in lateral permafrost thaw, which is reported to account for a significant fraction of permafrost loss in discontinuous permafrost

landscapes (McClymont *et al.*, 2013). This thaw occurs preferentially around wetland features, where the thermal energy stored in wetlands establishes a perennial thermal gradient from the wetland to the permafrost. Water moving adjacent to permafrost features acts to strengthen the thermal gradient between the permafrost body and the thawed wetland.

Some permafrost-free wetlands act predominantly as storage features, and are generally classified as bogs, while others convey water and are referred to as fens (Quinton *et al.*, 2003). Though a combination of vertical and lateral conduction and advection is likely to explain observed permafrost degradation rates in the landscape, it is unclear which of these processes dominates in each landscape feature. The aim of this work is to distinguish the dominant mechanisms for permafrost thaw in the different features of the discontinuous permafrost peatlands landscape. This can provide support from field observations for appropriate simplifying assumptions in representing thaw across the landscape in modelling applications.

7.2 Study Site

This study was undertaken at the Scotty Creek Research Station (SCRS) located approximately 70 km south of Fort Simpson in the Northwest Territories, Canada, as described in Section 3 (Quinton *et al.*, 2017). This site was selected because it has a long data record with instrumentation documenting the formation and evolution of taliks. It is representative of peatland headwaters regions of the Mackenzie and Liard rivers, and all stages from stable permafrost with no talik to permafrost-free wetlands can easily be found and distinguished in this landscape.

7.3 Methods

A combination of field data collection at the SCRS and modelling were used to assess the mechanisms for permafrost thaw in various parts of the discontinuous permafrost peatlands landscape.

7.3.1 Field methods

Field sites at the SCRS were selected to document permafrost degradation in each talik feature of the landscape. Figure 7.1 summarizes a progression in vertical thaw conditions

from (a) - the condition without a talik through to (d) depicting a talik which permits flow. Pane (e) depicts lateral thaw with advection (into the page), and (f) highlights the potential for permafrost degradation from below. Both (e) and (f) may be combined with the vertical talik formation from the soil surface depicted in (b), (c) and (d). Note that taliks here refer both the the confined regions sandwiched between the active layer and the top of the permafrost body, as well as permafrost-free wetland features abutting permafrost bodies.

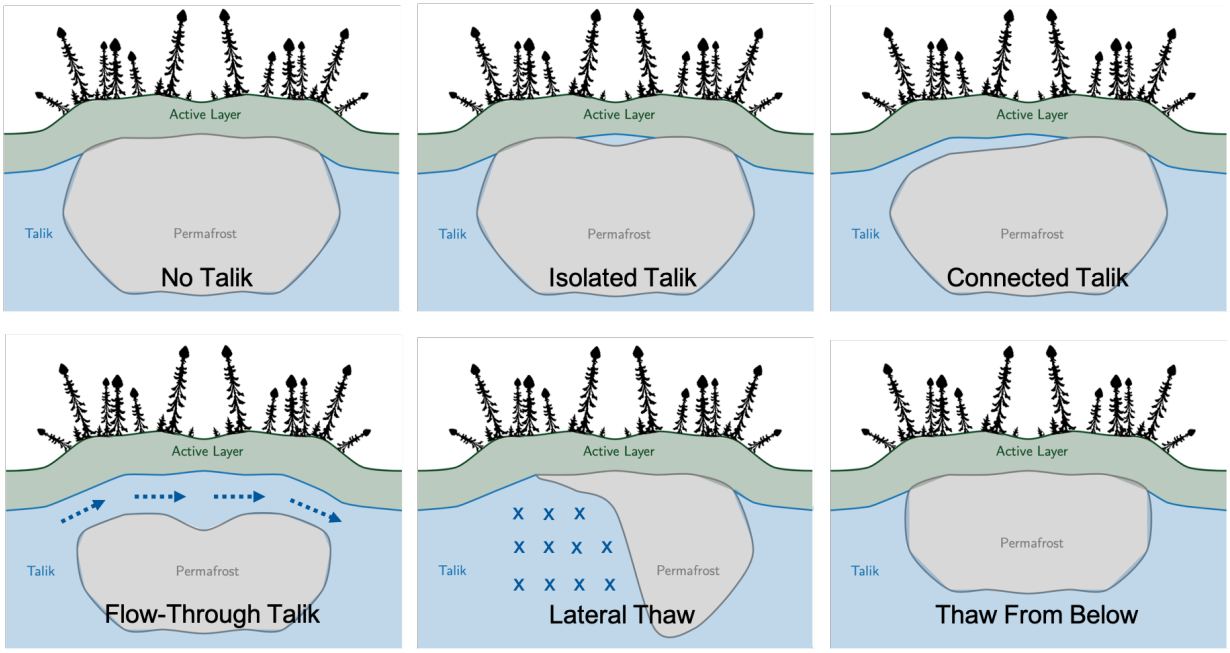

Figure 7.1: Different talik features observed at the SCRS. Here perennially thawed areas and taliks are shown in blue. Note that the diagram is conceptual and not to scale.

Frost table measurements were taken along ten transects and in a grid which can be seen in figure 3.1 using a frost probe. This graduated steel rod was inserted into the ground until the point of refusal. This measurement is taken annually at the end of the thawing season (typically August or early September), and indicates the maximal thaw extent. In addition to these measurements, temperature profiles were established at several sites - two deep thermistor profiles (RBR: 10 sensor temperature loggers) were installed to measure temperature to a depth of 6 - 10 m (also shown in figure 3.1. These sensors are located on a plateau adjacent to a cut line (winter road), and on the border of a fen. Shallower temperature data were collected at three additional sites: one in a connection between two

bog features (similar to pane (d) of figure 7.1), one on a plateau, and one in a bog. These profiles were measured using Campbell Scientific CS 107 or CS 109 thermistors connected to CR1000 or CR10X loggers. This data was augmented by Hoskin Scientific ground heat flux plates installed at an isolated talik site (black triangle located in grid in figure 3.1. Finally, HOBO U20L pressure transducers were used to report hydraulic gradients, and EnvironFlux passive flux meters (see chapter 5 for a description of these instruments and their installation) were used to establish flux through low-gradient talik connections. The location of these field sites is indicated in figure 3.1, where the frost table measurements fall on the transects and grid indicated in the map.

7.3.2 Modelling methods

An interface model of freeze thaw presented in Devoie & Craig (2020) (chapter 6) was used to test hypotheses regarding the interpretation of field measurements. This conduction-alone 1-D model was used with advection and unsaturated flow processes disabled to establish if conduction alone was sufficient to reproduce observed thaw rates. Initial and boundary conditions for model simulations were drawn from field data, including initial frost table positions and talik conditions as well as surface temperature timeseries and soil moisture. Soil thermal properties were drawn from peat properties reported at the SCRS and were compared to data in literature Price *et al.* (2005). A range of simulations were run for each case by sampling the initial and boundary conditions from an ensemble bootstrapped from observed data collected at the SCRS. The ensemble of temperature boundary conditions was generated using a SAMIRA analysis, as was discussed in section 4.2.3, with input temperatures collected at a site with an isolated talik and one with a connected talik. Model initial conditions were consistent with the permafrost configuration, which in the case of an isolated talik, is consistent with the centre of the "Isolated Talik" case in figure 7.1, while the connected and flow-through talik simulations are arranged as panes 3 and 4 of this figure.

7.4 Results

The four possible heat transfer mechanisms leading to permafrost thaw are: 1) vertical conduction, 2) vertical advection, 3) lateral conduction and 4) lateral advection. In both advective cases, thaw itself is conduction driven (as it is occurring in a solid) but the temperature gradient at the permafrost surface is impacted by flow adjacent to the permafrost surface. This term could as easily be interpreted as a convective flux to the permafrost,

but advection is used here for consistency with the theory presented in chapter 4. In order to understand the heterogeneity in observed thaw rates at the SCRS, the landscape is classified into five categories, and the drivers of permafrost thaw are considered in each of these categories.

7.4.1 Category 1: No Talik

The first permafrost category describes the case in which there is no talik present (figure 7.1a). In this case the active layer fully freezes from the soil surface to the top or the permafrost table overwinter. Without liquid water available, the only mechanism for heat transfer is vertical conduction, where ground heat flux is responsible for the freeze/thaw observed in the soil column. In a stable climate, this condition should be a stable one in which the depth of thaw and refreeze are equal year to year, or the depth of potential refreeze exceeds the maximum summer thaw. However field data (presented in figure 7.2 - no talik) indicate active layer thickening on the order of 2 cm/year. This is a process reported by Shiklomanov *et al.* (2012), in which active layers are observed to deepen due to increases in net ground heat flux. Active layer thickening can only persist until the depth of thaw reaches the maximal depth of refreeze. After this point, the winter is insufficiently cold to remove enough energy from the soil profile for complete refreeze, and a talik is formed. Data collected at the SCRS provides evidence for this process, where taliks increased in prevalence from 8% to 33% of measurements points distributed across plateau features between 2011 and 2016 (Connon *et al.*, 2018).

7.4.2 Category 2: Isolated Talik

Once a talik is formed, a perennially thawed soil layer exists between the active layer and the top of the permafrost table (Figure 7.1 b). This layer effectively isolates the permafrost from the atmosphere in the winter because it is above the freezing point. This prevents it from losing energy, and results in permafrost loss year-round (Connon *et al.*, 2018). In the case of an isolated talik surrounded on all sides by permafrost, it is hypothesized that permafrost loss can be attributed to vertical conduction alone. Lateral conduction is unlikely due to the lack of lateral thermal gradients, and the scarcity of water movement in isolated taliks means only a small energy input can be expected from summer precipitation events and advection is unlikely. This is supported by data collected in the field, where the mean rate of permafrost degradation in isolated taliks (Figure 7.2 - Isolated) is very similar to the rate of permafrost degradation calculated from the measured vertical ground heat flux in this study.

Ground heat flux plates were installed to quantify the cumulative vertical ground heat flux (Q_g [kJ/m^2]) annually. This energy is converted to cm of permafrost thaw using:

$$\Delta z = \frac{Q_g}{(\eta - S_{res})\rho_i \lambda_f} \tag{7.3}$$

where the porosity of peat is (η), the latent heat of fusion of water is (λ_f [kJ/kg]), and ρ_i [kg/m^3] is the density if ice. This results in 2.7 cm/year of thaw (green circle in figure 7.2 - Isolated). This aligns well with the observed mean permafrost degradation rate. In addition, the interface model described in chapter 6 incorporating heat conduction and changes in water table position was used to verify these results. Simulations of an unsaturated soil column forced with boundary and initial conditions sampled from field data collected in sites containing isolated taliks compare favourably with the observed thaw rates (figure 7.2 - Isolated Model). In fact, this conduction-only model over-estimates the observed thaw, indicating that vertical conduction is sufficient to describe permafrost degradation occurring in isolated taliks. Of course, this does not preclude other processes from contributing to thaw, only that this single process is sufficient to account for this thaw, and the likelihood is therefore high that the influence of other processes is negligible.

7.4.3 Category 3: Connected Talik

Taliks are also frequently found adjacent to wetland features (figure 7.1c). Observations of vertical permafrost thaw in connected talik features leads to the degradation rates presented in figure 7.2 - Connected. The observed mean thaw is somewhat higher than that observed in isolated taliks and the variance in observed thaw rates is also significantly greater. The increase in thaw rate may be partially explained by a mean increase in incoming radiation near wetland features, where the canopy-free wetlands allow for more radiation to reach the surrounding permafrost bodies, especially on south-facing edges where thaw was observed to progress more rapidly. The vertical conduction-only model is again used with consistent boundary and initial conditions to reproduce the mean observed thaw rate as seen in figure 7.2 - Connected Model. However, the model does not reproduce the observed spread in data. This variance can be either attributed to differences in canopy cover and incoming radiation to permafrost adjacent to different wetland features, or it may point to a need to consider advection in certain features where water is moving sufficiently to convey heat to the connected talik. Prior to talik development (Figure 7.1a), the active layer was the sole flowpath for conveying water from the plateaux to the adjacent wetlands. With the introduction of a talik, it seems that this function could be shared between active layer and

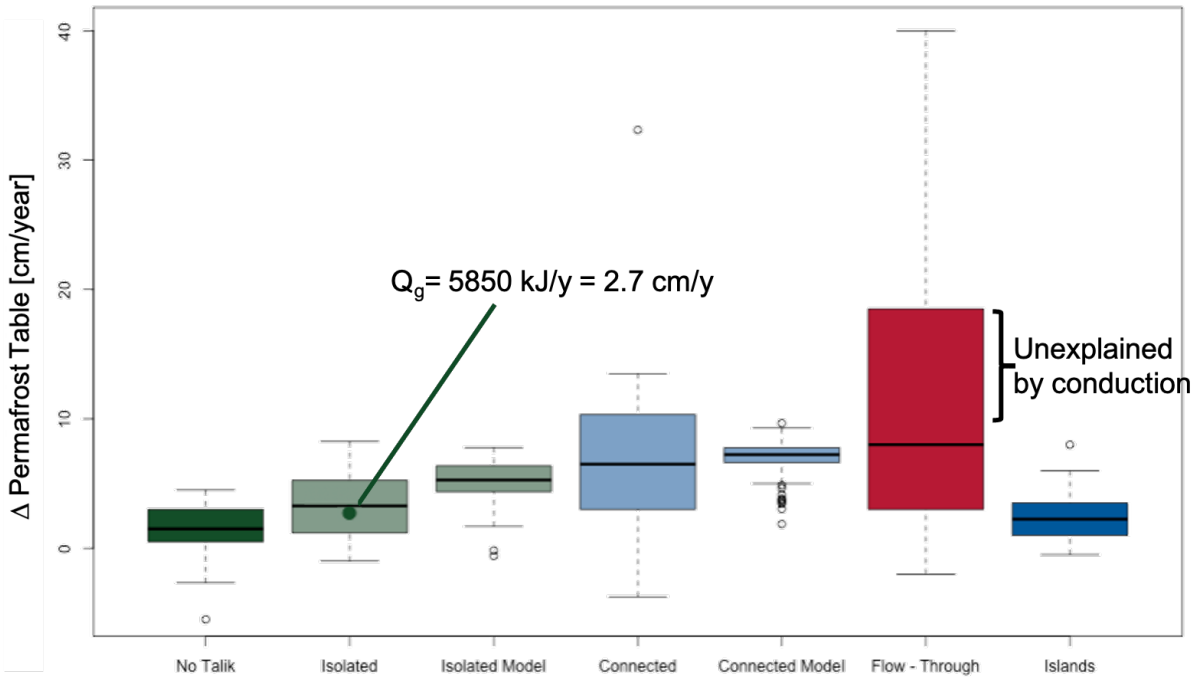

Figure 7.2: Vertical permafrost degradation rates in all types of taliks, measured and modelled using vertical conduction alone for the isolated talik and Connected talik cases, data aggregated between 2011 and 2020. Green point indicates computed thaw based on ground heat flux in 2011.

talik, implying that water (and energy) moves from the active layer to the talik and then to the adjacent wetland. That being said, the model results indicate that vertical conduction alone is sufficient to explain the mean thaw rate observed in these connected talik features, and is therefore likely the dominant thaw mechanism, as it was for the isolated case.

7.4.4 Category 4: Flow-through Talik

The landscape features in which the most rapid vertical permafrost degradation is observed are termed flow-through taliks (figure 7.1d). These are taliks confined between the

active layer and the permafrost table, but which are connected on each end to a different wetland feature. As seen in figure 7.2 (d), the more rapid permafrost thaw rates in these features cannot be explained by conduction alone. If the connected wetland features differ in hydraulic head, a gradient is established across the talik, driving lateral water flow over the permafrost surface. Depending on the temperature of the wetland features, this flow will transport thermal energy which can drive vertical permafrost degradation through advection. In order to quantify this thaw, subsurface flow data was collected using passive flux meters as detailed in Devoie *et al.* (2020), alongside subsurface soil temperature profiles. The observed seasonal mass flow data ($\dot{m}$ [kg/s]) and the specific heat of water were used with the mean seasonal subsurface temperatures ($T(z)$) over the depth of the profile assumed to influence the permafrost table, h, to quantify the energy available to drive thaw:

$$\int_0^{365d} \int_o^h \frac{\dot{m} C_p \Delta T(z)}{h} dz dt = \eta \rho \lambda \Delta z \Delta x \cdot 1m \tag{7.4}$$

The depth h was assumed to be one half of the depth of the talik in the winter - the bottom half of this feature would affect the underlying permafrost while the top half would interact with the active layer. In the summer, h was taken to be the full thawed depth of the profile as once the active layer is thawed, as it is not expected that energy contained in subsurface flow would be conveyed upwards. The right hand side of equation 7.4 represents the mean loss of permafrost along the transect, for a unit transect width. In this relation, η represents the soil porosity, ρ is the soil density, λ is the latent heat of fusion of water, and Δx represents the length of the transect. Δz is the resulting vertical loss of permafrost. For data collected at the SCRS, this loss can be anywhere between 0.6 and 8 cm of thaw annually. This value aligns well with the unexplained high thaw rates observed in flow-through taliks in figure 7.2 - (Flow - Through), and suggests that the combination of vertical conduction and advection are sufficient to provide the energy necessary to describe the observed thaw in these features.

7.4.5 Category 5: Remnant Permafrost

The final box and whisker plot in figure 7.2 - Remnant refers to the vertical permafrost degradation rate observed on small permafrost features surrounded by wetlands. These are thought to be remnants of permafrost features that have degraded. They often exhibit the no talik condition, and hence the vertical thaw rate (mean 2.5 cm/year) is similar to that observed in the active-layer thickening talik-free case (1.4 cm/year). This does not

mean that these features are not degrading. Much to the contrary, rapid thaw is observed at the periphery of these and other features.

7.4.6 Lateral Thaw

Lateral thaw observed in the discontinuous permafrost landscape occurs significantly more quickly than vertical thaw - the degradation rate is approximately one order of magnitude greater, as seen by comparing figures 7.2 and 7.4. Instead of being driven by seasonal temperature gradients from above, lateral thaw occurs year-round adjacent to permafrost-free wetlands. As in the vertical case, both conduction and advection can combine in lateral thaw. It is however challenging to quantify lateral thaw, and further investigation and instrumentation is needed. However, some extrapolations are possible from the available data. If the thaw could be explained through conduction alone, Fourier's law of conduction, equation 7.1 in the x direction, would imply that the rate of permafrost degradation is proportional to the temperature of the adjacent wetland feature. If lateral conduction alone was the key driver, the temperature of fens would be expected to be approximately three times that observed in bogs since the observed thaw rate is about 115 cm/year compared to about 30 cm/year near bogs. This is clearly not the case, as the average bog temperature at a depth of 90 cm is 3.96 °C, while the average fen temperature at 100 cm is 4.46 ° C. This indicates that advection must play a key role in lateral permafrost degradation, especially in flowing fen features. This also helps to explain the rapid thaw rates observed laterally as advection supplies warm water to maintain a thermal gradient laterally while the active layer is comparatively ineffective at maintaining a thermal gradient.

As shown in figure 7.3, the thaw adjacent to a winter road spans a very wide range, though the mean temperature recorded there is much lower than in the other permafrost-free features. This is because the winter road traverses bogs and fens, and thaw rates are strongly affected by these wetland features as opposed to the road itself. The mean temperature data is take from thermistors installed on the edge of a plateau bordering this features, hence the cool temperature. There is only one data point relating the thaw next to a lake. It indicates thaw rates similar to those adjacent to a bog - which is consistent with the concept of bogs and lakes as water storage features, however there is insufficient data to speculate further.

Considering both processes of advection and conduction, the rapid lateral thaw rates are still somewhat higher than would be expected for completely frozen permafrost with a large vertical extent. They indicate that the permafrost body that is thawing likely has a limited vertical extent, and was both exposed to degradation from above and potentially thaw from below.

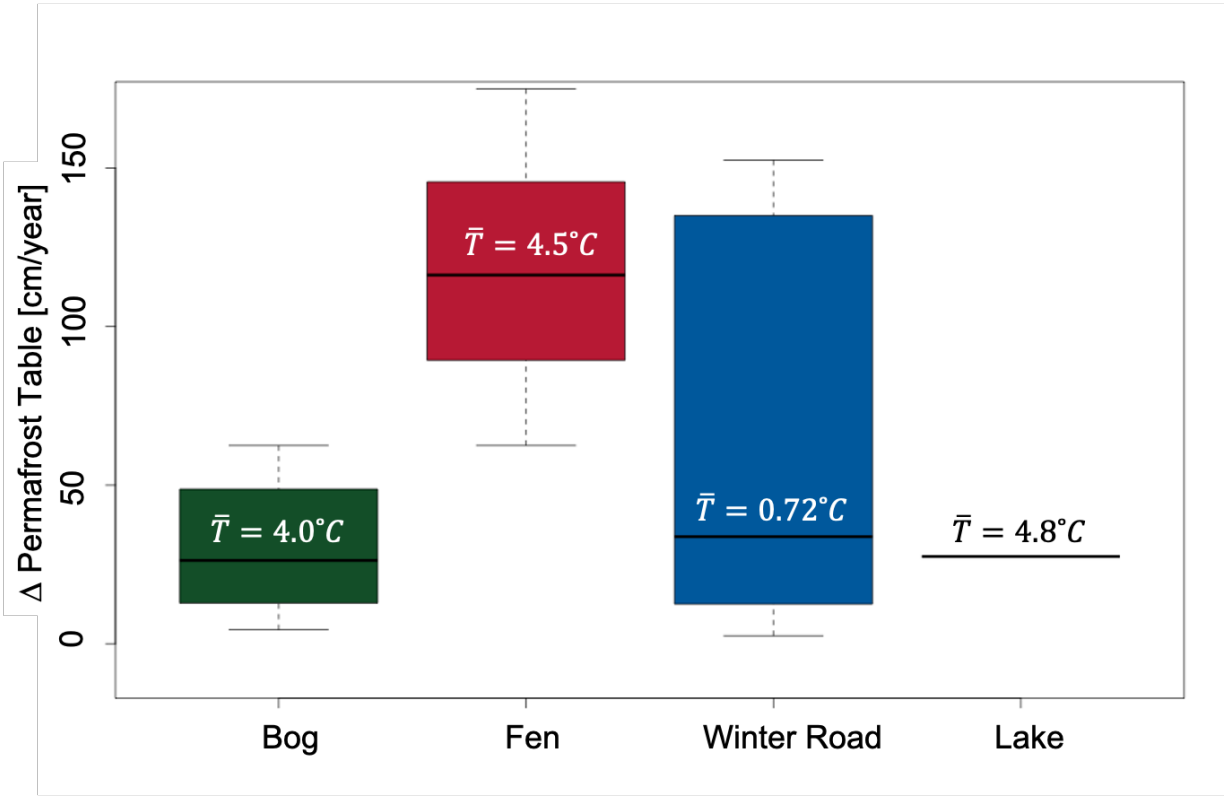

Figure 7.3: Lateral permafrost degradation rates adjacent to all wetland features.

7.4.7 Thaw from Below

After having considered vertical thaw from above, and lateral thaw, we should also consider the potential for permafrost degradation from below. The first consideration is the geothermal heat flux, which is known to have a magnitude of approximately 0.08 W/m^2 at a depth of 50 m in this region (McClymont *et al.*, 2013). This small flux would eventually degrade a permafrost body from below if it were not balanced by a net thermal loss from the surface. This heat flux would account for a maximal thaw rate of about 9.8 cm/year, assuming the permafrost were at the freezing point, none of the ground heat flux were consumed as sensible heat, and the permafrost lost no thermal energy over winter. In the absence of groundwater movement and lateral thermal gradients, it is expected that permafrost underlying a talik would degrade from below at this rate once it becomes isothermal as there is no mechanism for it to lose heat vertically from above. Lateral heat transfer within permafrost underlying taliks and permafrost under an active layer demonstrating

complete refreeze is still possible and merits further investigation. Given the increase in talik prevalence and a permafrost thickness of 5 - 13 m as reported by McClymont *et al.* (2013), this could result in total permafrost loss in the next century due to this process alone.

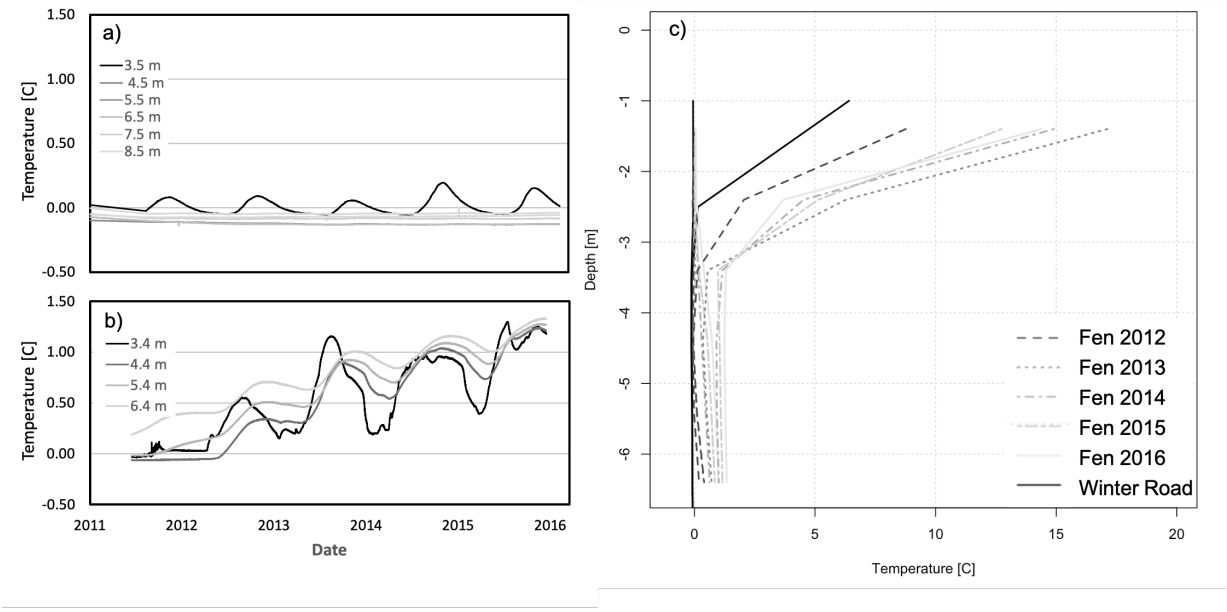

Figure 7.4: Subsurface temperature below a plateau (a) and near a fen (b) at multiple depths. Annual data for the fen is represented in a trumpet plot, and compared to the stationary data for the winter road in (c).

In addition to the geothermal heat flux, there is some evidence for groundwater-driven thaw in this field site. The warmest over-winter temperatures can be found in lakes with a minimum over-winter temperature of 1.87 °C, and mean annual temperature of 4.18 ° C at a depth of approximately 2 m. Evidence for subsurface water movement is provided by deep thermistor profiles, as shown in figure 7.4. Here it is clear that the subsurface temperature at the edge of a degrading fen is increasing, whereas that observed in a winter road not in proximity to a wetland feature indicates isothermal permafrost. Though the isothermal permafrost is likely indicative of phase change - the temperature is within the freezing point depression observed in this study site, and is likely within the zero curtain - it does not show evidence of a temperature gradient. The temperature at the edge of the fen feature however indicates a higher temperature at depth than near the surface. This noticeable thermal gradient (approximately 0.1 W/m^2 determined from the thermal profile

in figure 7.4) is somewhat greater than that expected due to geothermal heat flux, and indicates the possibility of a deep groundwater connection. This temperature profile also shows evidence for summer mixing (vertically) as the subsurface temperatures converge near their peak, but diverge in the cold winter months. Field observations of groundwater connections include upwelling and flooding of frozen wetland features in the early spring. This is further evidence that there is a groundwater source bringing energy to the system from below.

Finally, the rapid lateral permafrost thaw rate may in part be explained through low-ice content permafrost adjacent to wetlands. As shown in figure 7.4 (a), the deep subsurface in many regions is isothermal at the freezing point depression. This indicates that phase change is likely occurring, and any change in enthalpy of the system is associated with latent heat as opposed to sensible heat. The edges of permafrost bodies would be continuously exposed to thermal gradients which may drive this thaw as opposed to the centre of these bodies which are isolated. This could result in loss in lateral extent of permafrost exceeding vertical losses because the ice content may be as low as 40% where these features border wetlands. Anecdotal evidence from frost probe measurements taken in the field indicate that permafrost is 'softer' near the edge of wetland features, and as depths approach 2m. If thaw reaches a depth of 2 m, it is extremely rare to find permafrost below that depth. More investigations are needed to verify this hypothesis.

7.5 Discussion

The cases above can be summarized by adding to the conceptual diagram in figure 7.5, which indicates which thaw mechanisms dominate each landscape feature. Further to being indicative of the dominant thaw mechanisms, each of the talik configurations serves distinct functions in the discontinuous permafrost peatland environment.

7.5.1 Talik Function

Talik function can be categorized as hydrologic, thermodynamic, or geophysical.

Hydrologic Function

Taliks predominantly serve as hydrologic storage features, or extensions of wetlands in the topographically flat discontinuous permafrost peatlands environment. In the cases of

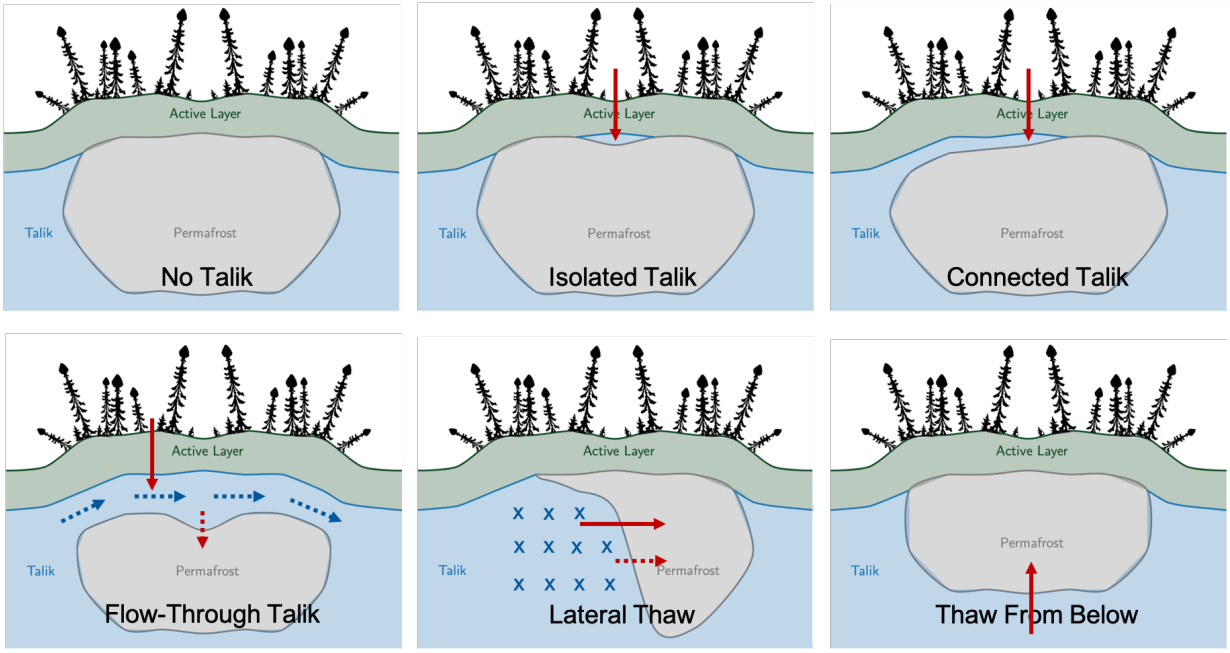

Figure 7.5: Different types of heat flux responsible for thaw in various taliks. Solid red arrows indicate conduction, dashed red arrows indicate advection-induced thaw. Dashed blue arrows indicate water flow, and blue crosses indicate flow into the page. Note that an estimate of the lateral width of these permafrost bodies is about 40 m, while their total depth is approximately 10 m. The talik configurations are symmetric to those presented in figure 7.1

isolated taliks, there is rarely a hydraulic gradient to drive flow between the taliks and surrounding features, and when there is, the storage features act to dampen the hydrologic response of the landscape. Connected taliks seem to function as extensions of the wetland to which they are connected. This is supported by water level data collected in taliks adjacent to fens, which shows water levels in the taliks tracking those observed in the fen (figure 7.6). Note that the water level is higher in the upstream locations relative to the downstream ones, and follows the trend expected in the fen.

In the case of flow-through taliks, their formation increases the hydrologic connectivity of the landscape. There are two major impacts of this increase in connectivity. The first is an increase in runoff ratio, where more of the water incident on the landscape is able to flow toward the basin outlet. This is supported by the observations presented in Connon *et al.* (2015), where there is evidence of increases in streamflow accompanying permafrost

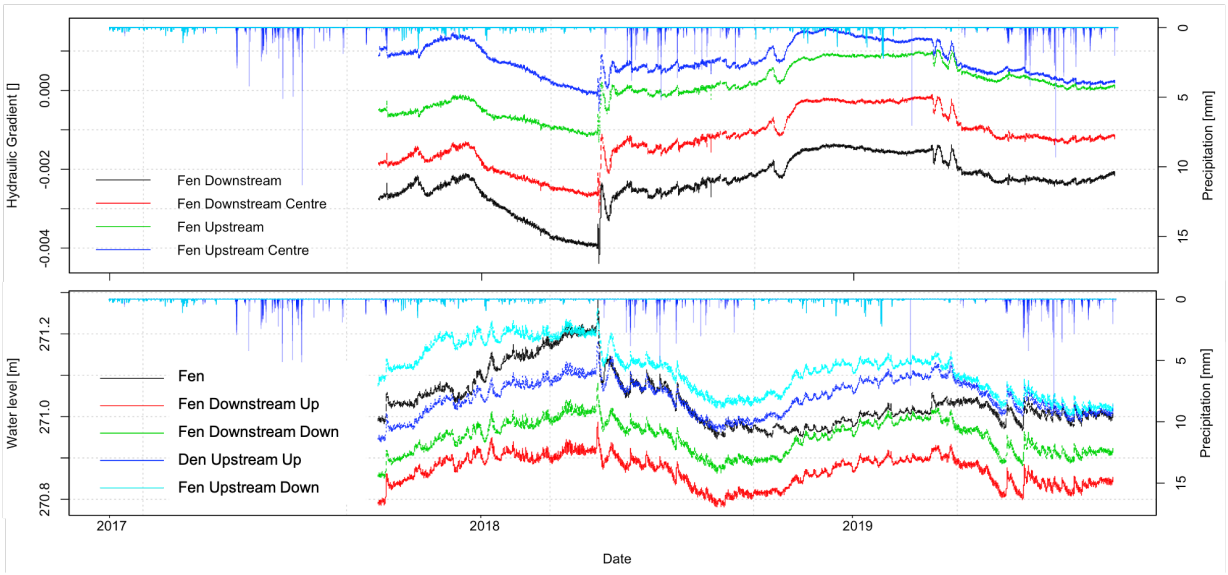

Figure 7.6: Water level records collected adjacent to a fen at SCRS. Similar trends in data show hydrologic connection, where talik acts as extension of fen feature. Precipitation shown along the top axis, where light blue is snow and dark blue is rain.

degradation, as seen in figure 7.7, modified from Connon *et al.* (In Preparation). This water may be coming from newly accessed storage features in the landscape, where water which would once have been stored in bogs or lost as ET is now routed to the basin outlet. Other studies have also observed a trend in which talik formation increases the surface-water ground-water interaction (McKenzie & Voss, 2013).

The second major hydrologic impact of these subsurface flow pathways is on the winter quiescence of the system. It is generally assumed that in the winter, flow in permafrost systems ceases as the active layer freezes down to the top of the permafrost table (Woo, 2012). However, once perennially thawed features exist in the landscape, they contribute to an increase in baseflow which is observed over the winter period, shown in the inset of figure 7.7. It is therefore clear that the presence of taliks has the potential to significantly impact the seasonal runoff and baseflow regimes.

Thermodynamic Function

Most of the transferable energy in this discontinuous permafrost landscape is associated with the sensible heat of liquid water, and so the thermodynamic function of taliks mirrors

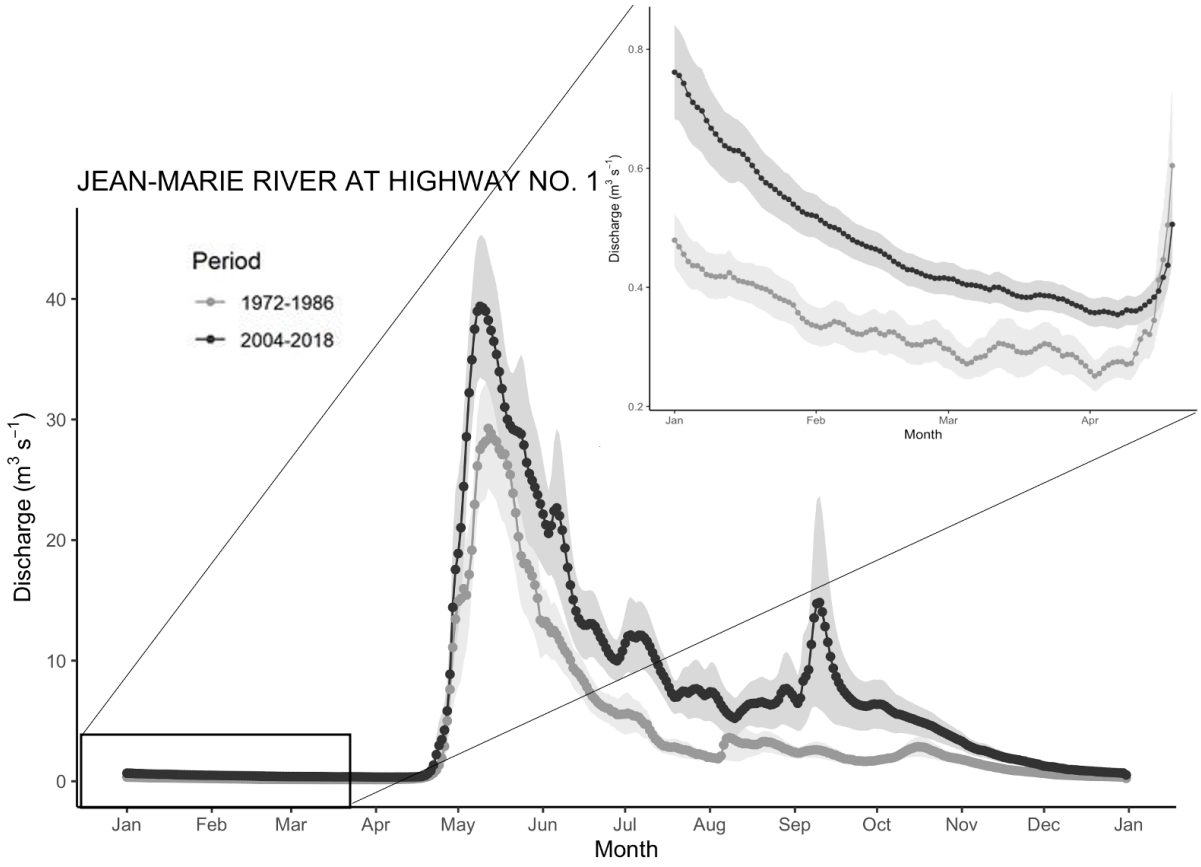

Figure 7.7: Increase in mean streamflow observed at the outlet of Jean-Marie river. This basin is adjacent to Scotty Creek with similar land cover classification, and a contributing area ten times that of the Scotty Creek catchment (Connon *et al.*, 2014). No remarkable change in precipitation was observed over the documented period. Modified from Connon *et al.* (In Preparation). Increase in baseflow observed especially over the winter months due to talik formation.

their hydrologic function. As such, isolated and connected taliks act as energy storage features, and accelerate permafrost thaw by preventing the over-winter cooling of the soil profile as discussed in section 7.4.2. Though flow-through features may convey heat with the water that is transported through them, it is more likely that the heat stored in water flowing through them is passed to the permafrost and active layer. This acts to accelerate thaw in these features, as well as alongside the edges of fens where lateral thaw progresses rapidly year-round. The presence of a talik often coincides with increased soil moisture

and depressions formed due to subsidence, leading to the positive feedback cycle discussed in the introduction (Quinton & Baltzer, 2013).

Geophysical Function

In a geophysical sense, ground ice lends significant structure to the discontinuous permafrost peatlands environment. It is clear from the landscape that forested areas are limited to peat plateaux which are generally underlain by permafrost. Once permafrost degradation takes place, subsidence causes the dry ground to meet the water table, flooding the roots of the canopy and resulting in the loss of the black spruce over-story (Baltzer *et al.*, 2014). Subsidence is especially evident in features adjacent to wetlands, and it is possible that thaw from below is causing this more rapid change in ground surface elevation. In some areas where permafrost has degraded and subsequent drainage has occurred, a tree canopy may return to the landscape, but it is unclear whether this is a stable condition, and if these treed environments are suited to future conditions (Disher, 2020). The fact that permafrost loss results in landscape transitions points to the nonstationarity of this system, indicating that it is perhaps inappropriate to represent any given location in the landscape using one model system. A schematic of this change is presented in the introduction of this thesis, shown in figure 3.5.

7.5.2 Nonstationarity

It is clear from the the results presented above that permafrost is changing rapidly at the SCRS, and in similar field sites across the NWT (Carpino *et al.*, 2020). This change necessitates an evolving description of the landscape in order to track processes. For instance, a flow-through talik was found and instrumented in 2016. As observed in figure 7.8, the subsurface temperature profile at this site was initially similar to that observed on a stable peat plateau (indicated in dark blue). However, by 2019 we observe that the temperature profile is now much more similar to the bog condition (gold). The evolution of the temperature profile over time can be seen in figure 7.9.

This extremely rapid transition is not unique to this particular site, in fact, similar results are observed in a flow-though talik that was instrumented much earlier in its formation. Figure 7.10 shows the degradation of this plateau feature separating two bogs over the last two decades (along with the shorter timeseries drawn from the site instrumented in 2016:"B100-NA"). The similarities in both vertical and lateral permafrost degradation over the past four years are remarkable. This figure also highlights the fact that any one

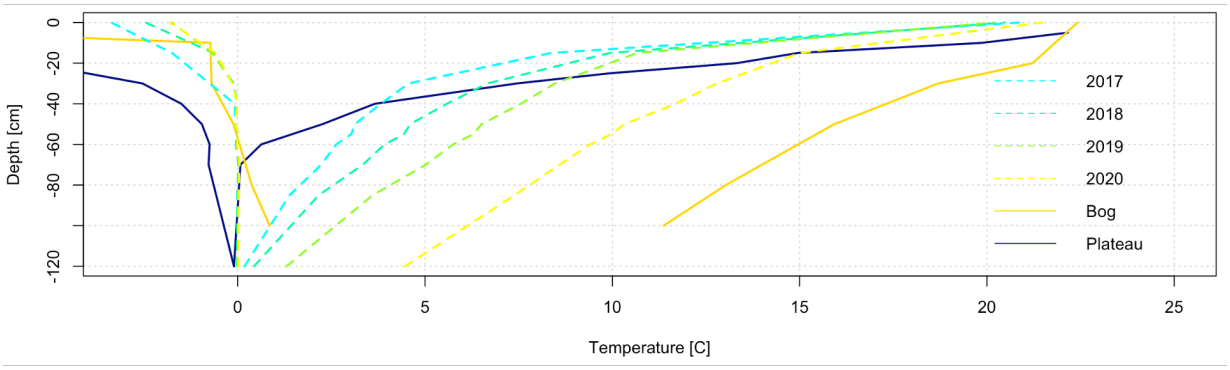

Figure 7.8: Trumpet plot of talik development with advection between two bogs. End members of permafrost warming are shown as plateau (dark blue) and bog (gold).

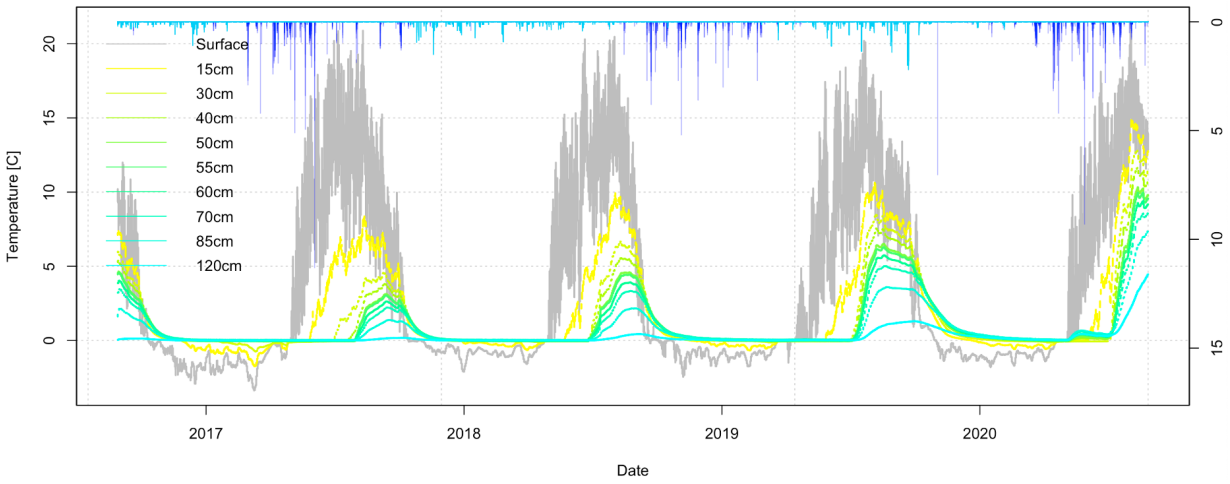

Figure 7.9: Temperature profile of talik with advection between two bogs. Air temperature shown in grey and subsurface temperatures shading from yellow to cyan as depth increases. Note the increasing depth of active layer warming in the summer and the isothermal conditions over winter indicating incomplete refreeze.

thaw mechanism is not acting independently - vertical and lateral thaw occur simultaneously and must both be represented to accurately predict permafrost degradation. Thus, figure 7.5 may describe the predominant mechanism for thaw in each case, but not the exclusive mechanism.

Not only are these processes occurring simultaneously, but the data in figure 7.10

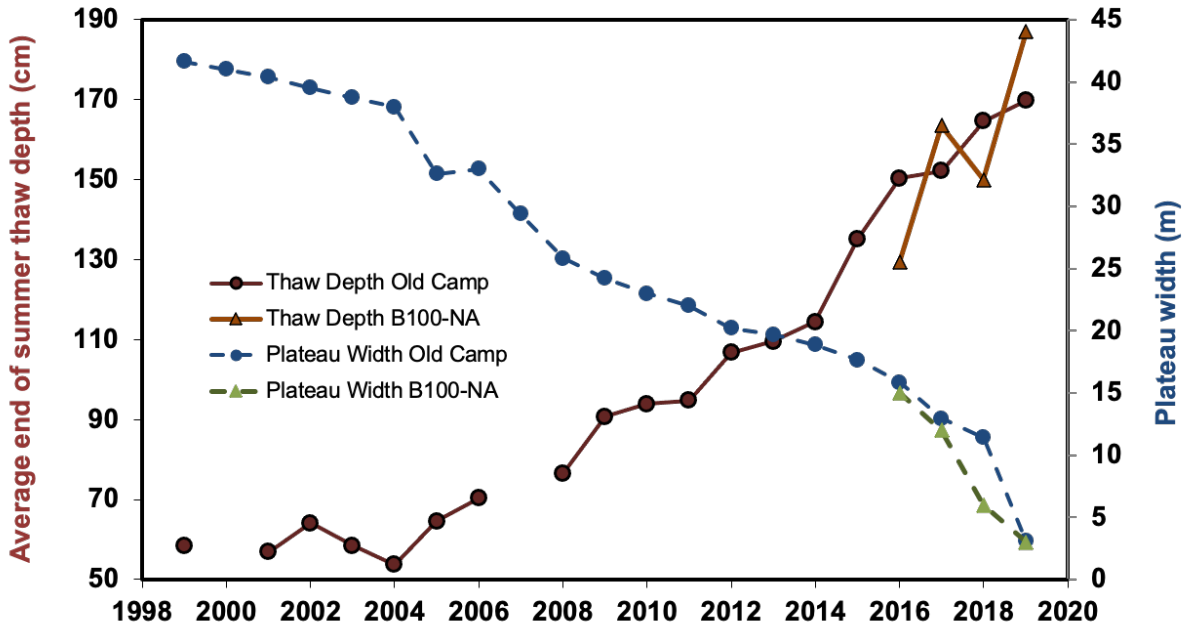

Figure 7.10: Simultaneous vertical and lateral permafrost thaw observed at two sites in the SCRS. There are two notable turning points: when the thaw depth exceeds about 70 cm, the rate of permafrost degradation increases, and again when the thaw depth reaches about 110 cm and the width is 15 - 20 m, there is an inflection point.

indicate co-dependence of thaw rates. There are two notable changes in this figure, the first is when the thaw depth exceeds 70 cm, and both the vertical and lateral thaw rates increase notably. This may indicate the point at which a connected talik was formed allowing for advection to act alongside vertical conduction. A second turning point can be picked out when the plateau width is 15 - 20 m, and the rate of permafrost thaw again increases. This may indicate the action of lateral as well as vertical thaw processes and thaw from below. Additionally, as the talik thickens there is potential for active layer thinning as the thermal storage in the talik increases and counteracts the maximum refreeze depth. This can be observed in figure 4.4 (c) from chapter 4, where the maximum depth of refreeze seems to increase with talik thickness. We also note that once permafrost is not present in the soil column, there is potential for the geothermal heat flux to limit refreeze depth as well.

7.5.3 Talik Evolution - Trajectory of Change

Figure 7.2 shows that the mean permafrost degradation rate across this landscape is positive. This indicates that permafrost at the SCRS is in disequilibrium with the climate, and due to changes in climate this region is headed towards permafrost-free conditions. As presented in Carpino *et al.* (2020), there is a trajectory of change in which the formation of an isolated talik results from increased incoming radiation. The positive feedback driven by subsidence, canopy thinning and increased thermal conductivity causes talik expansion, leading to connection(s) with wetland features. Degradation continues, with the potential for advection along with conduction, and lateral thaw in addition to the vertical thaw. Plateaux are then expected to degrade, forming either bogs or fens. Evidence for bog capture, in which bog features expand until they become hydrologically indistinct, is presented in Haynes *et al.* (2018). This process leads to landscape drying and it is thought that widespread thaw may result in drainage and the re-establishment of a tree canopy on a permafrost-free landscape (Carpino *et al.*, 2020).

7.6 Conclusion

This study shows that vertical thaw in isolated and connected taliks can be explained exclusively through (vertical) conduction, while advection is needed in addition to conduction to describe observed thaw in flow-through taliks. This was expected, however it was notable that connected taliks that did not allow for flow through features had thaw explained by conduction alone. The rate of thaw increases with the size and degree of connectivity of the talik feature. It highlights that lateral thaw rates adjacent to different wetland features show clear dependence on advection, and degradation occurs significantly faster in these features. Deep subsurface temperatures provide evidence for thaw from below, and potential for isothermal permafrost degradation in which soil at the freezing point depression is only partially frozen. The geothermal heat flux may be responsible for significant thinning of degrading permafrost bodies from below. The results show that we can readily represent the vertical evolution of isolated and connected taliks using 1D conduction-only models, but flow through taliks and lateral thaw likely require higher-dimensional models for long-term predictions. Though these governing processes can be distinguished and used for modelling purposes, the system is non-stationary, and thus different processes are expected to dominate permafrost thaw as the system changes. Not only is the behaviour non-stationary, but it is also likely site-specific and variable. In order to capture permafrost degradation at regional scales in future work, it is important to classify the wetland features according to their probability of conveying flow as this seems to dominate the rate of

lateral degradation. Vertical permafrost thaw can likely be adequately represented through conduction alone as flow-through taliks are rare in the landscape, and vertical thaw is slow compared to the lateral process. Degradation generally follows a pattern of talik formation and evolution in which isolated taliks become connected, with a potential for flow-through, and then degrade entirely merging with wetland features. Permafrost aggradation is not documented or expected in this landscape.

Chapter 8

Conclusions

This thesis addresses four main objectives, though there is overlap between these objectives and each of the four chapters. Here we present how each chapter is related to each major objective while highlighting the major findings of this PhD work.

The first objective was to **identify and quantify controls on local talik formation in the Taiga Plains discontinuous permafrost zone using a mixed field and modelling approach.** Chapter 4 focused on addressing this objective, where a combination of field data and 1D modelling was used to investigate the formation of isolated taliks and it was found that soil moisture, snowcover, and advection affect their formation and development. This work demonstrated that the formation of taliks in the discontinuous permafrost peatlands environment of the SCRS is essentially irreversible. The only conditions under which permafrost was reestablished once a talik was formed were significant drying of soils beyond the natural variability in the landscape. The scientific contributions of this work include identifying conditions under which taliks are likely to develop, and establishing a tool to predict patterns and rates of permafrost thaw at the hillslope scale.

The second objective was to **determine and compare the hydrologic function of taliks adjacent to bogs and fens by analyzing seasonal pressure and temperature gradients to understand the evolution and thaw mechanisms in the discontinuous permafrost peatland system.** Chapter 4 also partially addressed this objective by determining that the formation of an isolated talik results in accelerated and likely irreversible permafrost thaw. In the pursuit of understanding talik function, it was found that current methods for the estimation of subsurface flow were inadequate to quantify the flow through talik features. This led to the investigation of passive flux meters discussed in chapter 5. Here it was found that passive flux meters can be used to estimate

subsurface flow in permafrost regions under unsaturated and partially frozen conditions, and are useful when gradient-based measurements are highly uncertain. This study was the first application of PFMs in a permafrost environment. Once subsurface flows were quantified, it was possible to combine field data with modelling approaches to determine that taliks act predominantly as storage features or extensions of wetland features in this landscape. Chapter 7 shows that taliks can increase the hydrologic connectivity of the landscape when they connect wetland features, and this may contribute to the increase in discharge from this study basin observed over the last four decades. Taliks may also be responsible for the increase in overwinter flows which have been observed. The feedbacks between permafrost degradation and hydrology indicate a hydrologic regime shift from a system dominated by winter quiescence to one in which there is year-round flow. As noted in the first objective, this study confirms that taliks are thermal storage features in the landscape, and that their formation almost inevitably leads to permafrost loss.

The third objective was to **develop, validate and test a physically-based interface model of active layer evolution.** Chapter 6 describes this model development. A novel semi-analytical model of soil freeze and thaw was presented for application in hydrology. This model is numerically stable and scale insensitive, and up to three orders of magnitude faster than the continuum equivalent. Model validation was performed against both field data and a benchmarked numerical model. This is one of the most significant scientific contributions of this thesis. This interface model presents a new efficient approach to solve the heat equation, allowing for previously prohibitively computationally expensive simulations to be feasible. This includes sensitivity analyses, model calibration, hypothesis testing, long-term simulations, and many other applications.

The fourth and final goal of this thesis was to **distinguish thaw mechanisms in the discontinuous permafrost peatlands environment and use a combination of modelling and data collected in the filed to determine which processes lead to the spatially variable thaw observed at the SCRS.** First, this objective led to a much clearer process understanding of thaw in discontinuous permafrost peatlands outlined in chapter 7. It was found that vertical permafrost thaw **can** be explained exclusively through (vertical) conduction in both isolated and connected taliks, while advection was needed in addition to conduction to describe observed thaw in flow-through taliks. Lateral thaw rates adjacent to different wetland features showed a clear dependence on advection-driven thaw, and were significantly higher than vertical thaw rates. Deep subsurface temperatures provided evidence for thaw from below adjacent to fens partially attributed to the geothermal heat flux which may be playing an important role in lateral permafrost degradation. These thaw rates from below have not been previously considered in this landscape, but given current estimates of the geothermal gradient, this may lead to widespread permafrost

loss in the next century, especially in areas with taliks. Chapter 7 outlines the pattern of permafrost degradation in peatlands. It is postulated that permafrost thaw is initiated by the formation of an isolated talik which expands and coalesces with other thaw features to form a connection between wetland features. As features become connected, thaw rates are observed to increase, and thaw becomes dominated by lateral conduction and advection when taliks become connected to wetland features. This work categorizes thaw processes according to their mechanisms and dimensionality, which allows to distinguish when more efficient 1-D conduction-based models can be used as opposed to higher-dimension models including water movement. This work also contributed a discussion of the hydrological, geophysical and thermodynamic function of taliks which will become increasingly relevant as permafrost thaw extends further north.

In summary, this thesis has shed some light on the poorly understood process of permafrost degradation in peatlands, while contributing a versatile tool to permafrost and hydrologic modelling. It is hoped that the interface model presented here is useful in future work in various environments and applications.

Shortcomings and Limitations

Though useful, this thesis by no means addresses conclusively the function of discontinuous permafrost peatlands environment. Many limitations to this work exist, and the most important are listed here:

- Data was collected at one study site, and there may be inter-site variability
- Modelling work was mostly 1-D, and though source/sink terms were included to capture lateral processes, these were not evolving in time
- Process description mainly limited to a pseudo-stationary conception of the landscape, while likely permafrost evolution and loss is occurring due to many of the discussed processes simultaneously, and each feature is evolving in time so the process description should as well
- Data used for model simulations collected at a point scale as many measurements across the basin, however distributed and time-evolving measurements of permafrost table and soil moisture were not available to rigorously validate models
- Though some feedbacks between permafrost, soil moisture, ground elevation, snow cover, canopy cover etc. are discussed, it is likely that some factors are overlooked, presented conceptual models are a simplification of the observed system

- Measurements of several processes were not available - e.g. geothermal heat flux, lateral heat flux, deep groundwater movement, etc. These processes were estimated using the available modelling tools and what data was available to describe them indirectly, but this leaves room for misinterpretation of results
- Use and understanding of PFMs was limited by the proprietary information associated with the instruments, making it challenging to quantify error based on incomplete methodological information
- Flow in frozen or partially frozen soils is empirically based using impedance due to ice content, field data would be highly beneficial
- Simulating cryosuction in unsaturated soils was attempted, but representing this process is numerically challenging and little data and methodology exists explicitly indicating how this should be combined with matric potential, future work should support assumptions made herein regarding the additivity of cryosuction and matric potential terms
- Lateral heat transfer through permafrost underlying taliks and talik-free soil columns was not considered in simulations
- Hysteretic effects in soil moisture characteristic curves as well as in soil freezing functions were neglected

Future Research

Future work will involve extensions to the interface model so it is more suited to describe mineral soils, seasonal ground ice, and moisture migration. Once complete, the model will be added to a semi-distributed modelling framework to assess the impacts of permafrost loss and changes in seasonal ground ice dynamics on basin-scale hydrology. This will allow the local results detailed in this thesis to be upscaled to the basin scale and transferred to other study catchments. An extension of the interface model capable of representing subsidence would make this model even more relevant to the assessment of permafrost and ground stability.

Field studies should be conducted to quantify lateral permafrost thaw mechanisms, and to extend the conceptual understanding of thaw mechanisms beyond peatlands to other discontinuous and continuous permafrost environments. Studies in other environments would be valuable to determine if the mechanisms for and impacts of permafrost degradation at the SCRS are transferable to other landscapes. Additional work is especially

needed to elucidate the process of permafrost thaw from below - is this a phenomenon driven solely by the geothermal gradient, or does deep groundwater movement affect this thaw rate? Is this degradation distributed across the landscape, or confined to the periphery of permafrost bodies? What rates of degradation can be expected from the base of the permafrost body? This work also raises a definition question regarding taliks - if they are a perennially thawed feature in a permafrost environment, how much permafrost does there need to be and how far away can it be?

References

2017. *GEO SLOPE Temp/W*. https://www.geo-slope.com/products/temp-w. Accessed: 2017-09-06.

Ali, G, Oswald, CJ, Spence, C, Cammeraat, ELH, McGuire, KJ, Meixner, T, & Reaney, SM. 2013. Towards a unified threshold-based hydrological theory: necessary components and recurring challenges. *Hydrological Processes*, **27**(2), 313–318.

Amiri, Erfan A, & Craig, James R. 2019. Effect of Soil Thermal Heterogeneity on Permafrost Evolution. *Pages 492–499 of: Cold Regions Engineering 2019*. American Society of Civil Engineers Reston, VA.

Amiri, Erfan A, Craig, James R, & Kurylyk, Barret L. 2018. A theoretical extension of the soil freezing curve paradigm. *Advances in water resources*, **111**, 319–328.

Ankeny, Mark D., Ahmed, Mushtaque, Kaspar, Thomas C., & Horton, Robert. 1991. Simple Field Method for Determining Unsaturated Hydraulic Conductivity. *Soil Science Society*.

Annable, Michael D, Hatfield, Kirk, Cho, Jaehyun, Klammler, Harald, Parker, Beth L, Cherry, John A, & Rao, P Suresh C. 2005. Field-scale evaluation of the passive flux meter for simultaneous measurement of groundwater and contaminant fluxes. *Environmental science & technology*, **39**(18), 7194–7201.

Arnold, J. G., Srinivasan, R., Muttiah, R. S., & Williams, J. R. 1998. Large area hydrologic modeling and assessment – part I: Model development. *J. Am. Water Resour. Assoc.*, **34**, 73–89.

Atchley, Adam L, Painter, Scott L, Harp, Dylan R, Coon, Ethan T, Wilson, Cathy J, Liljedahl, Anna K, & Romanovsky, Vladimir E. 2015. Using field observations to inform thermal hydrology models of permafrost dynamics with ATS (v0. 83). *Geoscientific Model Development Discussions (Online)*, **8**(4).

Atchley, Adam L, Coon, Ethan T, Painter, Scott L, Harp, Dylan R, & Wilson, Cathy J. 2016. Influences and interactions of inundation, peat, and snow on active layer thickness. *Geophysical Research Letters*, **43**(10), 5116–5123.

Baltzer, Jennifer L, Veness, Tyler, Chasmer, Laura E, Sniderhan, Anastasia E, & Quinton, William L. 2014. Forests on thawing permafrost: fragmentation, edge effects, and net forest loss. *Global Change Biology*, **20**(3), 824–834.

Bay, RR. 1969. Runoff from small peatland watersheds. *Journal of Hydrology*, **9**(1), 90–102.

Bense, VF, Ferguson, G, & Kooi, H. 2009. Evolution of shallow groundwater flow systems in areas of degrading permafrost. *Geophysical Research Letters*, **36**(22).

Benton, Joshua, Schreiber, Madeline Eve, McGuire, Kevin J, Strahm, Brian D, Ross, Donald S, Bailey, Scott W, Bower, Jennifer, & Duston, Stephanie. 2018. Characterizing Subsurface Hydrologic Fluxes within a Glaciated Watershed. *AGUFM*, **2018**, H21K–1810.

Berghuijs, WR, Woods, R a, & Hrachowitz, M. 2014. A precipitation shift from snow towards rain leads to a decrease in streamflow-supplement. *Nature Climate Change*, **4**(7), 583–586.

Bloschl, G, & Sivapalan, M. 1995. Scale issues in hydrological modelling: a review. *Hydrological Processes*, **9**(September 1994).

Boelter, DH. 1966. Important physical properties of peat materials. *Proc. Third Internal Peat Congr.*, 150–154.

Boelter, DH. 1976. Methods for analyzing the hydrological characteristics of organic soils in marsh-ridden areas. *Forest Service, US Department of Agriculture, Grand Rapids, Minnesota, USA.*, 161–169.

Bonnaventure, Philip P, & Lamoureux, Scott F. 2013. The active layer: a conceptual review of monitoring, modelling techniques and changes in a warming climate. *Progress in Physical Geography*, **37**(3), 352–376.

Braverman, Michael, & Quinton, William L. 2016. Hydrological impacts of seismic lines in the wetland-dominated zone of thawing, discontinuous permafrost, Northwest Territories, Canada. *Hydrological Processes*, **30**(15), 2617–2627.

Briggs, Martin A, Walvoord, Michelle A, McKenzie, Jeffrey M, Voss, Clifford I, Day-Lewis, Frederick D, & Lane, John W. 2014. New permafrost is forming around shrinking Arctic lakes, but will it last? *Geophysical Research Letters*, **41**(5), 1585–1592.

Brown, Dana RN, Jorgenson, M Torre, Douglas, Thomas A, Romanovsky, Vladimir E, Kielland, Knut, Hiemstra, Christopher, Euskirchen, Eugenie S, & Ruess, Roger W. 2015. Interactive effects of wildfire and climate on permafrost degradation in Alaskan lowland forests. *Journal of Geophysical Research: Biogeosciences*, **120**(8), 1619–1637.

Bruulsema, A, Friesen, D, & Tanciongko, K. 2017. Soil frost measurement device. *4th Year Design Project, Mechanical Engineering, University of Waterloo.*

Burn, Christopher Robert. 1998. The active layer: two contrasting definitions. *Permafrost and Periglacial Processes*, **9**(4), 411–416.

Canada Soil Survey Committee. 1978. *The Canadian system of soil classification.* Research Branch, Canada Department of Agriculture.

Carey, SK. 2003. Dissolved organic carbon fluxes in a discontinuous permafrost subarctic alpine catchment. *Permafrost and Periglacial Processes*, **14**(2), 161–171.

Carey, SK, & Quinton, WL. 2004. Evaluating snowmelt runoff generation in a discontinuous permafrost catchment using stable isotope, hydrochemical and hydrometric data. *Nordic Hydrology*, **35**(4-5), 309–324.

Carpino, Olivia, Haynes, Kristine, Connon, Ryan, Craig, James, Devoie, Élise, & Quinton, William. 2020. The trajectory of landcover change in peatland complexes with discontinuous permafrost, northwestern Canada. *Hydrology and Earth System Sciences Discussions*, 1–40.

Carpino, Olivia A, Berg, Aaron A, Quinton, William L, & Adams, Justin R. 2018. Climate change and permafrost thaw-induced boreal forest loss in northwestern Canada. *Environmental Research Letters*, **13**(8), 084018.

Carslaw, H. S., & Jaeger, J. C. 1959. *Conduction of heat in solids.* Oxford at the Clarendon press.

Celia, M, Bouloutas, E, & Zarba, R. 1990. A general mass-conservative numerical solution for the unsaturated flow equation. *Water Resources Research*, **26**(7), 1483–1496.

Chappell, Nick A, & Lancaster, James W. 2007. Comparison of methodological uncertainties within permeability measurements. *Hydrological Processes: An International Journal*, **21**(18), 2504–2514.

Chasmer, L, Quinton, W, Hopkinson, C, Petrone, R, & Whittington, P. 2011. Vegetation canopy and radiation controls on permafrost plateau evolution within the discontinuous permafrost zone, Northwest Territories, Canada. *Permafrost and Periglacial Processes*, **22**(3), 199–213.

Chasmer, L, Quinton, W, Hopkinson, C, Veness, T, & Baltzer, J. 2014. A decision-tree classification for low-lying complex land cover types within the zone of discontinuous permafrost. *Remote Sensing of the Environment*, **143**, 73–84.

Chen, Hua, Xu, Chong-Yu, & Guo, Shenglian. 2012. Comparison and evaluation of multiple GCMs, statistical downscaling and hydrological models in the study of climate change impacts on runoff. *Journal of hydrology*, **434**, 36–45.

Cherkauer, KA, & Lettenmaier, DP. 1999. Hydrologic effects of frozen soils in the upper Mississippi River basin. *Journal of Geophysical Research*, **104**.

Christensen, Brendan. 2014 (2). *Permafrost development and active-layer hydrology of peat plateaus in wetland-dominated discontinuous permafrost*. M.Phil. thesis, University of Calgary.

Clymo, R. 2012. The origin of acidity in sphagnum bogs. *American Bryological and Lichenological Society*, **67**(4), 427–431.

Clymo, RS. 1984. The limits to peat bog growth. *Philosophical Transactions of the Royal Society of London. B, Biological Sciences*, **303**(1117), 605–654.

Connon, RF, Quinton, WL, Craig, JR, & Hayashi, M. 2014. Changing hydrologic connectivity due to permafrost thaw in the lower Liard River valley, NWT, Canada. *Hydrological Processes*, **28**(14), 4163–4178.

Connon, RF, Quinton, WL, Craig, JR, Hanisch, J, & Sonnentag, O. 2015. The hydrology of interconnected bog complexes in discontinuous permafrost terrains. *Hydrological Processes*, **29**(18), 3831–3847.

Connon, RF, Quinton, WL, & Haughness, E. In Preparation. Changes in snow and streamflow at Scotty Creek Research Station. *Hydrologic Processes*.

Connon, Ryan, Devoie, Élise, Hayashi, Masaki, Veness, Tyler, & Quinton, William. 2018. The influence of shallow taliks on permafrost thaw and active layer dynamics in subarctic Canada. *Journal of Geophysical Research: Earth Surface*, **123**(2), 281–297.

Côté, Jean, & Konrad, Jean-Marie. 2005. Thermal conductivity of base-course materials. *Canadian Geotechnical Journal*, **42**(1), 61–78.

Craig, James R, Brown, Genevieve, Chlumsky, Robert, Jenkinson, Wayne, Jost, Georg, Lee, Konhee, Mai, Juliane, Serrer, Martin, Snowdon, Andrew P, Sgro, Nicholas, *et al.* 2020. Flexible watershed simulation with the Raven hydrological modelling framework. *Environmental Modelling & Software*, 104728.

Cuntz, M, Mai, J, Zink, M, Thober, S, Kumar, R, Schäfer, D, Schrön, M, Craven, J, Rakovec, O, Spieler, D, *et al.* 2015. Computationally inexpensive identification of noninformative model parameters by sequential screening. *Water Resources Research*, **51**(8), 6417–6441.

Daanen, Ronald P, Misra, Debasmita, Epstein, Howard, Walker, Donald, & Romanovsky, Vladimir. 2008. Simulating nonsorted circle development in arctic tundra ecosystems. *Journal of Geophysical Research: Biogeosciences*, **113**(G3).

de Grandpré, Isabelle, Fortier, Daniel, & Stephani, Eva. 2012. Degradation of permafrost beneath a road embankment enhanced by heat advected in groundwater. *Canadian Journal of Earth Sciences*, **49**(8), 953–962.

Desormeaux, Amanda, Annable, Michael D, Dobberfuhl, Dean, & Jawitz, James W. 2019. In situ measurement of nitrate flux and attenuation using a soil passive flux meter. *Journal of environmental quality*, **48**(3), 709–716.

Devito, K, Waddington, JM, & Branfireun, BA. 1997. Flow reversals in peatlands influenced by local groundwater systems. *Hydrological Processes*, **11**, 103–110.

Devito, K, Creed, I, Gan, T, Mendoza, C, Petrone, R, Silins, U, & Smerdon, B. 2005. A framework for broad-scale classification of hydrologic response units on the Boreal Plain: is topography the last thing to consider? *Hydrological processes*, **19**(8), 1705–1714.

Devoie, Élise G, & Craig, James R. 2020. A Semianalytical Interface Model of Soil Freeze/Thaw and Permafrost Evolution. *Water Resources Research*, **56**(8), e2020WR027638.

Devoie, Élise G, Craig, James R, Connon, Ryan F, & Quinton, William L. 2019. Taliks: A tipping point in discontinuous permafrost degradation in peatlands. *Water Resources Research*, **55**(11), 9838–9857.

Devoie, Élise G, Connon, Ryan F, Craig, James R, & Quinton, William L. 2020. Subsurface flow measurements using passive flux meters in variably-saturated cold-regions landscapes. *Hydrological Processes*.

Disher, Brenden. 2020. Characterizing the hydrological function of treed bogs in the zone of discontinuous permafrost.

Edlefsen, N, Anderson, A, *et al.* 1943. Thermodynamics of soil moisture. *Hilgardia*, **15**(2), 31–298.

Endrizzi, S, Gruber, Stephan, Dall'Amico, M, & Rigon, R. 2014. GEOtop 2.0: simulating the combined energy and water balance at and below the land surface accounting for soil freezing, snow cover and terrain effects. *Geoscientific Model Development*, **7**(6), 2831–2857.

Evans, Sarah G, & Ge, Shemin. 2017. Contrasting hydrogeologic responses to warming in permafrost and seasonally frozen ground hillslopes. *Geophysical Research Letters*, **44**(4), 1803–1813.

Fabre, Clément, Sauvage, Sabine, Tananaev, Nikita, Srinivasan, Raghavan, Teisserenc, Roman, & Sánchez Pérez, José Miguel. 2017. Using modeling tools to better understand permafrost hydrology. *Water*, **9**(6), 418.

Fan, Y., Li, H., & Miguez-Macho, G. 2013. Global Patterns of Groundwater Table Depth. *Science*, **339**(6122), 940–943.

Fisher, James P, Estop-Aragonés, Cristian, Thierry, Aaron, Charman, Dan J, Wolfe, Stephen A, Hartley, Iain P, Murton, Julian B, Williams, Mathew, & Phoenix, Gareth K. 2016. The influence of vegetation and soil characteristics on active-layer thickness of permafrost soils in boreal forest. *Global Change Biology*, **22**(9), 3127–3140.

Fourier, Jean Baptiste Joseph. 1878. *The analytical theory of heat*. The University Press.

Frampton, A, Painter, S, Lyon, SW, & Destouni, G. 2011. Non-isothermal, three-phase simulations of near-surface flows in a model permafrost system under seasonal variability and climate change. *Journal of Hydrology*, **403**, 352–359.

Frampton, Andrew, Painter, Scott L, & Destouni, Georgia. 2013. Permafrost degradation and subsurface-flow changes caused by surface warming trends. *Hydrogeology Journal*, **21**(1), 271–280.

Fredlund, DG, Gan, JK, & Rahardjo, H. 1991. Measuring negative pore water pressures in a freezing environment. vol. 1307.

Gelfan, Alexander, Gustafsson, David, Motovilov, Yury, Arheimer, Berit, Kalugin, Andrey, Krylenko, Inna, & Lavrenov, Alexander. 2017. Climate change impact on the water regime of two great Arctic rivers: modeling and uncertainty issues. *Climatic change*, **141**(3), 499–515.

Gharedaghloo, Behrad, Price, Jonathan S, Rezanezhad, Fereidoun, & Quinton, William L. 2018. Evaluating the hydraulic and transport properties of peat soil using pore network modeling and X-ray micro computed tomography. *Journal of Hydrology*, **561**, 494–508.

Gharedaghloo, Behrad, Berg, Steven J, & Sudicky, Edward A. 2020. Water freezing characteristics in granular soils: Insights from pore-scale simulations. *Advances in Water Resources*, **143**, 103681.

Gillespie, AW, Sanei, H, Diochon, A, Ellert, BH, Regier, TZ, Chevrier, D, Dynes, JJ, Tarnocai, C, & Gregorich, EG. 2014. Perennially and annually frozen soil carbon differ in their susceptibility to decomposition: analysis of Subarctic earth hummocks by bioassay, XANES and pyrolysis. *Soil Biology and Biochemistry*, **68**, 106–116.

Goodrich, LE. 1978. Efficient numerical technique for one-dimensional thermal problems with phase change. *International Journal of Heat and Mass Transfer*, **21**(5), 615–621.

Gordon, J, Quinton, W, Branfireun, BA, & Olefeldt, D. 2016. Mercury and methylmercury biogeochemistry in a thawing permafrost wetland complex, Northwest Territories, Canada. *Hydrological Processes*, **30**(20), 3627–3638.

Grant, RF, Mekonnen, ZA, Riley, WJ, Wainwright, HM, Graham, D, & Torn, MS. 2017. Mathematical modelling of arctic polygonal tundra with ecosys: 1. Microtopography determines how active layer depths respond to changes in temperature and precipitation. *Journal of Geophysical Research: Biogeosciences*, **122**(12), 3161–3173.

Gray, DM, Toth, Brenda, Zhao, Litong, Pomeroy, JW, & Granger, RJ. 2001. Estimating areal snowmelt infiltration into frozen soils. *Hydrological Processes*, **15**(16), 3095–3111.

Grosse, Guido, Goetz, Scott, McGuire, A. Dave, Romanovsky, Vladimir E., & Schuur, Edward A.G. 2016. Review and Synthesis: Changing Permafrost in a Warming World and Feedbacks to the Earth System. *Environmental Research Letters*.

Gupta, N, Rudra, RP, & Parkin, G. 2006. Analysis of spatial variability of hydraulic conductivity at field scale. *Canadian Biosystems Engineering*, **48**, 1.

Hallett, PD, Nunan, N, Douglas, JT, & Young, IM. 2004. Millimeter-scale spatial variability in soil water sorptivity: Scale, surface elevation, and subcritical repellency effects. *Soil Science Society of America Journal*, **68**(2), 352–358.

Haluska, Alexander A, Thiemann, Meghan S, Evans, Patrick J, Cho, Jaehyun, & Annable, Michael D. 2018. Expanded application of the passive flux meter: In-situ measurements of 1, 4-dioxane, sulfate, Cr (VI) and RDX. *Water*, **10**(10), 1335.

Harlan, RL. 1973. Analysis of coupled heat-fluid transport in partially frozen soil. *Water Resources Research*, **9**.

Harris, A. 2008. Spectral reflectance and photosynthetic properties of Sphagnum mosses exposed to progressive drought. *Ecohydrology*, **130**(February), 126–130.

Hatfield, Kirk, Rao, P. Suresh C., Annable, Michael D., & Campbell, Timothy J. 2002. *Device and method for measuring fluid and solute fluxes in flow systems*. Tech. rept. United States Patent.

Hatfield, Kirk, Annable, Michael, Cho, Jaehyun, Rao, PSC, & Klammler, Harald. 2004. A direct passive method for measuring water and contaminant fluxes in porous media. *Journal of contaminant hydrology*, **75**(3-4), 155–181.

Hayashi, M, Goeller, N, Quinton, WL, & Wright, N. 2007. A simple heat-conduction method for simulating the frost-table depth in hydrological models. *Hydrological Processes*, 2610–2622.

Hayashi, Masaki. 2013. The cold vadose zone: Hydrological and ecological significance of frozen-soil processes. *Vadose Zone Journal*, **12**(4).

Hayashi, Masaki, van der Kamp, Garth, & Rudolph, David L. 1997. Use of tensiometer response time to determine the hydraulic conductivity of unsaturated soil. *Soil science*, **162**(8), 566–575.

Haynes, KM, Connon, RF, & Quinton, WL. 2018. Permafrost thaw induced drying of wetlands at Scotty Creek, NWT, Canada. *Environmental Research Letters*, **13**(11), 114001.

Hewlett, JD, & Hibbert, AR. 1967. Factors affecting the response of small watersheds to precipitation in humid areas. *Forest Hydrology*, **1**, 275–290.

Hinkel, KM, Paetzold, F, Nelson, FE, & Bockheim, JG. 2001. Patterns of soil temperature and moisture in the active layer and upper permafrost at Barrow, Alaska: 1993–1999. *Global and Planetary Change*, **29**(3-4), 293–309.

Hinzman, LD, Goering, DJ, & Kane, DL. 1998. A distributed thermal model for calculaing soil temperature profiles and depth of thaw in permafrost regions. *Journal of Geophysical Research*, **103**, 975–991.

Hipel, K. W., & McLeod, A. I. 1994. *Time series modelling of water resources and environmental systems*. Elsevier Science.

Holden, J, & Burt, TP. 2002. Piping and pipeflow in a deep peat catchment. *Catena*, **48**(3), 163–199.

Hyder, Zafar, Butler Jr, James J, McElwee, Carl D, & Liu, Wenzhi. 1994. Slug tests in partially penetrating wells. *Water Resources Research*, **30**(11), 2945–2957.

Jafarov, Elchin E, Romanovsky, Vladimir E, Genet, Helene, McGuire, A David, & Marchenko, Sergey S. 2013. The effects of fire on the thermal stability of permafrost in lowland and upland black spruce forests of interior Alaska in a changing climate. *Environmental Research Letters*, **8**(3), 035030.

Jafarov, Elchin E, Coon, Ethan T, Harp, Dylan R, Wilson, Cathy J, Painter, Scott L, Atchley, Adam L, & Romanovsky, Vladimir E. 2018. Modeling the role of preferential snow accumulation in through talik development and hillslope groundwater flow in a transitional permafrost landscape. *Environmental Research Letters*, **13**(10), 105006.

Jorgenson, M Torre, Romanovsky, Vladimir, Harden, Jennifer, Shur, Yuri, O'Donnell, Jonathan, Schuur, Edward AG, Kanevskiy, Mikhail, & Marchenko, Sergei. 2010. Resilience and vulnerability of permafrost to climate change. *Canadian Journal of Forest Research*, **40**(7), 1219–1236.

Jorgenson, MT, & Osterkamp, TE. 2005. Response of boreal ecosystems to varying modes of permafrost degradation. *Canadian Journal of Forest Research*, **35**(9), 2100–2111.

Jutras, Sylvain, Rousseau, Alain N, & Clerc. 2009. Implementation of a Peatland-Specific Water Budget Algorithm in HYDROTEL. **34**(4), 349–364.

Kane, DL, Yoshikawa, K, & Mcnamara, JP. 2013. Regional groundwater flow in an area mapped as continuous permafrost , NE Alaska (USA). 41–52.

Karra, S, Painter, SL, & Lichtner, PC. 2014. Three-phase numerical model for subsurface hydrology in permafrost-affected regions (PFLOTRAN-ICE v1. 0). *The Cryosphere (Online)*, **8**(5).

Kimmel, K, & Mander, U. 2010. Ecosystem services of peatlands: implications for restoration. *Progress in Physical Geography*, **34**(4), 491–514.

Klammler, Harald, Parker, Beth L, Cherry, John A, & Rao, P Suresh C. 2005. Field-Scale Evaluation of the Passive Flux Meter for Simultaneous Measurement of Groundwater and Contaminant Fluxes. **39**(18), 7194–7201.

Klammler, Harald, Hatfield, Kirk, & Annable, Michael D. 2007. Concepts for measuring horizontal groundwater flow directions using the passive flux meter. *Advances in water resources*, **30**(4), 984–997.

Koven, Charles D, Riley, William J, & Stern, Alex. 2013. Analysis of permafrost thermal dynamics and response to climate change in the CMIP5 Earth System Models. *Journal of Climate*, **26**(6), 1877–1900.

Krogh, Sebastian A, Pomeroy, John W, & Marsh, Philip. 2017. Diagnosis of the hydrology of a small Arctic basin at the tundra-taiga transition using a physically based hydrological model. *Journal of Hydrology*, **550**, 685–703.

Kuchment, L, Gelfan, A & Demidov, V. 2000. A distributed model of runoff generation in the permafrost regions. *Journal of Hydrology*, **240**, 1–22.

Kunz, Julia Vanessa, Annable, Michael D, Cho, Jaehyun, Tümpling, Wolf von, Hatfield, Kirk, Rao, Suresh, Borchardt, Dietrich, & Rode, Michael. 2017. Quantifying nutrient fluxes with a new hyporheic passive flux meter (HPFM). *Biogeosciences*, **14**(3), 631–649.

Kurylyk, Barret L, & Hayashi, Masaki. 2016. Improved Stefan equation correction factors to accommodate sensible heat storage during soil freezing or thawing. *Permafrost and Periglacial Processes*, **27**(2), 189–203.

Kurylyk, Barret L, Hayashi, Masaki, Quinton, William L, McKenzie, Jeffrey M, & Voss, Clifford I. 2016. Influence of vertical and lateral heat transfer on permafrost thaw, peatland landscape transition, and groundwater flow. *Water Resources Research*, **52**(2), 1286–1305.

Kurylyk, BL, & Watanabe, K. 2013. The mathematical representation of freezing and thawing processes in variably-saturated, non-deformable soils. *Advances in Water Resources*, **60**, 160–177.

Kurylyk, BL, McKenzie, JM, MacQuarrie, KB, & Voss, CI. 2014. Analytical solutions for benchmarking cold regions subsurface water flow and energy transport models: one-dimensional soil thaw with conduction and advection. *Advances in Water Resources*, **70**, 172–184.

Kwong, YT John, & Gan, TY. 1994. Northward migration of permafrost along the Mackenzie Highway and climatic warming. *Climatic Change*, **26**(4), 399–419.

Lafleur, PM, Hember, RA, Admiral, SW, & Roulet, NT. 2005. Annual and seasonal variability in evapotranspiration and water table at a shrub-covered bog in southern Ontario, Canada. *Hydrological Processes*, **19**(18), 3533–3550.

Langford, Joelle E, Schincariol, Robert A, Nagare, Ranjeet M, Quinton, William L, & Mohammed, Aaron A. 2020. Transient and transition factors in modeling permafrost thaw and groundwater flow. *Groundwater*, **58**(2), 258–268.

Larsen, James A. 2013. *The boreal ecosystem*. Elsevier.

Lawrence, David M, Slater, Andrew Gi, Romanovsky, Vladimr E, & Nicolsky, Dmitry J. 2008. Sensitivity of a model projection of near-surface permafrost degradation to soil column depth and representation of soil organic matter. *Journal of Geophysical Research*, **113**, 1–14.

Lebeau, Marc, & Konrad, Jean-Marie. 2012. An extension of the capillary and thin film flow model for predicting the hydraulic conductivity of air-free frozen porous media. *Water Resources Research*, **48**(7).

Lee, Jimi, Rao, PSC, Poyer, Irene C, Toole, Robyn M, Annable, MD, & Hatfield, K. 2007. Oxyanion flux characterization using passive flux meters: Development and field testing of surfactant-modified granular activated carbon. *Journal of contaminant hydrology*, **92**(3-4), 208–229.

Leibowitz, Scott G, Mushet, David M, & Newton, Wesley E. 2016. Intermittent surface water connectivity: fill and spill vs. fill and merge dynamics. *Wetlands*, **36**(2), 323–342.

Lewis, Ciaran, Albertson, John, Xu, Xianli, & Kiely, Ger. 2012. Spatial variability of hydraulic conductivity and bulk density along a blanket peatland hillslope. *Hydrological Processes*, **26**(10), 1527–1537.

Li, Qian, Sun, Shufen, & Xue, Yongkang. 2010. Analyses and development of a hierarchy of frozen soil models for cold region study. *Journal of Geophysical Research*, **115**.

Magnusson, Jan, Gustafsson, David, Hüsler, Fabia, & Jonas, Tobias. 2014. Assimilation of point SWE data into a distributed snow cover model comparing two contrasting methods. *Water resources research*, **50**(10), 7816–7835.

McBean, G. 2007. *Arctic climate impact assessment*.

McClymont, AF, Hayashi, M, Bentley, LR, & Christensen, BS. 2013. Geophysical imaging and thermal modeling of subsurface morphology and thaw evolution of discontinuous permafrost. *Journal of Geophysical Research: Earth Surface*, **118**, 1826–1837.

McDonnell, J. 2003. Where does water go when it rains? Moving beyond the variable source area concept of rainfall-runoff response. *Hydrological processes*, **17**(9), 1869–1875.

McGuire, A David, Koven, Charles, Lawrence, David M, Clein, Joy S, Xia, Jiangyang, Beer, Christian, Burke, Eleanor, Chen, Guangsheng, Chen, Xiaodong, Delire, Christine, *et al.* 2016. Variability in the sensitivity among model simulations of permafrost and carbon dynamics in the permafrost region between 1960 and 2009. *Global Biogeochemical Cycles*, **30**(7), 1015–1037.

McKenzie, Jeffrey M, & Voss, Clifford I. 2013. Permafrost thaw in a nested groundwater-flow system. *Hydrogeology Journal*, **21**(1), 299–316.

McKenzie, Jeffrey M, Voss, Clifford I, & Siegel, Donald I. 2007. Groundwater flow with energy transport and water–ice phase change: numerical simulations, benchmarks, and application to freezing in peat bogs. *Advances in water resources*, **30**(4), 966–983.

Meteorological Service of Canada. 2012. National climate data archive of Canada.

Morris, Paul J, Baird, Andy J, & Belyea, Lisa R. 2015. Bridging the gap between models and measurements of peat hydraulic conductivity. *Water Resources Research*, **51**(7), 5353–5364.

Morris, PJ, & Waddington, JM. 2011. Groundwater residence time distributions in peatlands: implications for peat decomposition and accumulation. *Water Resources Research*, **47**(2), 1–12.

Naasz, R, Michel, J-C, & Charpentier, Sylvain. 2005. Measuring hysteretic hydraulic properties of peat and pine bark using a transient method. *Soil science society of America Journal*, **69**(1), 13–22.

Natural Resources Canada. 1995. *Permafrost in Canada*. data retrieved from Natural Resources Canada, http://geogratis.gc.ca/api/en/nrcan-rncan/ess-sst/d1e2048b-ccff-5852-aaa5-b861bd55c367.

Nicolsky, D J, Romanovsky, V E, Alexeev, V A, & Lawrence, D M. 2007. Improved modeling of permafrost dynamics in a GCM land-surface scheme. *Geophysical Research Letters*, **34**(April), 2–6.

Nicolsky, Dmitry J, Romanovsky, Vladimir E, Panda, Santosh K, Marchenko, Sergey S, & Muskett, Reginald R. 2017. Applicability of the ecosystem type approach to model permafrost dynamics across the Alaska North Slope. *Journal of Geophysical Research: Earth Surface*, **122**(1), 50–75.

Obu, Jaroslav, Westermann, Sebastian, Bartsch, Annett, Berdnikov, Nikolai, Christiansen, Hanne H, Dashtseren, Avirmed, Delaloye, Reynald, Elberling, Bo, Etzelmüller, Bernd, Kholodov, Alexander, *et al.* 2019. Northern Hemisphere permafrost map based on TTOP modelling for 2000–2016 at 1 km^2 scale. *Earth-Science Reviews*, **193**, 299–316.

O'Donnell, Jonathan A, Romanovsky, Vladimir E, Harden, Jennifer W, & McGuire, A David. 2009. The effect of moisture content on the thermal conductivity of moss and organic soil horizons from black spruce ecosystems in interior Alaska. *Soil Science*, **174**(12), 646–651.

Oelke, C, Zhang, T, Serreze, MC, & Armstrong, RL. 2003. Regional-scale modeling of soil freeze / thaw over the Arctic drainage basin. *Journal of Geophysical Research*, **108**, 1–19.

Ogden, Fred L, Lai, Wencong, Steinke, Robert C, Zhu, Jianting, Talbot, Cary A, & Wilson, John L. 2015. A new general 1-D vadose zone flow solution method. *Water Resources Research*, **51**(6), 4282–4300.

Ogden, Fred L., Allen, Myron B., Lai, Wencong, Zhu, Jianting, Seo, Mookwon, Douglas, Craig C., & Talbot, Cary A. 2017. The soil moisture velocity equation. *Journal of Advances in Modeling Earth Systems*, **9**.

Oledefeldt, D. 2016. Fire, thaw, droughts and floods: impacts on wetland and wetland catchments in Alberta. *AEP Conference, oral presentation.*

Oriol, Felipo, De Boodt, M, Verdonck, O, & Cappaert, I. 1978. Thermal properties of two organic (peat, pine bark) and two inorganic (perlite, clay) horticultural substrates. *Catena*, **5**(3-4), 389–394.

Price, Jonathan S. 1991. Evaporation from a blanket bog in a foggy coastal environment. *Boundary-Layer Meteorology*, **57**(4), 391–406.

Price, Jonathan S, & Ketcheson, Scott J. 2009. Water relations in cutover peatlands. *Carbon Cycling in Northern Peatlands*, **184**, 277–287.

Price, Jonathan S, Cagampan, Jason, & Kellner, Erik. 2005. Assessment of peat compressibility: is there an easy way? *Hydrological Processes: An International Journal*, **19**(17), 3469–3475.

Price, JS, & Maloney, DA. 1994. Hydrology of a Patterned Bog-Fen Complex in Southeastern Labrador , Canada. *Nordic Hydrology*, **25**, 313–330.

Prowse, Terry D, & Furgal, Chris. 2009. Northern Canada in a changing climate: major findings and conclusions. *Ambio*, **38**(5), 290–292.

Putkonen, Jaakko. 1998. Soil thermal processes and heat transfer processes near Ny-Ålesund, northwestern Spitsbergen, Svalbard. *Polar research*, **17**(2), 165–179.

Pörtner, H.-O., Roberts, D.C., Masson-Delmotte, V., Zhai, P., Tignor, M., Poloczanska, E., Mintenbeck, K., Alegría, A., Nicolai, M., Okem, A., Petzold, J., Rama, B., & Weyer, N.M. 2019. IPCC, 2019: IPCC Special Report on the Ocean and Cryosphere in a Changing Climate.

Quinton, W L, & Baltzer, JL. 2013. The active-layer hydrology of a peat plateau with thawing permafrost (Scotty Creek, Canada). *Hydrogeology Journal*, **21**(1), 201–220.

Quinton, William, Berg, Aaron, Braverman, Michael, Carpino, Olivia, Chasmer, Laura, Connon, Ryan, Craig, James, Devoie, Élise, Hayashi, Masaki, Haynes, Kristine, *et al.* 2018. A Synthesis of Three Decades of Eco-Hydrological Research at Scotty Creek, NWT, Canada. *Hydrology and Earth System Sciences Discussions*, **2018**, 1–36.

Quinton, William L, Hayashi, Masaki, & Carey, Sean K. 2008. Peat hydraulic conductivity in cold regions and its relation to pore size and geometry. *Hydrological Processes: An International Journal*, **22**(15), 2829–2837.

Quinton, WL, Hayashi, M, & Pietroniro, A. 2003. Connectivity and storage functions of channel fens and flat bogs in northern basins. *Hydrological Processes*, **17**(18), 3665–3684.

Quinton, WL, Hayashi, M, & Chasmer, LE. 2009. Peatland hydrology of discontinuous permafrost in the Northwest Territories: overview and synthesis. *Canadian Water Resources Journal*, **34**(4), 311–328.

Quinton, WL, Hayashi, M, & Chasmer, LE. 2011. Permafrost-thaw-induced land-cover change in the Canadian subarctic: implications for water resources. *Hydrological Processes*, **25**(1), 152–158.

Quinton, WL, Berg, AA, Carpino, O, Connon, RF, Craig, JR, Devoie, E, & Johnson, E. 2017. Toward understanding the trajectory of hydrological change in the southern Taiga Plains, northeastern British Columbia and southwestern Northwest Territories. *Geoscience BC Summary of Activities*, 2018–4.

Raven, Development Team. 2017. Raven: User's and Developer's Manual v2.7.

Rawlins, MA, Nicolsky, DJ, McDonald, KC, & Romanovsky, VE. 2013. Simulating soil freeze/thaw dynamics with an improved pan-Arctic water balance model. *Journal of Advances in Modeling Earth Systems*, **5**(4), 659–675.

Reeve, AS, Warzocha, Jon, Glaser, PH, & Siegel, DI. 2001. Regional ground-water flow modeling of the Glacial Lake Agassiz Peatlands, Minnesota. *Journal of Hydrology*, **243**(1), 91–100.

Richards, L. A. 1941. Soil moisture tensiometer materials and construction. *U. S. Department of Agriculture*.

Robinson, Stephen D, & Moore, Timothy R. 2000. The influence of permafrost and fire upon carbon accumulation in high boreal peatlands, Northwest Territories, Canada. *Arctic, Antarctic, and Alpine Research*, **32**(2), 155–166.

Romanovsky, VE, Osterkamp, TE, & Duxbury, NS. 1997. An evaluation of three numerical models used in simulations of the active layer and permafrost temperature regimes. *Cold Regions Science and Technology*, **26**(3), 195–203.

Roulet, NT, & Woo, M. 1986. Hydrology of a wetland in the continuous permafrost region. *Journal of Hydrology*, **89**, 73–91.

Rowland, JC, Jones, CE, Altmann, G, Bryan, R, Crosby, BT, Hinzman, LD, Kane, DL, Lawrence, DM, Mancino, A, Marsh, P, *et al.* 2010. Arctic landscapes in transition: responses to thawing permafrost. *Eos, Transactions American Geophysical Union*, **91**(26), 229–230.

Rowland, JC, Travis, BJ, & Wilson, CJ. 2011. The role of advective heat transport in talik development beneath lakes and ponds in discontinuous permafrost. **38**(September), 1–5.

Rowlands, Aled, Pomeroy, John, Hardy, Janet, Marks, Danny, Elder, Kelly, & Melloh, Rae. 2002. Small-scale spatial variability of radiant energy for snowmelt in a mid-latitude subalpine forest. **9**.

Rydin, H, & Jeglum, JK. 2013. *The biology of peatlands*. Oxford university press.

Schaefer, Kevin, Zhang, Tingjun, Slater, Andrew G, Lu, Lixin, Etringer, Andrew, & Baker, Ian. 2009. Improving simulated soil temperatures and soil freeze/thaw at high-latitude regions in the Simple Biosphere/Carnegie-Ames-Stanford Approach model. *Journal of Geophysical Research: Earth Surface*, **114**(F2).

Semenova, O, Lebedeva, L, & Vinogradov, Y. 2013. Simulation of subsurface heat and water dynamics, and runoff generation in mountainous permafrost conditions, in the Upper Kolyma River basin, Russia. *Hydrogeology Journal*, **21**(1), 107–119.

Shen, Mingxi, Chen, Jie, Zhuan, Meijia, Chen, Hua, Xu, Chong-Yu, & Xiong, Lihua. 2018. Estimating uncertainty and its temporal variation related to global climate models in quantifying climate change impacts on hydrology. *Journal of Hydrology*, **556**, 10–24.

Shiklomanov, Nikolay I, Streletskiy, Dmitry A, & Nelson, Frederick E. 2012. Northern hemisphere component of the global circumpolar active layer monitoring (CALM) program. **1**, 377–382.

Shook, K, Pomeroy, JW, Spence, C, & Boychuk, L. 2013. Storage dynamics simulations in prairie wetland hydrology models: Evaluation and parameterization. *Hydrological Processes*, **27**(13), 1875–1889.

Shook, Kevin, Pomeroy, John, & van der Kamp, Garth. 2015. The transformation of frequency distributions of winter precipitation to spring streamflow probabilities in cold regions; case studies from the Canadian Prairies. *Journal of Hydrology*, **521**, 395–409.

Shur, Yu L, & Jorgenson, MT. 2007. Patterns of permafrost formation and degradation in relation to climate and ecosystems. *Permafrost and Periglacial Processes*, **18**(1), 7–19.

Sjöberg, Ylva, Coon, Ethan, K. Sannel, A Britta, Pannetier, Romain, Harp, Dylan, Frampton, Andrew, Painter, Scott L, & Lyon, Steve W. 2016. Thermal effects of groundwater flow through subarctic fens: A case study based on field observations and numerical modeling. *Water Resources Research*, **52**(3), 1591–1606.

Slater, AG, Pitman, AJ, & Desborough, CE. 1998. Simulation of freeze-thaw cycles in a general circulation model land surface scheme. *Journal of Geophysical Research*, **103**(97).

Smith, RI Lewis. 1985. Nutrient cycling in relation to biological productivity in Antarctic and sub-Antarctic terrestrial and freshwater ecosystems. *Pages 138–155 of: Antarctic nutrient cycles and food webs*. Springer.

Smith, Sharon Lee. 2011. *Trends in permafrost conditions and ecology in northern Canada*. Canadian Councils of Resource Ministers.

Solomon, AD. 1979. An easily computable solution to a two-phase Stefan problem. *Solar energy*, **23**(6), 525–528.

Solomon, S., Qin, D., Manning, M., Averyt, K., & Marquis, M. 2007. *Climate change 2007 - the physical science basis: working group I contribution to the fourth assesment report of the IPCC*. Cambridge University Press.

Spaans, Egbert JA, & Baker, John M. 1996. The soil freezing characteristic: its measurement and similarity to the soil moisture characteristic. *Soil Science Society of America Journal*, **60**, 13–19.

St Jacques, JM, & Sauchyn, DJ. 2009. Increasing winter baseflow and mean annual streamflow from possible permafrost thawing in the Northwest Territories, Canada. *Geophysical Research Letters*, **36**(1), 1–6.

Stähli, Manfred, Jansson, Per-Erik, & Lundin, Lars-Christer. 1999. Soil moisture redistribution and infiltration in frozen sandy soils. *Water Resources Research*, **35**(1), 95–103.

Stendel, M, & Christensen, JH. 2002. Impact of global warming on permafrost conditions in a coupled GCM. *Geophysical Research Letters*, **29**(13), 10–1.

Stephens, DB. 1995. *Vadose zone hydrology*. CRC press.

Stone, Lindsay E. 2018. *The role of channel fens in permafrost degradation induced changes in peatland discharge at Scotty Creek, NT.* M.Phil. thesis, Wilfrid Laurier University.

Stormont, John C, & Anderson, Clifford E. 1999. Capillary barrier effect from underlying coarser soil layer. *Journal of Geotechnical and Geoenvironmental Engineering*, **125**(8), 641–648.

Sudicky, Edward A. 1986. A natural gradient experiment on solute transport in a sand aquifer: Spatial variability of hydraulic conductivity and its role in the dispersion process. *Water Resources Research*, **22**(13), 2069–2082.

Swindles, Graeme T, Morris, Paul J, Mullan, Donal, Watson, Elizabeth J, Turner, T Edward, Roland, Thomas P, Amesbury, Matthew J, Kokfelt, Ulla, Schoning, Kristian, Pratte, Steve, *et al.* 2015. The long-term fate of permafrost peatlands under rapid climate warming. *Scientific reports*, **5**(1), 1–6.

Tananaev, NI, Makarieva, OM, & Lebedeva, LS. 2016. Trends in annual and extreme flows in the Lena River basin, Northern Eurasia. *Geophysical Research Letters*, **43**(20).

Tao, Y-X, & Gray, DM. 1994. Prediction of snowmelt infiltration into frozen soils. *Numerical Heat Transfer*, **26**(6), 643–665.

Tarnocai, C. 2009. The impact of climate change on Canadian peatlands. **34**(4), 453–466.

Tarnocai, C, Kettles, IM, & Lacelle, B. 2011. *Peatlands of Canada database.* data retrieved from Peat Moss Association of Canada, http://peatmoss.com.

Taylor, G. S., & Luthin, J. N. 1978. A model for coupled heat and moisture transfer during soil freezing. *Canadian Geotechnical Journal*, **15**(4), 548–555.

Tromp-Van Meerveld, HJ, & McDonnell, JJ. 2006. Threshold relations in subsurface stormflow: 2. The fill and spill hypothesis. *Water Resources Research*, **42**, 1–11.

Van Genuchten, M Th. 1980. A closed-form equation for predicting the hydraulic conductivity of unsaturated soils. *Soil science society of America journal*, **44**(5), 892–898.

Walvoord, MA, & Kurylyk, BL. 2016. Hydrologic impacts of thawing permafrost: a review. *Vadose Zone Journal*, **15**(6).

Walvoord, Michelle A, Voss, Clifford I, Ebel, Brian A, & Minsley, Burke J. 2019. Development of perennial thaw zones in Boreal hillslopes enhances potential mobilization of permafrost carbon. *Environmental Research Letters*, **14**(1), 015003.

Wania, R, Ross, I, & Prentice, IC. 2009. Integrating peatlands and permafrost into a dynamic global vegetation model: 1. Evaluation and sensitivity of physical land surface processes. *Global Biogeochemical Cycles*, **23**(3), 1–19.

Warner, BG. 2016 (december). *What came first, the peatlands or the permafrost?* personal communication.

Water Survey of Canada. 2020. Historical Hydrometric Data.

Wellman, Tristan P, Voss, Clifford I, & Walvoord, Michelle A. 2013. Impacts of climate, lake size, and supra-and sub-permafrost groundwater flow on lake-talik evolution, Yukon Flats, Alaska (USA). *Hydrogeology Journal*, **21**(1), 281–298.

Whitfield, PH, St-Hilaire, A, & van der Kamp, G. 2009. Improving hydrological predictions in peatlands. *Canadian Water Resources Journal*, **34**(4), 467–478.

Winter, Thomas C. 1983. The interaction of lakes with variably saturated porous media. *Water Resources Research*, **19**(5), 1203–1218.

Woo, M. 1986. Permafrost Hydrology in North America 1. *Atmosphere-Ocean*, **24**(3), 201–234.

Woo, M, & Winter, TC. 1993. The role of permafrost and seasonal frost in the hydrology of northern wetlands in North America. *Journal of hydrology*, **141**(1), 5–31.

Woo, M-K, Arain, MA, Mollinga, M, & Yi, S. 2004. A two-directional freeze and thaw algorithm for hydrologic and land surface modelling. *Geophysical Research Letters*, **31**(12).

Woo, Ming-ko. 2012. *Permafrost hydrology*. Springer Science & Business Media.

Wright, N, Quinton, WL, & Hayashi, M. 2008. Hillslope runoff from an ice-cored peat plateau in a discontinuous permafrost basin, Northwest Territories, Canada. *Hydrological Processes*, **22**(15), 2816–2828.

Wright, N, Hayashi, M, & Quinton, WL. 2009. Spatial and temporal variations in active layer thawing and their implication on runoff generation in peat-covered permafrost terrain. *Water Resources Research*, **45**(5).

Yi, S, Wischnewski, K, Langer, Moritz, Muster, S, & Boike, J. 2014. Freeze/thaw processes in complex permafrost landscapes of northern Siberia simulated using the TEM ecosystem model: impact of thermokarst ponds and lakes. *Geoscientific Model Development*, **7**(4), 1671–1689.

Yi, Yonghong, Kimball, John S, Chen, Richard, Moghaddam, Mahta, Reichle, Rolf H, Mishra, Umakant, Zona, Donatella, & Oechel, Walter C. 2018. Characterizing permafrost active layer dynamics and sensitivity to landscape spatial heterogeneity in Alaska. *The Cryosphere*, **12**(1), 145.

Yoshikawa, K, & Hinzman, LD. 2003. Shrinking thermokarst ponds and groundwater dynamics in discontinuous permafrost near Council Alaska. *Permafrost and Periglacial Processes*, **14**(2), 151–160.

Zhang, Y, Chen, W, & Cihlar, J. 2003. A process-based model for quantifying the impact of climate change on permafrost thermal regimes. *Journal of Geophysical Research: Atmospheres*, **108**(D22).

Zhang, Yinsuo, Wang, Shusen, Barr, Alan G, & Black, TA. 2008a. Impact of snow cover on soil temperature and its simulation in a boreal aspen forest. *Cold Regions Science and Technology*, **52**(3), 355–370.

Zhang, Yu, Chen, Wenjun, & Riseborough, Daniel W. 2008b. Disequilibrium response of permafrost thaw to climate warming in Canada over 1850–2100. *Geophysical Research Letters*, **35**(2).

Zhao, Lin, Wu, Qingbai, Marchenko, SS, & Sharkhuu, N. 2010. Thermal state of permafrost and active layer in Central Asia during the International Polar Year. *Permafrost and Periglacial Processes*, **21**(2), 198–207.

Zhou. 2014. Simulating cold regions hydrological processes using a modular model in the west of China. *Journal of Hydrology*, **509**, 13–24.

Zoltai, SC. 1972. Palsas and peat plateaus in central Manitoba and Saskatchewan. *Canadian Journal of Forest Research*, **2**(3), 291–302.

APPENDICES

Appendix A

Repositories of Field data and Model Code

A.1 Field Data

The data presented in this work as well as a significant quantity of additional field data which helped in the understanding of this system and will be used in future work is available in the Scotty Creek Data Archive. This archive is hosted by Wilfrid Laurier University, and can be accessed by contacting Dr. William Quinton (wquinton@wlu.ca) who heads this research station.

A.2 Model Code

Similarly, the model code is living, and is therefore best referred to in its repository. There are two relevant repositories. The finite volume model discussed in chapter 4 is available here: `https://github.com/egdevoie/FiniteVolumeModel` and the interface model described in chapter 6 is available here: `https://github.com/egdevoie/InterfaceModel`